



UNIVERSIDAD DE MÁLAGA

# Analysis, Design and Optimization of Electric Vehicle Wireless Chargers

A thesis submitted in fulfilment of the requirements for the  
degree of Doctor of Philosophy of Electrical Power Systems

José Manuel González González

Departamento de Ingeniería Eléctrica  
Escuela de Ingenierías Industriales  
Universidad de Málaga


Doctoral Thesis  
Málaga, Spain

Monday 26<sup>th</sup> July, 2021



UNIVERSIDAD  
DE MÁLAGA

AUTOR: José Manuel González González

 <https://orcid.org/0000-0002-3406-629X>

EDITA: Publicaciones y Divulgación Científica. Universidad de Málaga



Esta obra está bajo una licencia de Creative Commons Reconocimiento-NoComercial-SinObraDerivada 4.0 Internacional:

<http://creativecommons.org/licenses/by-nc-nd/4.0/legalcode>

Cualquier parte de esta obra se puede reproducir sin autorización pero con el reconocimiento y atribución de los autores.

No se puede hacer uso comercial de la obra y no se puede alterar, transformar o hacer obras derivadas.

Esta Tesis Doctoral está depositada en el Repositorio Institucional de la Universidad de Málaga (RIUMA): [riuma.uma.es](http://riuma.uma.es)



Tesis Doctoral

# Análisis, Diseño y Optimización de Cargadores Inalámbricos para Vehículos Eléctricos

José Manuel González González

Tesis dirigida por el Dr. D. José Antonio Aguado Sánchez y  
la Dra. Dña. Alicia Triviño Cabrera.

Programa Interuniversitario en Sistemas de Energía Eléctrica



UNIVERSIDAD DE MÁLAGA



UNIVERSITAT POLITÈCNICA  
DE CATALUNYA  
BARCELONATECH



eman ta zabal zazu  
Universidad del País Vasco Euskal Herriko  
Unibertsitatea

Departamento de Ingeniería Eléctrica  
Escuela de Ingenierías Industriales  
Universidad de Málaga

Málaga, 2021



## DECLARACIÓN DE AUTORÍA Y ORIGINALIDAD DE LA TESIS PRESENTADA PARA OBTENER EL TÍTULO DE DOCTOR

D. José Manuel González González, estudiante del programa de doctorado interuniversitario en Sistemas de Energía Eléctrica de la Universidad de Málaga, autor/a de la tesis, presentada para la obtención del título de doctor por la Universidad de Málaga, titulada: *Analysis, Design and Optimization of Electric Vehicle Wireless Chargers*.

Realizada bajo la tutorización y dirección del Dr. D. José Antonio Aguado Sánchez y la dirección de la Dra. Dña. Alicia Triviño Cabrera.

DECLARO QUE:

La tesis presentada es una obra original que no infringe los derechos de propiedad intelectual ni los derechos de propiedad industrial u otros, conforme al ordenamiento jurídico vigente (Real Decreto Legislativo 1/1996, de 12 de abril, por el que se aprueba el texto refundido de la Ley de Propiedad Intelectual, regularizando, aclarando y armonizando las disposiciones legales vigentes sobre la materia), modificado por la Ley 2/2019, de 1 de marzo.

Igualmente asumo, ante a la Universidad de Málaga y ante cualquier otra instancia, la responsabilidad que pudiera derivarse en caso de plagio de contenidos en la tesis presentada, conforme al ordenamiento jurídico vigente.

En Málaga, a 17 de junio de 2021

Fdo.: José Manuel González González Doctorando/a	Fdo.: D. José Antonio Aguado Sánchez Tutor/a
Fdo.: D. José Antonio Aguado Sánchez Directores de tesis	Dña. Alicia Triviño Cabrera





## Abstract

The transition to a decarbonized economy that many countries have undertaken in recent years has focused closely on sustainable transportation. Governments are backing Electric Vehicles (EVs) as a solution that will help to reduce their countries' carbon footprint. As part of this effort, they provide tax benefits and direct aid to promote the acquisition of EVs in order to meet the objectives established in the Paris Agreement.

Nowadays, one of the biggest concerns of potential users of these vehicles is their autonomy, which is limited both by the capacity of the batteries and by their charging. The charging is currently carried out using conductive chargers, which requires user intervention and raises safety concerns. However, wireless charging, especially magnetic-resonance technology, is considered a real alternative to conductive charging as it provides additional advantages such as greater security and ease of charging. This technology has a very rich field of development to which this thesis has contributed in a number of aspects.

The first of these contributions lies in the analytical characterization of the magnetic field generated by inductive chargers. Although there are several complex tools available to carry out this task, the proposed solution allows the magnetic field to be calculated in a simple way at any position in space. This tool, which has been validated with a 3.7-kW wireless charger prototype, facilitates the design tasks of coils, as well as the control of the exposure of external objects to the magnetic field.

One of the main difficulties that wireless chargers will have to face lies in the future transition to this technology. Wireless technology is expected to coexist with conductive technology. This thesis provides a solution for this transition, proposing an *on-board* charger topology in which a large number of components are shared between both technologies. In this way, we can reduce implementation costs and the weight of the vehicle, thereby improving its autonomy.

Developing prototypes is essential for implementing and analysing new solutions. In view of this, a prototype has been developed for the laboratory with the flexibility to test topologies and control strategies. We have also designed and implemented a final prototype for charging an electric bicycle. All the design stages have been taken into account when developing this latest prototype, from the coils to the power electronics, which are regulated to operate following a Constant Current-Constant Voltage (CC/CV) strategy. The use of a real vehicle has allowed us to propose and evaluate an analytical model to quantify the impact of the position of the secondary coil.

The charging strategy is not the only relevant aspect that controllers must monitor. The operation of the chargers outside their nominal conditions, such as in the case of misalignment between coils, produces an increase in some electrical variables of the circuit that must be controlled. This problem has

been analysed in depth in order to develop a control that limits the most critical variables and prevents damage to system components.

The control of wireless chargers also affects efficiency, which will play a fundamental role in the adoption of this technology as it is the main disadvantage compared to conductive chargers. The final contribution of this Thesis focuses on this aspect, for which a Model Predictive Control (MPC) is proposed. The control maximizes efficiency by simultaneously adjusting variables such as the operating frequency, the phase shift angle of the inverter and the equivalent resistance of the battery.

**Keywords:** electric vehicle, wireless charging, magnetic-resonance power transfer, model predictive control, maximum efficiency

## Resumen

El proceso de descarbonización de las economías que muchos países han experimentado en los últimos años ha puesto el foco en el transporte sostenible. Los gobiernos están apostando por los vehículos eléctricos (VEs) como una solución que ayudará a reducir la huella de carbono de los países, proporcionando beneficios fiscales y ayudas directas para su adquisición con los que pretenden cumplir con el Acuerdo de París.

Una de las mayores preocupaciones de los potenciales usuarios de estos vehículos está en su autonomía, que se encuentra limitada tanto por la capacidad de las baterías como por su carga. La carga se realiza actualmente mediante cargadores conductivos, que requiere la intervención del usuario y presenta problemas de seguridad. Sin embargo, la carga inalámbrica, especialmente la tecnología magnético resonante, se plantea como una alternativa real a la carga conductiva, aportando ventajas adicionales como mayor seguridad y facilidad de carga o la carga en movimiento. Esta última ventaja permite reducir el tamaño de las baterías y el consumo de los vehículos sin afectar a su autonomía.

La carga magnética resonante se basa en las leyes de Ampère y Faraday, que definen la interacción entre los campos magnéticos y las corrientes que circulan por los conductores. La transmisión de energía se realiza por medio de dos bobinas conocidas como primaria o emisora y secundaria o receptora. La bobina primaria se encarga de generar un campo magnético de alta frecuencia gracias a la corriente de la misma frecuencia que circula por ella. Este campo magnético atraviesa la bobina secundaria, en la que se induce una fuerza electromotriz que puede alimentar una carga conectada en ella.

El diseño de las bobinas afecta a los parámetros eléctricos del circuito y, por tanto, al comportamiento del sistema. Entre los factores considerados para el diseño se incluyen el coste, la robustez ante el desalineamiento y el tipo de carga, es decir, estática o dinámica. La alta frecuencia de operación de estos cargadores hace que se recurra al hilo de Litz para su construcción, con la que se consigue reducir el efecto Skin y las pérdidas asociadas. Sin embargo, no solo las bobinas juegan un papel fundamental en la tecnología magnético resonante. El sistema de compensación es el encargado de operar el cargador en resonancia gracias a sus elementos capacitivos, que compensan el carácter reactivo de las bobinas y mejoran la eficiencia del sistema. Las topologías más simples son las monoresonantes, compuestas por un único condensador conectado en serie o en paralelo a cada una de las bobinas. Las topologías multiresonantes también incorporan elementos reactivos al sistema de compensación, que ayudan a mejorar el comportamiento ante desalineamientos y a reducir el fenómeno de bifurcación.

Uno de los principales retos de la carga magnética resonante es la corriente de alta frecuencia requerida para la generación del campo magnético. La

frecuencia de la red eléctrica es demasiado baja para esta función, por lo que se recurre a la electrónica de potencia para el proceso de conversión. La combinación de alta frecuencia con potencias del orden de kW produce pérdidas elevadas en los tradicionales semiconductores de silicio. La tecnología de carburo de silicio (SiC) es una alternativa adecuada ya que mejora la eficiencia de la conversión gracias a sus características superiores, entre las que destaca la menor resistencia en conducción. El proceso de aumento de frecuencia consiste en una rectificación de la corriente de la red a Corriente Continua (CC) para después convertirla en Corriente Alterna (CA) de alta frecuencia utilizando un inversor. Algunas topologías incluyen una etapa intermedia de conversión CC/CC para adaptar la tensión. La estructura de inversor más utilizada es la de puente completo, ya que es el más equilibrado en términos de eficiencia, costo, peso y complejidad.

La fuerza electromotriz inducida en el secundario es también de alta frecuencia y debe ser adaptada a la CC utilizada por las baterías de los vehículos. Esta tarea es realizada por un rectificador, que en su topología más básica recurre a un puente de diodos y a un convertidor CC/CC si la tensión necesita ser adaptada en el lado secundario del cargador. Los rectificadores controlados pueden prescindir de etapas adicionales de conversión en el secundario, ya que son capaces de ajustar la tensión de salida. A pesar de que el control de estos convertidores es más complejo, su uso está cada vez más extendido gracias a sus ventajas frente a los rectificadores no controlados: capacidad bidireccional, mejor eficiencia gracias a la menor caída de tensión, menor pérdidas debido al menor número de componentes frente a soluciones multietapa y control de la energía reactiva del circuito.

La carga de la batería es regulada por el sistema de control. La estrategia de carga más utilizada es la de corriente constante-tensión constante, que maximiza la vida de la batería al garantizar que no se superan los valores de corriente y tensión máximos recomendados por el fabricante de la batería. Esta regulación de la carga puede ser realizada desde distintos puntos del cargador. El control desde el lado primario es utilizado porque permite simplificar los componentes del secundario, reduciendo así el peso del vehículo. El control por desplazamiento de fase es el más utilizado en el inversor, ya que regula la tensión de salida utilizando una técnica sencilla que no requiere de etapas de conversión adicionales. A pesar de la mayor sencillez del control del convertidor CC/CC, su uso está menos extendido ya que requiere la instalación de esta etapa adicional. La principal desventaja de estas topologías de control se encuentra en la necesidad de establecer comunicaciones con el secundario para controlar la carga de la batería.

El control secundario, además de eliminar la necesidad de establecer comunicaciones, permite implementar estrategias de máxima eficiencia. Para ello, el convertidor CC/CC o el rectificador controlado debe trabajar como un adaptador de impedancias. El principal inconveniente de aplicar este tipo de estrategias se encuentra en la imposibilidad de regular la carga de la batería simultáneamente. Esta limitación puede ser eliminada aplicando el sistema de control a ambos lados del cargador, ya que de esta forma se puede operar con

tres grados de control que incluyen la tensión, la frecuencia de operación y la resistencia equivalente de la batería.

Para garantizar el despegue de esta tecnología y la compatibilidad entre distintos fabricantes, la carga magnética resonante ha sido regulada con varios estándares internacionales. El más relevante en la industria internacional es el SAE J2954, que define diversos aspectos de estos cargadores. La frecuencia de operación, la potencia de carga y la distancia entre bobinas son algunos de los parámetros definidos en esta normativa.

Las perspectivas de mercado de los cargadores inalámbricos son inciertas debido a la actual etapa de desarrollo en la que se encuentra. El coste, la eficiencia y las potencias de carga son algunos de los retos a los que se debe hacer frente para adquirir cuota de mercado frente a la tecnología conductiva. Las previsiones apuntan a una Tasa de Crecimiento Anual Compuesto (TCAC) de entre el 30 y el 50 % hasta el año 2025, con Europa liderando este mercado. Algunos fabricantes de vehículos ya han mostrado su interés en esta tecnología, aunque el principal impulso viene de compañías externas al sector, que ya han implementado soluciones en entornos reales. La hibridación de cargadores conductivos e inductivos puede colaborar a mejorar la implementación de la carga inalámbrica gracias a la reducción de costes. Sin embargo, es de esperar que el impulso definitivo venga del desarrollo de esta tecnología, al que esta tesis ha contribuido con diversas aportaciones.

### **Contribución 1**

La caracterización del campo magnético es una herramienta fundamental para el diseño de las bobinas. Aunque esta tarea puede ser realizada utilizando software costoso y complejo basado en método de elementos finitos (como Ansys Maxwell), estos no son capacidades de proporcionar un análisis rápido de las distintas posibilidades para el diseño de las bobinas de un prototipo. Esta aportación busca eliminar las limitaciones de estos softwares, proponiendo un método que permite realizar estudios mediante un simple script.

La propuesta ha sido desarrollada centrándose en las bobinas rectangulares. Aunque las bobinas circulares presentan una mejor eficiencia en situaciones ideales, las rectangulares mejoran su rendimiento bajo desalineamiento, por lo que en la práctica son más utilizadas.

La solución propuesta tiene una serie de ventajas respecto a otras presentes en la literatura, como la posibilidad de obtener el valor del campo magnético en cualquier punto del espacio, el no uso de dipolos magnéticos y la facilidad de incorporar apantallamiento o elementos ferromagnéticos en el modelo modificando los parámetros eléctricos equivalentes. La metodología de cálculo se basa en la relación entre el campo magnético estático y el vector de potencial magnético. Los dos componentes del vector de potencial magnético se calculan aplicando la ley de Biot-Savart. El campo magnético final se calcula multiplicando el campo magnético estático resultante por el número de vueltas y un factor dependiente del tiempo.

El campo magnético generado por los cargadores magnético resonantes debe incluir los efectos de ambas bobinas, pero si asumimos que operan en un

medio lineal, este valor se puede calcular sumando las contribuciones del campo magnético generado por la bobina primaria y el creado por bobina secundaria. Para cada bobina, el campo magnético básico se calcula para un único bucle. El número de bucles se utiliza posteriormente como una constante proporcional de la derivada del campo magnético. Dado que el desalineamiento también afecta la fase de la corriente que circula por el sistema, las ecuaciones desarrolladas han considerado este fenómeno.

La herramienta se ha validado con el prototipo de laboratorio en un amplio conjunto de configuraciones con diferentes condiciones de desalineación. El campo magnético ha sido medido utilizando una bobina auxiliar desarrollada en el laboratorio. La comparación entre las mediciones y los resultados teóricos concluye con un error medio del 8 % y una desviación estándar igual al 6,5 %.

## **Contribución 2**

A pesar de las ventajas que tienen los cargadores inalámbricos sobre los conductivos, su implementación será un proceso lento en el que probablemente ambas tecnologías coexistan simultáneamente para aprovechar la infraestructura de carga conductiva existente.

Los VEs se pueden cargar con cargadores externos e internos. Los cargadores externos están relacionados con los cargadores de CC porque realizan la conversión de energía con la electrónica de potencia ubicada en un dispositivo externo. Estos cargadores no se utilizan en entornos domésticos porque son peligrosos y requieren mucha potencia y espacio disponible. Por otro lado, los cargadores de a bordo están integrados en el vehículo y pueden conectarse directamente a la red. La hibridación de cargadores no es un tema ampliamente estudiado. La bibliografía es escasa con un número limitado de trabajos y solo dos patentes de Tesla y Toyota. La propuesta realizada por estos fabricantes es compartir el convertidor CC/CC del lado secundario entre ambas tecnologías.

Este trabajo tiene como objetivo aprovechar la electrónica de potencia de a bordo encargada de la carga de la batería en los VEs actuales para que los cargadores inalámbricos y conductores compartan más componentes que los propuestos en las patentes. Esto permitirá aprovechar las ventajas de ambas tecnologías sin un aumento significativo de peso y coste del vehículo.

Para ello, este trabajo propone un novedoso concepto de carga en el que el transformador utilizado para aislar el vehículo de la red se sustituye por dos bobinas construidas con hilo de Litz que, a su vez, son utilizadas por el sistema inalámbrico como bobinas receptoras. Por tanto, el rectificador instalado en el vehículo puede ser compartido por ambas tecnologías. Este cambio es significativo porque los componentes electrónicos deben poder funcionar a alta frecuencia. La frecuencia de la corriente de la red también debe incrementarse para que este concepto sea viable. Este proceso también se puede utilizar para regular la potencia de carga, lo que podría simplificar otras etapas de un cargador de a bordo tradicional.

Uno de los principales retos de este trabajo es el diseño de las bobinas, que se ha realizado mediante un método de elementos finitos en el software

ANSYS Maxwell 3D. Por un lado, ambas bobinas instaladas en el vehículo deben tener especificaciones que permitan regular la potencia de carga y aislar el vehículo de la red, mientras que por otro lado también deben actuar como bobinas receptoras para la carga inalámbrica, lo que requiere tener un espacio muy pequeño entre ambas bobinas y ser del mismo tamaño. La diferencia en el espacio entre las dos bobinas plantea un problema para la carga inductiva ya que la inductancia mutua con la bobina primaria es diferente y esto produce una corriente circulante que aumenta las pérdidas del sistema. Por lo tanto, minimizar esta brecha es esencial para mejorar la eficiencia del sistema.

Ambos modos de carga funcionan con un perfil corriente constante-tensión constante. La carga inalámbrica del vehículo se realiza gracias a un inversor primario externo que convierte la corriente de la red en una corriente de alta frecuencia de 85 kHz. Esta corriente alimenta la bobina primaria, que incluye un tanque resonante LCC para mejorar la eficiencia ante desalineamientos. El campo magnético generado pasa por las dos bobinas instaladas en el vehículo e induce una tensión de alta frecuencia, que se convierte a CC mediante un rectificador no controlado y los diodos antiparalelos del inversor de a bordo. Por lo tanto, hay dos vías desde las que la corriente fluye hacia la batería. La regulación de la carga se realiza utilizando la técnica de desplazamiento de fase en el inversor primario.

La carga conductiva utiliza solo las dos bobinas instaladas en el vehículo en un proceso similar al de la carga inalámbrica. En este caso, un inversor integrado genera la corriente de alta frecuencia necesaria para la transferencia. La potencia de carga se regula mediante un control de frecuencia que opera en el rango entre 100 y 140 kHz.

La propuesta se ha implementado en un prototipo de cargador híbrido de 3 kW que ha permitido verificar su viabilidad. Los resultados muestran que el funcionamiento del sistema es válido en todo el rango de cargas de la batería, con eficiencias superiores al 93 % en modo conductor y al 87 % en modo inductivo. Estos niveles de eficiencia se alcanzan porque el sistema opera con conmutación a cero voltaje (ZVS) cuando el ángulo de fase de la impedancia de entrada es alto, aunque este parámetro aumenta la potencia reactiva en el circuito. También se analiza la eficiencia bajo desalineación con una resistencia equivalente de 53,3  $\Omega$ , alcanzando valores superiores al 90 % con 15 cm de desalineación y superiores al 80 % con 30 cm. Finalmente, se ha verificado que el prototipo cumple con los límites de emisiones electromagnéticas.

### **Contribución 3**

La carga inalámbrica de vehículos se asocia tradicionalmente con los automóviles. Sin embargo, esta tecnología también es compatible con otro tipo de vehículos, como autobuses, motocicletas, drones y bicicletas eléctricas.

Desarrollar un prototipo para cualquier vehículo es siempre un desafío, ya que su diseño debe adaptarse a sus requisitos técnicos. Los vehículos más grandes suelen incluir baterías de gran capacidad, por lo que sus cargadores deben poder funcionar a alta potencia para que el proceso no conlleve demasiado tiempo. Además, estas baterías funcionan con altos valores de tensión



que requieren una electrónica de potencia adecuada para estos niveles. Sin embargo, los requisitos para los vehículos más ligeros son diferentes: la potencia de carga ya no es un factor determinante porque está limitada por C-rate de sus baterías. La prioridad de estos sistemas es encontrar una solución lo suficientemente compacta para que pueda ser instalada en el vehículo, a la vez que mantiene un bajo coste para que su implementación sea atractiva para los usuarios.

Esta aportación tiene como objetivo desarrollar un prototipo de 84 W para la carga inalámbrica de una e-bike Torrot City Surfer, incluyendo el diseño e implementación de todos los componentes del cargador, así como el sistema de control, que regula la carga de la batería de forma sencilla y robusta.

El proceso de diseño del prototipo comienza con las bobinas de transmisión, que se han diseñado utilizando una estructura circular. Este tipo de bobina tiene una tolerancia menor a la desalineación que las bobinas rectangulares. Sin embargo, para esta aplicación, se ha instalado sobre un soporte físico que garantiza su alineación con la bobina secundaria. En estas circunstancias, las bobinas circulares proporcionan una mejor eficiencia que las bobinas rectangulares. El diseño finalmente se implementó utilizando hilo de Litz, que reduce el efecto Skin y por lo tanto las pérdidas.

La implementación del prototipo en un vehículo real plantea desafíos adicionales al diseño de las bobinas, ya que las condiciones de trabajo dejan de ser ideales. Una de las principales dificultades es el efecto que tienen las partes metálicas del vehículo sobre el campo magnético. En el análisis realizado en laboratorio, se puede observar que los materiales conductores circundantes afectan el circuito equivalente del cargador. Los materiales que interfieren se pueden modelar agregando una tercera malla compuesta por un inductor y una resistencia.

Para simplificar el análisis, este trabajo propone una solución que permite reducir el circuito a una topología equivalente de dos mallas. Los efectos de los materiales interferentes circundantes se incorporan modificando los valores de las inductancias y las resistencias.

El posicionamiento final de las bobinas se ha decidido en base al análisis experimental de tres posiciones. La zona delantera de la bicicleta (posiciones A y B) tiene un efecto negativo en la eficiencia, ya que los radios de la rueda, la horquilla y el sistema de frenado son de acero. Este efecto es aún más significativo en la posición B (zona interior de la rueda delantera) debido a la inclinación de la horquilla y la mayor proximidad al cuadro de la bicicleta. Por el contrario, la posición C (detrás del asiento) consigue un buen nivel de eficiencia gracias al bajo contenido metálico del asiento. Tanto el cuadro -porque incorpora la batería en su interior- como la rueda trasera -por la cantidad de metal en el sistema de cambio- fueron descartados del análisis al no ser factible incorporar la bobina en esas posiciones.

El proceso de diseño del cargador también incluye el dimensionamiento del sistema de compensación y la topología de la electrónica de potencia. El sistema de compensación se ha implementado utilizando una estructura serie-serie, que proporciona un buen rendimiento utilizando una estructura sencilla.



Estas estructuras están compuestas por condensadores de polipropileno como único componente. La señal de alta frecuencia es generada por un inversor de puente completo que integra MOSFETs de SiC. Este inversor también se encarga de regular el flujo de energía transmitida. La topología de puente completo también se utiliza para el rectificador secundario, que está compuesto por diodos de SiC para reducir las pérdidas.

Otro desafío a la hora de implementar un prototipo en un sistema real radica en la batería de la bicicleta. En las configuraciones de laboratorio, se utiliza una resistencia que mantiene su valor constante para emular la batería. Sin embargo, el comportamiento de las baterías evoluciona durante el proceso de carga, es decir, a medida que aumenta el estado de carga (SOC). Este efecto debe ser considerado por el sistema de control. Para ello, se ha implementado un algoritmo de carga corriente constante-tensión constante simple pero robusto, que establece la corriente de carga de la batería en 2 A hasta que se alcanza la tensión máxima de la batería (42 V). Cuando esto sucede, la corriente de carga se regula para evitar que la tensión supere el valor máximo.

Los resultados experimentales han demostrado que la posición de las bobinas afecta en gran medida a la eficiencia del sistema, obteniendo un 92 % cuando está en la posición C frente a aproximadamente el 80 % alcanzado en las otras dos posiciones. También se ha validado el proceso de carga, regulado por el control corriente constante-tensión constante. Se ha observado que la eficiencia disminuye cuando aumenta el SOC de la batería. Estos resultados concluyen que tanto la posición de la bobina como el algoritmo de control deben seleccionarse cuidadosamente durante el proceso de diseño en prototipos reales porque afectan a la eficiencia y, por tanto, a la viabilidad de un cargador inalámbrico.

#### **Contribución 4**

Existe un amplio número de estrategias de control para cargadores inalámbricos de VEs disponibles en la bibliografía. Su objetivo principal es ajustar la potencia de carga o maximizar la eficiencia. Sin embargo, el desarrollo de este trabajo permitió observar la necesidad de diseñar y desarrollar un control que combine el objetivo de regular la potencia de salida y proteger los componentes del sistema. En un prototipo real, los condensadores y bobinas deben estar sujetos a restricciones de corriente y tensión, ya que pueden dañarse o destruirse si se exceden los límites del fabricante. Aunque estas restricciones pueden ser consideradas en el proceso de diseño y configuración específica, el funcionamiento real de los cargadores inalámbricos EV puede conducir a un aumento en la tensión y/o corriente. Este problema surge en particular cuando el cargador no funciona con los parámetros nominales considerados en el proceso de diseño. Tres eventualidades principales pueden causar esto: (i) desalineamiento de la bobina; (ii) diferentes valores de resistencia equivalente de la batería; y (iii) una frecuencia de operación diferente a la nominal. Dado que la frecuencia está limitada por regulaciones y las variaciones en la resistencia equivalente son reducidas, el desalineamiento de las bobinas es la contingencia que afecta principalmente a la desviación de las variables del sistema. Además,

el desalineamiento de la bobina es común tanto en la carga estática como en la dinámica, con desplazamientos horizontales y/o verticales.

Esta contribución incluye el diseño y desarrollo de un sistema de control con la capacidad de regular la potencia de carga y operar el sistema en un rango adecuado de valores para las variables eléctricas. El control también está adaptado a las especificaciones definidas en el estándar internacional SAE J2954.

El control está respaldado por un modelo teórico de los efectos del desalineamiento en un sistema con compensación SS. La formulación completa se puede encontrar en el documento publicado. Este modelo está validado en MATLAB para facilitar el análisis del rendimiento del sistema para múltiples variaciones de la inductancia mutua (causadas por desalineamiento). Este análisis se realiza con desalineamiento tanto vertical como horizontal, para lo que se utilizan valores reales de inductancia mutua medidos en laboratorio. Los resultados de este estudio muestran un aumento en la corriente que fluye a través de la bobina primaria para todos los casos de desalineamiento horizontal, mientras que los desalineamientos verticales aumentan la corriente solo cuando aumenta la distancia entre bobinas.

Los resultados obtenidos en el análisis confirman la necesidad de controlar la corriente en el lado primario del cargador para limitar su valor. Por esta razón, se ha propuesto un control que regula la potencia de carga de la batería y limita la corriente que fluye por el lado primario utilizando la técnica de cambio de fase. El controlador principal está ubicado en el lado primario del cargador y es responsable de aplicar la estrategia de control, así como de medir la corriente que fluye a través del lado primario. Como la estrategia de control requiere mediciones en el lado secundario, es necesario instalar un controlador auxiliar en ese lado, que mide la corriente de carga y el voltaje de la batería y envía la información al controlador principal. Esta propuesta incluye un sistema compuesto por dos controladores PI, en el que uno compara la potencia de carga medida con la potencia de referencia, mientras que el segundo controlador limita la corriente máxima que fluye por el lado primario. La salida de este sistema regula el ángulo de desplazamiento de fase, que posteriormente se envía a un generador de señal encargado de activar los MOSFETs del inversor primario.

La principal dificultad de este controlador radica en la puesta a punto de sus parámetros, ya que una actuación excesivamente rápida por parte de uno de ellos puede provocar que el sistema se comporte de forma inestable. Este problema se ve agravado por los retrasos en la conversión analógica-digital de la medida y en la comunicación entre los lados primario y secundario. Los parámetros de configuración se han establecido cuidadosamente para que el sistema regule un desalineamiento repentino entre bobinas en un tiempo inferior al segundo.

El control finalmente ha sido validado en el laboratorio. Su implementación se ha realizado en una placa principal Intel Edison que trabaja de forma coordinada utilizando tecnología Bluetooth con una placa auxiliar Intel Edison que se encarga de las medidas. Las pruebas verifican las conclusiones

derivadas del análisis teórico, mostrando un aumento de la corriente primaria cuando se producen desalineamientos. El control funciona correctamente y en un tiempo razonable para limitar valores superiores a los máximos recomendados. A pesar de los resultados satisfactorios, la técnica de desplazamiento de fase produce una ligera disminución en la eficiencia del sistema debido a la inclusión de armónicos adicionales.

### **Contribución 5**

Los cargadores inalámbricos son menos competitivos que los cargadores conductivos en términos de eficiencia. Por esta razón, uno de los principales objetivos es maximizar la eficiencia de estos cargadores. Tanto el hilo de Litz como los semiconductores de SiC ayudan a mejorar la eficiencia. Sin embargo, se pueden lograr valores de eficiencia más altos ajustando los parámetros de operación de estos sistemas.

El objetivo de este trabajo es maximizar la eficiencia en cargadores inalámbricos magnético resonantes al reducir las pérdidas en bobinas y electrónica de potencia. Esta no es una tarea pequeña ya que las pérdidas están fuertemente relacionadas con el modo de operación de los convertidores de potencia.

Así, el desarrollo de este trabajo comienza con un análisis exhaustivo de las pérdidas en el sistema que no están relacionadas con el factor de acoplamiento entre ambas bobinas. En este punto, no solo es importante calcular las pérdidas, sino identificar qué parámetros operativos del sistema impactan en la magnitud de las pérdidas en cada componente. Además, las pérdidas en un cargador inalámbrico dependen de la topología del sistema. Este estudio se basa en una topología serie-serie.

Al realizar un análisis de mallas, se puede deducir que la frecuencia de operación y la resistencia equivalente de la batería son los dos parámetros que tienen el mayor impacto en la eficiencia. El primer parámetro controla si el sistema está funcionando en resonancia o no. Su importancia está principalmente relacionada con la tolerancia de fabricación, es decir, la falta de precisión en la fabricación de las bobinas y los condensadores, provocando que el factor de potencia en el circuito sea menor que la unidad. El segundo parámetro impacta en las corrientes que circulan por los lados primario y secundario del cargador, afectando de forma directa en la eficiencia del sistema.

El análisis teórico concluye que la curva correspondiente a una frecuencia de operación de 82 kHz (límite inferior del rango permitido en SAE J2954) alcanza el valor de eficiencia más alto con una resistencia equivalente de 7  $\Omega$  para un sistema con las mismas características que el prototipo del laboratorio. Los valores máximos de eficiencia disminuyen a medida que aumenta la frecuencia de funcionamiento del sistema, mientras que estos máximos se alcanzan con valores de resistencia equivalente ligeramente superiores. En el rango analizado se consiguen mejoras de eficiencia de hasta un 6 %.

Por tanto, un control de máxima eficiencia debe determinar la perfecta sintonía de ambos parámetros, además de proporcionar capacidad para regular la potencia de carga. Controlar estos parámetros simultáneamente requiere actuar en ambos lados del cargador, ya que la frecuencia de operación se regula

en el inversor primario y la resistencia equivalente en el lado secundario, ya sea por un rectificador controlado o un convertidor CC/CC. La potencia de carga se puede ajustar mediante la técnica de desplazamiento de fase en el inversor principal. Esto hace que las comunicaciones sean esenciales en este tipo de control si se permite la desalineación.

La bibliografía incluye múltiples controles que persiguen el objetivo de máxima eficiencia. La técnica de control más utilizada para este propósito en la literatura se basa en el seguimiento del punto de máxima eficiencia (MEPT), en el que el controlador realiza pequeñas variaciones en los parámetros de control y verifica las mejoras en la eficiencia. Sin embargo, los controladores MEPT requieren tiempos de respuesta altos y pueden controlar dos parámetros de control como máximo, como la potencia de carga y la resistencia equivalente de la batería, o la potencia de carga y la frecuencia. Esta restricción reduce la capacidad del sistema para alcanzar la eficiencia óptima con la entrega de potencia deseada.

Los controles predictivos basados en modelo (MPC) permiten abordar la configuración de todas las variables de control (los parámetros de configuración de los convertidores de potencia) simultáneamente. Esto se realiza con tiempos de respuesta y cálculo reducidos. Para implementar un MPC correcto, se requiere un modelo preciso para predecir el comportamiento de las variables del sistema cuando se cambian los parámetros de configuración. Este modelo está definido por cuatro ecuaciones para la parte real e imaginaria de los lados primario y secundario. Las ecuaciones derivan de un análisis basado en mallas.

La inductancia mutua es un parámetro fundamental del modelo, por lo que el prototipo debe medirlo en tiempo real porque puede verse afectado por varios factores, como el desalineamiento de las bobinas. Para lograr una implementación factible, este parámetro se estima utilizando las medidas de corriente primaria y tensión secundaria en circuito abierto.

Los valores óptimos para las variables de control se calculan con una herramienta de optimización que utiliza la eficiencia como función objetivo. Además de las pérdidas consideradas en el análisis teórico anterior, el modelo utilizado para la optimización también incluye las pérdidas de los convertidores de potencia, es decir, pérdidas en diodos y MOSFET. Las pérdidas de los diodos corresponden a las pérdidas en el rectificador secundario y su cálculo se basa en su resistencia dinámica. Además, las pérdidas de los MOSFETs corresponden a las pérdidas en el inversor primario y están relacionadas con pérdidas de conducción, conmutación, ciclo de trabajo y snubbers.

Usando el modelo del sistema, sus pérdidas correspondientes, las restricciones operativas y la función objetivo, el algoritmo de optimización proporciona los valores óptimos para la frecuencia de operación, el desplazamiento de fase del inversor y el ciclo de trabajo del convertidor CC/CC secundario. Si no es posible alcanzar la potencia de carga establecida con el valor máximo de eficiencia, el algoritmo opta por reducir esta eficiencia para garantizar la potencia de carga.

La eficacia del MPC propuesto se ha validado en el prototipo de laborato-

rio. Esta tarea se ha llevado a cabo midiendo la eficiencia del cargador en diferentes situaciones de funcionamiento y comparando los resultados con los proporcionados por otros controladores basados en una única variable de control. La comparación muestra una mejor eficiencia no solo en situaciones ideales sino también cuando ocurren desalineaciones. El control propuesto consigue aumentar la eficiencia hasta en un 5 % en comparación con otros controladores.

**Palabras clave:** vehículos eléctricos, carga inalámbrica, transferencia magnético-resonante, control predictivo, máxima eficiencia



# Acknowledgements

---

This work is dedicated to my two grandfathers, who are no longer with us but who would surely be very proud of their grandson. Also to my three-year-old nephew Pablo, the youngest member of the family and the one who teaches us to live our lives with hope.

First and foremost, I must thank my Thesis Directors, José Antonio Aguado Sánchez and Alicia Triviño Cabrera, for all the help they have given me over the years. Without them, none of this would have been possible. The time we have shared has also allowed us to establish a friendship that I hope will last for many more years.

My family has also been a fundamental part of this work. It is wonderful to have a mother who is always there when you are most overwhelmed, a sister who helps you in any way she can (even if it means accompanying you to the lab), a father who cares about you, and a brother-in-law who organizes good sushi and movie nights to clear your head.

I cannot thank all my friends individually because they are too numerous. I hope, however, that they all know how important they are to me and that I need them to keep me going through both good and bad times.

Lastly, I would like to thank my colleagues from the university for their encouragement and collaboration. In particular, these include Pedro, a laboratory technician, who is always ready to help and make you smile, and Sebastián, with whom I have worked closely and shared some great moments.





# Contents

---

<b>1</b>	<b>Introduction</b>	<b>1</b>
1.1	Motivation . . . . .	3
1.2	Objectives . . . . .	6
1.3	Contributions . . . . .	7
1.4	Structure of the document . . . . .	9
<b>2</b>	<b>Electric vehicle wireless charging</b>	<b>11</b>
2.1	Wireless power transfer . . . . .	13
2.1.1	Inductive power transfer . . . . .	14
2.1.2	Magnetic resonance power transfer . . . . .	16
2.1.3	Strongly coupled magnetic resonance power transfer . . . . .	17
2.1.4	Capacitive power transfer . . . . .	18
2.1.5	Microwave power transfer . . . . .	20
2.1.6	Optical power transfer . . . . .	21
2.1.7	Application to electric vehicles . . . . .	22
2.2	Design of magnetic-resonance chargers . . . . .	22
2.2.1	Coils . . . . .	23
2.2.2	Compensation networks . . . . .	25
2.2.3	Misalignment . . . . .	27
2.2.4	Design procedure . . . . .	28
2.3	Power electronics in WPT . . . . .	29
2.3.1	Grid rectifier . . . . .	32
2.3.2	Primary inverter . . . . .	34
2.3.3	Secondary rectifier . . . . .	35
2.3.4	Secondary DC/DC converter . . . . .	36
2.4	Control in WPT . . . . .	38
2.4.1	Primary-side control . . . . .	38
2.4.2	Secondary-side control . . . . .	44
2.4.3	Dual-side control . . . . .	46
2.4.4	Control summary . . . . .	48

2.5	Standards for EV wireless chargers . . . . .	50
2.6	Market perspectives . . . . .	53
<b>3</b>	<b>Contributions</b>	<b>57</b>
3.1	Analytical characterisation of magnetic field generated by ICPT wireless charger . . . . .	59
3.2	A hybrid charger of conductive and inductive modes for electric vehicles .	63
3.3	Design and implementation of a cost-effective wireless charger for an electric bicycle . . . . .	79
3.4	Design and validation of a control algorithm for a SAE J2954-compliant wireless charger to guarantee the operational electrical constraints . . . . .	96
3.5	Model predictive control to maximize the efficiency in EV wireless chargers	115
<b>4</b>	<b>Conclusions and future work</b>	<b>129</b>
4.1	Conclusions . . . . .	131
4.2	Future work . . . . .	132
	<b>Bibliography</b>	<b>135</b>

# List of Figures

---

1.1	Global electric car stock, 2010-2019. . . . .	3
1.2	Future prospects for global electric car stock. . . . .	4
1.3	Developmental stages of the Thesis. . . . .	7
2.1	Generic diagram of WPT. . . . .	13
2.2	Illustration of the magnetic field generated by a coil passing through a secondary coil. . . . .	15
2.3	Generic diagram for inductive wireless chargers. . . . .	15
2.4	Generic diagram for magnetic resonant wireless chargers. . . . .	17
2.5	Generic diagram for a four-coil strongly coupled magnetic resonance system. . . . .	17
2.6	Generic diagram for capacitive wireless chargers. . . . .	19
2.7	Compensation topologies for capacitive WPT. . . . .	19
2.8	Generic diagram for microwave wireless chargers. . . . .	20
2.9	Generic diagram for optical power transfer systems. . . . .	21
2.10	WPT operation modes. . . . .	23
2.11	Generic flowchart for the design of a magnetic-resonance charger. . . . .	24
2.12	Mono-resonant compensation topologies. . . . .	26
2.13	Multi-resonant compensation topologies. . . . .	27
2.14	Effects of horizontal misalignment in both axes and a distance between the coils of 0.25 m. . . . .	28
2.15	Flowchart of the iterative algorithm used to design the coils and the compensation system. . . . .	30
2.16	Generic structure of a magnetic resonance wireless charger. . . . .	31
2.17	Power/operating frequency regions of the main controllable semiconductor devices. . . . .	32
2.18	Topology of a full-bridge inverter. . . . .	34
2.19	Comparison between battery resistance and equivalent resistance. . . . .	36
2.20	Single-phase active rectifiers. . . . .	37
2.21	CC/CV battery charging process. . . . .	40
2.22	Classification of controls according to the converter they operate. . . . .	40

---

2.23	Operation of phase-shifting technique in a full-bridge inverter. . . . .	42
2.24	Voltages in a full-bridge inverter with an square-wave activation and phase-shifting. . . . .	42
3.1	Proposed concept of inductive and conductive EV hybrid charger. . . . .	64
3.2	The proposed hybrid charger with inductive mode configuration. . . . .	64
3.3	Picture of e-bike wireless charger prototype. . . . .	79
3.4	Model of the magnetic coupling of the e-bike and the surrounding interfering materials. . . . .	80
3.5	Tested positions of the secondary coils. . . . .	81
3.6	Proposed prototype and control schemes. . . . .	81
3.7	Scheme of the proposed control system. . . . .	97
3.8	Generic diagram for magnetic resonance wireless chargers with SS compensation networks. . . . .	115
3.9	Efficiency as a function of $R_{eq}$ and frequency. . . . .	116

# List of Tables

---

1.1	Charging modes according to IEC 61851-1. . . . .	5
1.2	List of contributions and relationship with objectives. . . . .	7
1.2	List of contributions and relationship with objectives (continued) . . . . .	8
1.2	List of contributions and relationship with objectives (continued) . . . . .	9
2.1	Capacitor values and AC efficiency for mono-resonant compensation topologies. . . . .	26
2.2	Common DC/DC converters and the relationship between the input and output voltage. . . . .	39
2.3	Control strategies summary. . . . .	48
2.3	Control strategies summary (continued) . . . . .	49
2.4	WPT power classifications for light-duty vehicles. . . . .	50
2.5	Interoperability by Power Class. . . . .	51
2.6	Positioning tolerance requirements for Test Stand VAs and Product VAs. . . . .	51
2.7	Electromagnetic restrictions set by ICNIRP in the 3 kHz-10 MHz range. . . . .	52
3.1	Comparison of the efficiency under different $M$ values. . . . .	118



# List of acronyms

---

<b>AC</b>	Alternating Current
<b>BMS</b>	Battery Management System
<b>CAGR</b>	Compound Annual Growth Rate
<b>CC</b>	Constant Current
<b>CC-CV</b>	Constant Current-Constant Voltage
<b>CV</b>	Constant Voltage
<b>DC</b>	Direct Current
<b>DoD</b>	Depth of Discharge
<b>EV</b>	Electric Vehicle
<b>ICNIRP</b>	International Commission on Non-Ionizing Radiation Protection
<b>ICPT</b>	Inductively Coupled Power Transfer
<b>IEC</b>	International Electrotechnical Commission
<b>ISO</b>	International Organization for Standardization
<b>MEPT</b>	Maximum Efficiency Point Tracking
<b>MPC</b>	Model Predictive Control
<b>MPPT</b>	Maximum Power Point Tracking
<b>MPT</b>	Microwave Power Transfer
<b>OCC-PD</b>	One Cycle Control and Proportional Differential
<b>PDM</b>	Pulse Density Modulation

<b>PFC</b>	Power Factor Correction
<b>PID</b>	Proportional–Integral–Derivative
<b>PLL</b>	Phase Locked Loop
<b>PP</b>	Parallel-Parallel
<b>PS</b>	Parallel-Series
<b>PWM</b>	Pulse-Width Modulation
<b>RFID</b>	Radio Frequency Identification
<b>SAE</b>	Society of Automotive Engineers
<b>SCMR</b>	Strongly Coupled Magnetic Resonance
<b>SEPIC</b>	Single-Ended Primary-Inductor Converter
<b>SiC</b>	Silicon Carbide
<b>SOC</b>	State-Of-Charge
<b>SP</b>	Series-Parallel
<b>SS</b>	Series-Series
<b>V2G</b>	Vehicle-to-Grid
<b>VA</b>	Vehicle Assembly
<b>WBG</b>	Wide BandGap
<b>WPT</b>	Wireless Power Transfer
<b>ZPA</b>	Zero Phase Angle
<b>ZVS</b>	Zero Voltage Switching



# List of symbols

---

Symbol	Description	Unit
$\bar{A}$	Magnetic potential vector	V·s/m
$\bar{B}_s$	Magnetic field	T
$C_1$	Primary side capacitor	F
$C_2$	Secondary side capacitor	F
$D$	Duty cycle	-
$e_{ind}$	Induced voltage	V
$f$	Frequency	Hz
$\bar{H}$	Magnetic field intensity	A/m
$I_1$	Primary coil current	A
$I_2$	Secondary coil current	A
$I_L$	Load current	A
$I_P$	Primary current	A
$K_{DT}$	Coupling coefficient between the driver and the transmitter	-
$K_{TR}$	Coupling coefficient between the transmitter and the receiver	-
$K_{RL}$	Coupling coefficient between the receiver and the load	-
$L_1$	Primary coil self-inductance	H
$L_2$	Secondary coil self-inductance	H
$L_3$	Surrounding conductive material self-inductance	H
$\lambda$	Wavelength	nm
$L_{DEV}$	Maximum dimension of the emitter	m
$M$	Mutual inductance	H

<b>Symbol</b>	<b>Description</b>	<b>Unit</b>
$N_1$	Number of turns of primary coil	-
$N_2$	Number of turns of secondary coil	-
$\omega$	Angular frequency	rad/s
$\phi$	Magnetic flux	Wb
$q_1$	Primary coil quality factor	-
$q_2$	Secondary coil quality factor	-
$R_1$	Primary coil resistance	$\Omega$
$R_2$	Secondary coil resistance	$\Omega$
$R_3$	Surrounding conductive material resistance	$\Omega$
$R_{eq}$	Battery equivalent resistance	$\Omega$
$R_L$	Load resistance or battery resistance	$\Omega$
$t_{charge}$	Charging time	s
$V_{DC}$	DC-link voltage	V
$V_{in}$	Input voltage	V
$V_{out}$	Output voltage	V
$V_P$	Primary voltage	V

# Chapter 1

## Introduction

---

This first chapter of the Thesis introduces the reader to the work carried out by the author throughout the doctoral program. The motivation for developing this work is presented in the first section, which analyses the evolution of the EV market and its growth expectations. The main problem of these vehicles - i.e. their autonomy - is also studied in this section and wireless charging is proposed as a solution to this problem.

The chapter also presents the objectives of this Thesis and associates them with the corresponding publication.

Finally, the organization of the document is described in order to guide the reader through the Thesis.



## 1.1 Motivation

In a world committed to the objectives of the Paris Agreement [1], it is becoming increasingly important to generate renewable energy and reduce greenhouse gas emissions. Electric Vehicles (EVs) are foreseen as the transportation of the future as they position themselves as the main alternative to internal combustion vehicles. This is particularly significant when we consider that CO<sub>2</sub> emissions in the transport sector in 2018 reached 24.6% of total emissions and 74% of these emissions were derived from road transport [2].

The introduction of EVs on the market began in 2010, with almost negligible sales of 17,000 vehicles worldwide. The sector did not start to take off until the 2015-2019 period, with an annual average increase of 60%. In 2019, a global stock of over 7 million units was reached [3]. China stands out as the main consumer, followed by Europe and the USA.

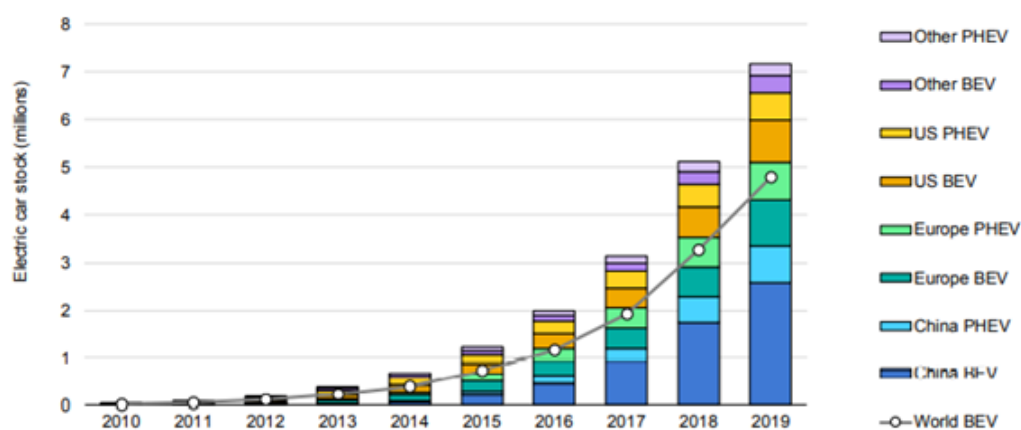


**Figure 1.1:** Global electric car stock, 2010-2019 [3].

At present, the figure is not particularly significant due to several factors. The main limitations include the price of the vehicles, their limited autonomy and the lack of an extensive infrastructure of chargers to facilitate charging. However, future forecasts are extremely promising because governments seem determined to invest in this technology. Indeed, they are providing purchasing incentives [4] and establishing regulations that penalize the pollution of traditional vehicles, such as the Euro 7 standard [5].

Despite the higher cost of EVs, they provide economic advantages to owners since they receive tax benefits [4]; in addition, the cost per kilometer is lower [6] and it possible to take greater advantage of users' self-consumption facilities. As shown in Figure 1.2, the global fleet of EVs is expected to exceed 50 million units by 2025 if stated policies are maintained. If sustainability continues to be promoted, we will achieve the most optimistic scenario in which nearly 250 million vehicles will be operative by 2030.

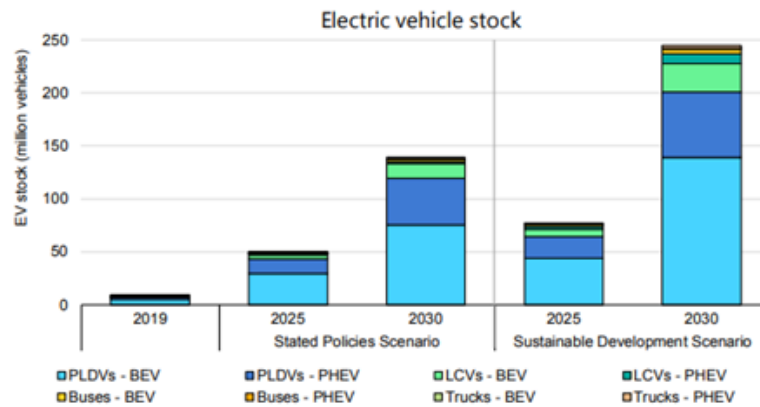


**Figure 1.2:** Future prospects for global electric car stock [3].

However, the factor that is undoubtedly the main concern of potential EV users is their autonomy [7, 8]. The autonomy of these vehicles depends on the battery and on the vehicle's consumption. The use of a battery with a higher capacity helps to improve the vehicle's autonomy, but it reduces the useful volume of the vehicle and increases its weight, with the consequent increase in consumption. The evolution of storage technology has improved battery energy density and this advance has resulted in vehicles on the market with an autonomy greater than 500 km (i.e. some models by Tesla, Audi, Mercedes and BMW).

One of the main ways to improve EVs' limited autonomy is by providing advanced charging technologies. The charging modes are classified mainly according to two international standards: SAE J1772 [9] and IEC 61851-1 [10]. In Europe, the predominant standard is IEC-61851-1, which classifies the charging in four modes, three of which operate with Alternating Current (AC) and one uses Direct Current (DC). AC chargers include the power electronics in the vehicle, which is why they are known as on-board chargers. This is the technology mainly used in the domestic sphere, in which mode 1 stands out with powers of up to 3.7 kW in single phase. This power level gives a range of 5 km per 15-minute charge. The highest charging speed is achieved with mode 4, in which the process is performed in DC. Specifically, an off-board system including all the power electronics is used. Currently, the most powerful commercial chargers reach a power level of up to 150 kW, which allows a range of 200 km per 15-minute charge. It is forecast that 250-kW chargers will be available in the near future.

However, ultra-fast chargers also have some drawbacks. Their charging power is directly related to the power extracted from the grid. Specific installations may be required, which is why these chargers have high associated fixed costs. Moreover, ultra-fast charging impacts on the lifespan of the batteries. Battery degradation depends on both the C-rate of the battery and the Depth of Discharge (DoD) of the batteries [11].

**Table 1.1:** Charging modes according to IEC 61851-1 [10].

Charging mode	Charging type	Maximum current	Maximum power	Charging time for 50 kWh	Kilometers from a 15 min charge <sup>1</sup>
<b>Mode 1</b>	Slow	16 A, AC Single-Phase	3.7 kW	14 h	5 km
<b>Mode 2</b>	Fast	32 A, AC Single-Phase	7.4 kW	7 h	9 km
		32 A, AC Three-Phase	22 kW	> 2 h	27 km
<b>Mode 3</b>	Rapid	62 A, AC Three-Phase	43 kW	> 1 h	54 km
<b>Mode 4</b>	Ultra-Rapid	400 A, DC	200 kW	15 min <sup>2</sup>	250 km <sup>2</sup>

<sup>1</sup> Using an average consumption of 0.20 kWh/km.

<sup>2</sup> Batteries cannot be fully charged at maximum power.

Wireless chargers are proposed as an alternative solution to conductive charging systems. Their main advantage is that handling by users is minimized. In addition, they reduce the safety concerns of conductive chargers as they are safe to use in rain or snow. Since cables are avoided, charging can be accomplished even on the move, which extends the scenarios in which EVs may be charged.

Although commercial-grade wireless EV chargers exist, technology in wireless chargers is currently in a developmental stage. Component design, control techniques and regulations are still works-in-progress. The design of wireless chargers is challenging due to the high operating frequency. This affects both the topology of the system and the materials used. Power electronics therefore play a crucial role, using new semiconductor materials which make it possible to reduce system losses during the switching. This results in greater efficiency, which makes them more competitive in relation to conductive chargers.

Control strategies are associated with power semiconductors, and are one of the main focuses of wireless technology development. In addition to regulating the charge of the batteries, they also implement secondary objectives such as maximizing the charging power or their efficiency, or easing their integration with conductive chargers. Hybrid chargers (combining conductive and wireless charger technology) are expected to attract consumers as they share components and, in turn, reduce costs.

Although some commercial EV wireless chargers do exist, all these considerations lay the foundations for the future development of advanced and effective prototypes of wireless

chargers.

## 1.2 Objectives

The main objective of this doctoral Thesis is to contribute to the development of EV wireless charging technology, specifically magnetic-resonant technology. The contributions cover several aspects, centred on the review of the state of art, the design and construction of experimental prototypes, and the implementation of novel charging strategies.

More specifically, the objectives of this Thesis are the following:

- 01.** Review of the state of art, which includes a general analysis of the different WPT technologies as well as a specific study of magnetic resonance technology. For this technology, it will be necessary to carry out a review of the components, the electromagnetic field, the losses, the control strategies and the international regulations in place.
- 02.** Design and development of a laboratory prototype adapted to the international standard SAE J2954 [12]. The prototype will integrate Silicon Carbide (SiC) technology in power electronics. The prototype will be used to verify some theoretical analyses such as the performance of the system and the characterization of losses with variations of nominal parameters, such as misalignment, operating frequency or equivalent resistance of the battery.
- 03.** Design, implementation and evaluation of a wireless charger and its control algorithm for a low-cost commercial EV. The process will include the design of the coils, the compensation system, the power electronics and the charging control. The evaluation will be oriented to analyse the impact of the surrounding interfering materials, which are present in real EVs.
- 04.** Design and implementation of a hybrid charger to facilitate the transition between conductive and magnetic resonance chargers. These types of chargers share the power electronics, reducing implementation costs and volume.
- 05.** Design, development and evaluation of a maximum efficiency control algorithm based on a Model Predictive Control (MPC) to improve the performance of wireless chargers.



## 1.3 Contributions

Figure 1.3 summarizes the main contributions that underpin this Thesis. The first stage consists in reviewing the state of art, i.e. the study of WPT technologies, the topologies of wireless chargers, their control strategies and the international standards that govern these systems. As a second stage, the work described in the Thesis has focused on fulfilling the other objectives.

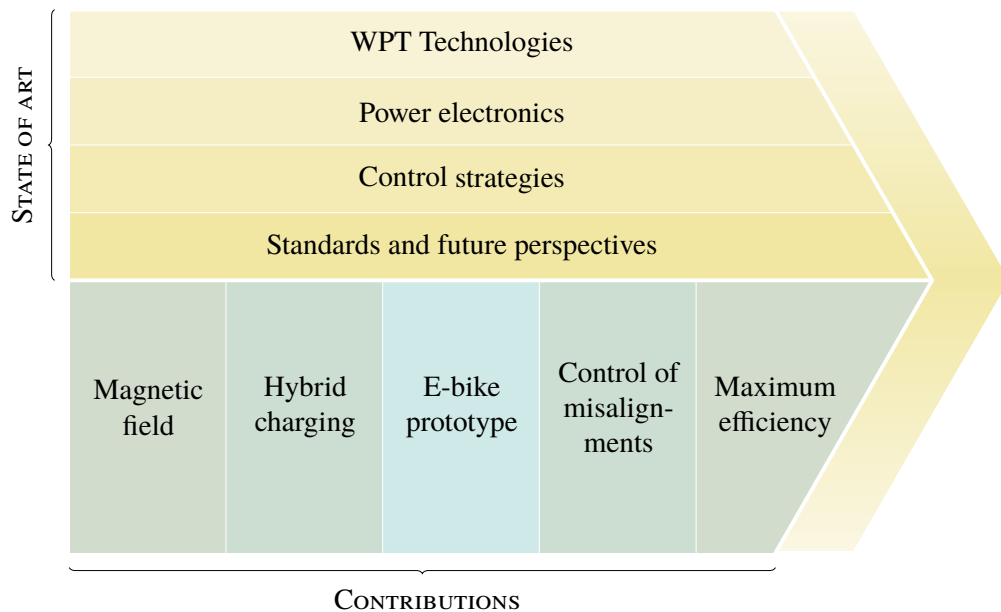


**Figure 1.3:** Developmental stages of the Thesis.

The objectives proposed for this Thesis are part of a research process, in which each one is the basis for the others. The fulfillment of some of these objectives has given rise to relevant publications or else has indirectly contributed to their development. Table 1.2 presents a list of contributions and their relationship with the objectives of this Thesis.

**Table 1.2:** List of contributions and relationship with objectives.

Contribution	Objective
A. Triviño-Cabrera, J. M. González-González, and J. A. Aguado, <i>Wireless Power Transfer for Electric Vehicles: Foundations and Design Approach</i> , Cham: Springer International Publishing, 2020. <b>Book.</b>	O1
Continued on the next page	

**Table 1.2:** List of contributions and relationship with objectives (continued)

Contribution	Objective
A. Triviño, J. M. González-González, and J. A. Aguado, "Wireless Power Transfer Technologies Applied to Electric Vehicles: A Review," <i>Energies</i> , vol. 14, no. 6, p. 1547, Mar. 2021. doi: 10.3390/en14061547 <b>JCR Impact Factor (2019): 2.702 (Q3).</b>	O1
A. Triviño, J. M. González-González and J. A. Aguado, "Evaluation of losses in a bidirectional wireless power transfer system for electric vehicles," <i>2017 IEEE International Conference on Environment and Electrical Engineering and 2017 IEEE Industrial and Commercial Power Systems Europe (EEEIC / I&amp;CPS Europe)</i> , 2017, pp. 1-5, doi: 10.1109/EEEIC.2017.7977706. <b>International conference.</b>	O1, O2
A. Triviño, J. M. González-González and J. A. Aguado, "Theoretical analysis of the efficiency of a V2G wireless charger for Electric Vehicles," <i>Transactions on Environment and Electrical Engineering</i> , vol. 3, no.1, pp. 1-6, 2019. doi: 10.22149/tee.v3i1.118. <b>Non JCR indexed journal.</b>	O1, O2
A. Triviño-Cabrera, J. Aguado and J. González, "Analytical characterisation of magnetic field generated by ICPT wireless charger," <i>Electronic Letters</i> , vol. 53, pp. 871-873, 2017. doi: 10.1049/el.2017.0968. <b>JCR Impact Factor (2017): 1.232 (Q3).</b>	O1, O2
J. M. González González, D. Fernández Cabrera, A. Triviño Cabrera, J. A. Aguado Sánchez, "Power Factor Corrector Design applied to an 85-kHz Wireless Charger," <i>International Conference on Renewable Energies and Power Quality (ICREPQ'16)</i> , 2016, pp. 521-525. <b>International conference.</b>	O2
B. Vu, J. M. Gonzalez-Gonzalez, V. Pickert, M. Dahidah and A. Trivino, "A hybrid charger of conductive and inductive modes for Electric Vehicles," <i>IEEE Transactions on Industrial Electronics</i> , Early Access, 2020. doi: 10.1109/TIE.2020.3042162. <b>JCR Impact Factor (2019): 7.515 (Q1).</b>	O4

Continued on the next page

**Table 1.2:** List of contributions and relationship with objectives (continued)

Contribution	Objective
A. Triviño, J. M. González-González, and J. A. Aguado, "Design and implementation of a cost-effective wireless charger for an electric bicycle". <i>IEEE Access</i> <b>Accepted. Pending publication. JCR Impact Factor (2019): 3.745 (Q1).</b>	O3
J. M. González-González, A. Triviño-Cabrera and J. A. Aguado, "Control algorithm for wireless EV charger considering operational constraints of electrical components," <i>2017 11th IEEE International Conference on Compatibility, Power Electronics and Power Engineering (CPE-POWERENG)</i> , 2017, pp. 211-216, doi: 10.1109/CPE.2017.7915171. <b>International conference.</b>	O2
J.M. González-González, A. Triviño-Cabrera and J.A. Aguado, "Design and Validation of a Control Algorithm for a SAE J2954-Compliant Wireless Charger to Guarantee the Operational Electrical Constraints," <i>Energies</i> , vol. 11, no. 3, pp. 604, 2018. doi: 10.3390/en11030604. <b>JCR Impact Factor (2017): 2.707 (Q3).</b>	O2
J. M. Gonzalez-Gonzalez, A. Trivino and J. A. Aguado, "Model Predictive Control to Maximize the Efficiency in EV Wireless Chargers," <i>IEEE Transactions on Industrial Electronics</i> , Early Access, 2020. doi: 10.1109/TIE.2021.3057006. <b>JCR Impact Factor (2019): 7.515 (Q1).</b>	O2, O5

## 1.4 Structure of the document

The document is divided into four chapters. Their contents are summarized as follows:

- **Chapter 1.** This chapter introduces the reader to the motivations of the doctoral student to carry out this work. It also describes the proposed objectives for its development.
- **Chapter 2.** This chapter provides an in-depth review of the state of art, starting with the study of the most popular WPT technologies, and then focusing on the magnetic-resonant technology. This is the most popular technology for EVs. The analysis of this technology includes power electronics and control techniques developed in the

literature. Finally, a review of the existing regulations on wireless charging of EVs and the market prospects for this technology is included.

- **Chapter 3.** This chapter includes the author's contributions for the development of the proposed objectives. For each contribution, a summary is included in order to facilitate the reader's understanding of these contributions.
- **Chapter 4.** The final chapter includes the conclusions of this work and the future research lines.

## Chapter 2

# Electric vehicle wireless charging

---

This chapter begins by introducing the reader to the field of Wireless Power Transfer (WPT). First, it presents the most relevant technologies and, in some cases, their application to EVs. After this presentation and a discussion of magnetic resonant technology (the most popular technology in EV charging), we make a detailed analysis of the components that make the operation of these systems possible. We then study the different control techniques proposed in the literature. Finally, the chapter concludes with a review of the most relevant international standards and future market prospects.

The content presented is based on two relevant contributions in which the author has participated: a paper entitled "Wireless power transfer technologies applied to electric vehicles: a review", published in the journal *Energies* [13], and a book called *Wireless Power Transfer for Electric Vehicles: Foundations and Design Approach*, published in Springer [14].



## 2.1 Wireless power transfer

WPT is the technology by which it is possible to transmit power without cables through an electromagnetic field. In this technology, there is a transmitting element that converts the energy from a power supply and converts it into a time-varying electromagnetic field. This electromagnetic field is used by a receiver device, which converts it into electrical energy to power a load. The transfer is characterized by the maximum dimension of the transmitting element, the distance between the transmitter and the receiver, and the properties of the electromagnetic waves, i.e. their wavelength or their frequency. Figure 2.1 depicts a diagram of this process, where  $R_L$  is the load resistance or, in charging systems, the battery equivalent resistance.

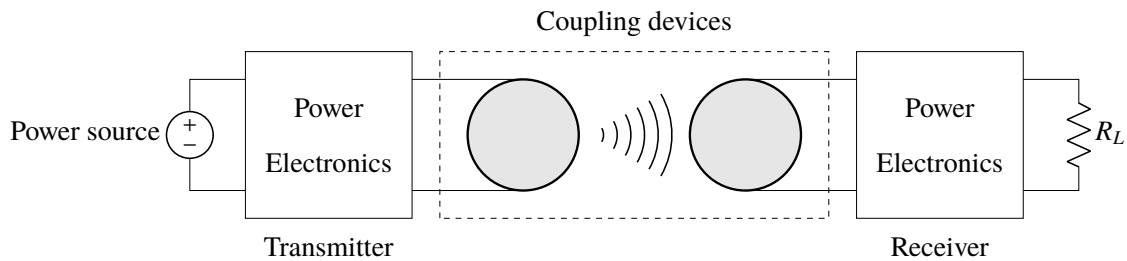


**Figure 2.1:** Generic diagram of WPT.

There are multiple technologies for WPT, the choice of which depends on the required use criteria. These criteria include:

- Transferred power
- Bidirectionality
- Gap
- Capability to work with misalignment
- Potential existence of intermediate objects
- Number of receivers
- Stationary/Mobile receiver

WPT technologies can be mainly classified into two techniques:

- **Near-field or non-radiative techniques.** Power is transmitted over short distances using a magnetic field (inductive coupling), or an electrical field (capacitive coupling). The conditions that are satisfied in these techniques are:

1. The maximum dimension of the emitter  $L_{DEV}$  is very small compared to the wavelength  $\lambda$ .
  2. The gap between the transmitter and the receiver is very small compared to the wavelength  $\lambda$ .
  3. The gap between the emitter and the receiver is very small compared to  $2 \cdot (L_{DEV}^2)/\lambda$ .
- **Far-field or radiative techniques.** Power is transmitted by means of electromagnetic radiation, such as microwaves or laser beams. In this case, the conditions are:
    1. The gap between the transmitter and the receiver is greater than the wavelength  $\lambda$ .
    2. The maximum dimension of the emitter  $L_{DEV}$  is more than 10 times greater than the wavelength  $\lambda$ .

### 2.1.1 Inductive power transfer

Inductive WPT is performed with the magnetic field of the electromagnetic wave. The operation principle is explained by the interaction of the magnetic and electrical behaviour described by Ampère's Law and Faraday's Law.

According to Ampère's Law, a current-carrying wire generates a magnetic field around it. The intensity of the magnetic field and its orientation depend on the topology of the wire. Specifically, Ampère's Law states that:

$$\oint \bar{H} \cdot dl = I \quad (2.1)$$

where  $\bar{H}$  is the magnetic field intensity of the magnetic field generated by the electric current  $I$  and  $dl$  is the differential element of length along the path on which the current travels.

As a consequence of this physical phenomenon, the frequency at which the intensity of the magnetic field varies is equal to the frequency of the current in the wire. Figure 2.2 illustrates the magnetic field of a common structure used in inductive wireless chargers.

As shown, coils are able to concentrate the magnetic field around the area in which they are defined to a higher degree than a simple wire.

If that time-varying magnetic field traverses a different coil, a voltage ( $e_{ind}$ ) is induced in its terminals. This effect is described by Faraday's Law as follows:

$$e_{ind} = -\frac{d\phi}{dt} \quad (2.2)$$



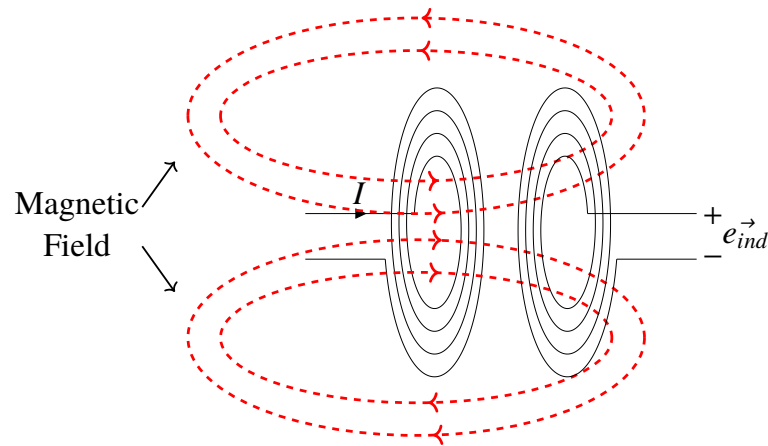


**Figure 2.2:** Illustration of the magnetic field generated by a coil passing through a secondary coil.

where  $\phi$  is the flux of the magnetic field passing in the area limited by the coil.

The combination of these two phenomena forms the basis of inductive and other magnetic-based WPT technologies. Inductive WPT technology requires a pair of coils referred to as the primary and secondary coils. This is presented as a diagram in Figure 2.3, where  $V_p$  is the primary voltage,  $I_p$  is the primary current,  $L_1$  and  $R_1$  are the self-inductance and resistance of the primary coil and  $L_2$  and  $R_2$  are the self-inductance and resistance of the secondary coil. In the primary coil, a time-varying current  $I_p$  must be produced by a generator. The magnetic field resulting from this must traverse the area of the secondary coil to which the load to be powered/charged ( $R_L$ ) is connected. There are usually intermediate electronic components positioned between the generator and the primary coil. Similarly, there are other electric systems between the secondary coil and the load. These additional elements are included to improve the WPT efficiency as explained next.

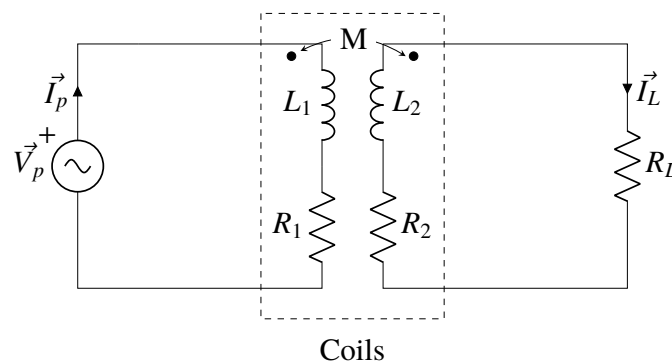


**Figure 2.3:** Generic diagram for inductive wireless chargers.

In general terms, we can state that the best approach is to produce an induced voltage that is as high as possible. As shown by Faraday's Law, the induced voltage is proportional to the rate of change of the flux traversing the secondary coil. This means that a coil

traversed by two magnetic fields with the same magnitude but different frequencies at two distinct moments will experience two different induced voltages. When the magnetic field passing through the coil is of the highest frequency, it will result in a higher induced voltage. Thus, the variation of magnetic flux in the secondary coil should preferably be as high as possible.

Thus, it is of interest for an inductive-based WPT to hold these two conditions:

- Most of the magnetic field generated by the primary coil traverses the secondary coil.
- The frequency of the magnetic field involved in the WPT is as high as possible while allowing for a near-field operation.

The first condition initially implies that large coils are preferable on the secondary side, but the application imposes some limits for this component in terms of size, weight and cost. This restriction is clearly observed in biomedical applications. With regard to EV applications, there is a limit to the size of the coils because of the structures in which the WPT components must be inserted and the cost of the materials. Please note that WPT for EVs is not supported by inductive WPT but by advanced technologies based on this kind of magnetic WPT.

Considering that inductive WPT also benefits from a higher rate of flux change, the main strategy for enhancing the WPT in inductive systems is to increase the frequency of the electrical current in the primary coil. This will lead to an increase in the frequency of the magnetic field and, consequently, the rate of flux change is also increased. Power converters are part of the magnetic-based WPT systems in order to elevate the operational frequency.

Radio Frequency Identification (RFID) [15] and Qi [16] are commercial technologies that are based on inductive WPT.

## 2.1.2 Magnetic resonance power transfer

One of the main problems of inductive WPT technology is its reduced efficiency due to the losses produced by the reactive energy that circulates through the system. Magnetic Resonance WPT technology solves this problem, since inductive systems are forced to work in resonance thanks to structures known as compensation networks. Figure 2.4 shows a diagram of a magnetic resonance WPT system, where  $I_1$  and  $I_2$  are the current flowing through the primary and secondary coils.

This technology is the most mature and widely used for wireless charging of EVs, so it is detailed in depth in the successive sections of this chapter.

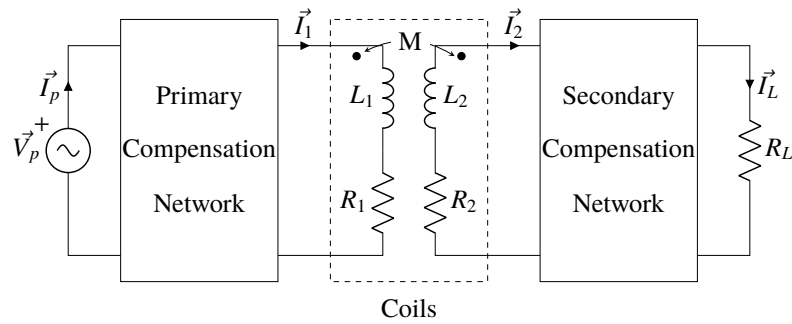


**Figure 2.4:** Generic diagram for magnetic resonant wireless chargers.

### 2.1.3 Strongly coupled magnetic resonance power transfer

Strongly Coupled Magnetic Resonance (SCMR), or WPT based on magnetically coupled resonance, is a variant of the magnetic resonance technology. It is mainly classified as mid-range WPT because the distance between the emitter and the receiver does not fit exactly in near-field or far-field operation.

The main properties of the most popular SCMR topology are the following [17]:

- **4-coil topology.** This topology is the most common configuration for SCMR circuits. It is composed of two coils in the power source (the driver and the transmitter) and two in the load (the receiver and the load). The driver and load coils are a simple loop. The four coils are connected by means of magnetic coupling. The structure of this topology is presented in Figure 2.5, where  $K_{DT}$  is the coupling coefficient between the driver and the transmitter,  $K_{TR}$  is the coupling coefficient between the transmitter and the receiver and  $K_{RL}$  is the coupling coefficient between the receiver and the load.

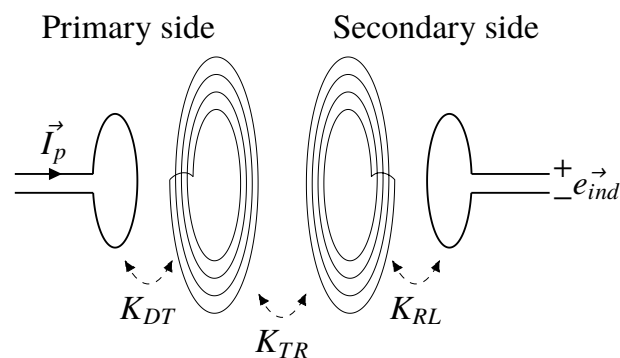


**Figure 2.5:** Generic diagram for a four-coil strongly coupled magnetic resonance system.

- **The intermediate coils are self-resonant.** The intermediate coils are designed in such a way that their parasitic capacitance makes them work in resonance. The resonant frequency is usually in the interval from 100 kHz to 20 MHz.
- **Compensation topologies in the driver and the load loops.** In this technology it is essential that the system operates in resonance, since the efficiency decreases drastically. Therefore, the driver and load coils include a matching network [18].

The control algorithms for this technology are designed considering two main objectives [19]: maximizing the power transfer in the load and the efficiency of this process. These goals can be achieved using various strategies: (i) adjusting the operational frequency; (ii) including regulable matching networks; and (iii) altering the distance between the driver and the transmitter coils. However, the application of these strategies can lead to bifurcation phenomena.

Some studies have also shown the effectiveness of this technology even with external objects [17], since this does not greatly affect the transmitted power as long as they are not too close to the transmitter or receiver. People and some materials such as aluminium have an effect on the resonant frequency, although this problem can be overcome with a suitable control strategy.

## 2.1.4 Capacitive power transfer

Capacitive WPT is another short-range technology with a topology similar to inductive technology but which transmits power through an electric field rather than a magnetic one. The electric field is created between two metallic plates located at the emitter and two others located at the receiver. Each of the emitter plates is located in parallel with a corresponding receiver plate, acting as electrodes (anode and cathode). In this way, there are two capacitors with a capacitance value in the range of picofarad [20] when the distance between them is close enough. Both capacitors are part of an electrical circuit and allow the current to flow from the emitter to the receiver (forward capacitor) and vice versa (return capacitor). Figure 2.6 shows a diagram of this technology.

In addition to this arrangement of the plates, there are other variants that provide additional advantages [21]. These include the Four-Plate Stacked structure [22], which is more compact and reduces the external capacitances, and the Six-Plate Stacked structure [23], which uses two large external plates that provide insulation, thereby reducing electric field emissions.

Compensation networks are also part of these chargers. The mono-resonant compensation topologies are coils, which may be connected in series or in parallel. We also

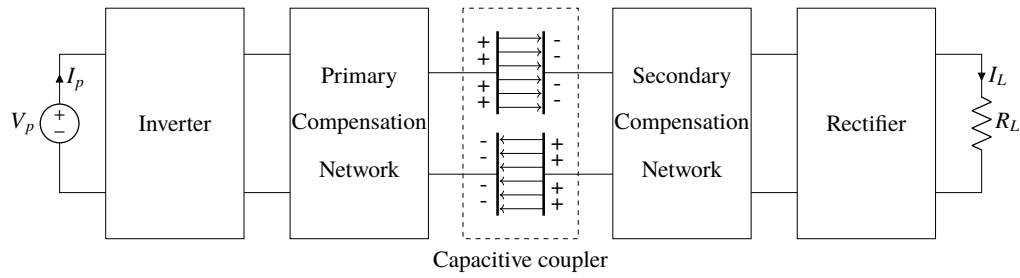


**Figure 2.6:** Generic diagram for capacitive wireless chargers.

find Series-Series (SS), Series-Parallel (SP), Parallel-Series (PS) or Parallel-Parallel (PP) structures, as with magnetic based chargers. With regard to multi-resonant compensation topologies, double-side LCL [22], double-side LCLC and double-side LC are the most popular in capacitive chargers [24]. These topologies are presented in Figure 2.7.

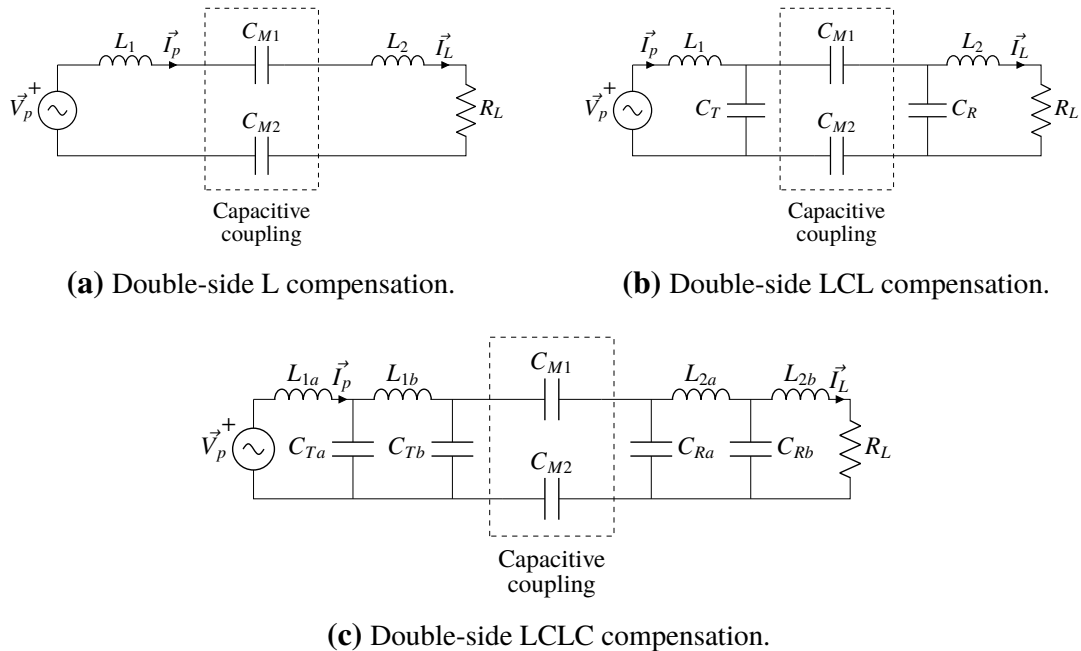


**Figure 2.7:** Compensation topologies for capacitive WPT.

The induced voltage on the secondary side is proportional to the rate of change of the electric field flux between the plates. In order to increase the transmitted power, it is also essential to operate the system at high frequencies, which is achieved through power electronics. The operating frequency is higher than the inductive one — in the order of MHz [22, 24, 25].

Capacitive wireless chargers were initially developed with low-power and low-gap applications in mind [26]. These capacities have improved as this technology has evolved, which currently allows us to find prototypes of several kilowatts and gaps of up to 300 mm with an efficiency greater than 85% [22, 24, 27]. Capacitive technology has also been

associated with inductive technology to improve power transmission capabilities [25, 28], using inductive charging for static applications and capacitive charging for dynamic ones.

The main advantages of capacitive WPT to charge an EV are:

- Limited electric emissions, because the magnetic field is restricted to the area comprising the plates.
- Non-relevant losses where transferring power with metallic barriers.
- Capacitive wireless chargers require aluminium plates, which is an inexpensive material and has good conductivity and low weight.

In contrast, the most relevant disadvantages for capacitive wireless chargers are:

- The limited space available under the vehicle, especially on bicycles and scooters, prevents bulky capacitors from being used.
- The vehicle produces parasitic capacitances, which affect the system's performance [20].

### 2.1.5 Microwave power transfer

Microwave Power Transfer (MPT) is a far-field WPT technology based on microwaves. Figure 2.8 presents a generic diagram of this technology. The generation of the microwave is performed by a magnetron, which is powered by a high-voltage DC source. This microwave is radiated by the transmitting antenna. The receiver uses a rectenna to convert the signal to DC, which finally powers a power electronics device. The operating frequency of these systems is in the GHz range.

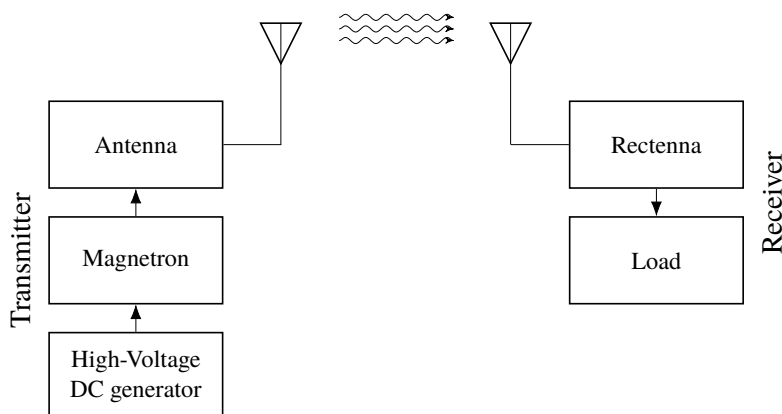


**Figure 2.8:** Generic diagram for microwave wireless chargers.

Some companies have developed products based on this technology [29, 30, 31], but its use is restricted to low-power devices. There are more powerful prototypes in the literature,

such as [32], in which the authors develop a system for an agricultural vehicle with 250 W and an efficiency of 44%, although this value is very sensitive to misalignment. Near-field technologies are more suitable solutions for charging land vehicles, but MPT technology enables charging at a greater distance and can be of interest for the aerospace field.

The main limitations of this technology in the EV context are:

- The transmitter and the receiver cannot be used to work bidirectionally, so Vehicle-to-Grid (V2G) operations require the system to be replicated.
- It requires bulky antennas for high-power devices, which restricts its applications.
- Lower efficiency than inductive and capacitive systems [33].

## 2.1.6 Optical power transfer

Optical WPT or laser power beaming systems is a far-field technology in which the power is transmitted with a laser beam and received with photovoltaic cells. A laser diode generates the optical wave in the transmitter, operating in the THz range. Figure 2.9 presents a generic diagram of an optical WPT.

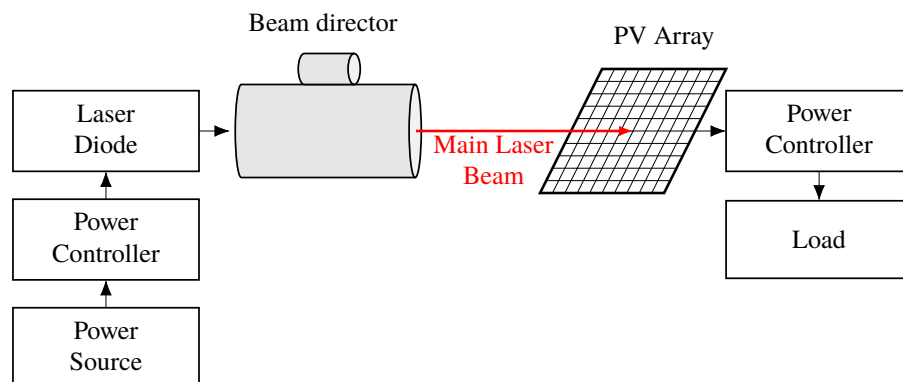


**Figure 2.9:** Generic diagram for optical power transfer systems.

This technology requires there to be no obstacle between the transmitter and the receiver. Furthermore, alignment is also an important factor in its operation, which is why a directing beam adjusts the direction of the laser. In addition to these difficulties, the optical WPT has a low efficiency (<25%) [34] and its operation carries potential risks for humans [35], which increase with the power level.

For low power applications, WPT optical systems (especially in the infrared region) are safe for use in domestic environments. Wi-Charge markets a system with this technology. The emitters have the capacity to transmit 250 mW at a distance greater than 5 meters [36]. For high power applications, PowerLight Technologies showed a prototype capable of transmitting 400 W of power through 325 meters with an efficiency of 20% [37].

### 2.1.7 Application to electric vehicles

In the field of EVs, wireless chargers have a series of advantages over conductive ones. These are:

- **No user intervention.** The vehicle starts charging without the need for the driver to connect it to a power source. The simplicity of this operation makes scheduling easier, which could result in notable advantages [38].
- **Increased safety.** Since user intervention is not required, contact risks are suppressed. This is especially relevant in the charging of EVs due to the high currents and voltages that are handled. Electromagnetic fields are not a health concern when the established limits are not exceeded. [39].
- **V2G.** Some of the WPT technologies support bidirectional power transmission, allowing the energy stored in vehicle batteries to be used to power an external load. This technology may acquire special relevance in the future by complementing self-consumption [40], since it can provide energy to consumption points in periods without generation, or by providing ancillary services to the grid [41].
- **On-the-move charging.** The absence of physical links allows other charging modes to exist in addition to static charging [42]. Thus, the charging modes are static, stationary and dynamic. Static charging is the traditional charging method, in which a vehicle parked in a parking space performs the charging process. Stationary charging is a mode similar to static, but charging is done in short periods of time. A specific example of this type of charging is stopping at traffic lights. Bus stops would also be included in this category: they are particularly relevant for these vehicles because it would be possible to charge multiple buses at the same stop, providing them with enough energy to complete one bus route. This type of charge reduces the size of the batteries and the consumption of the vehicle, which increases the useful space of the bus. Finally, dynamic charging provides the vehicle with power while driving. This technology presents a great challenge for the industry not only due to costs but also to misalignments and the drop in efficiency that this entails. Figure 2.10 represents the three charging modes.

## 2.2 Design of magnetic-resonance chargers

The design of a magnetic-resonance charger takes into account multiple requirements related to regulatory compliance, cost, efficiency and dimensions. These requirements are

---



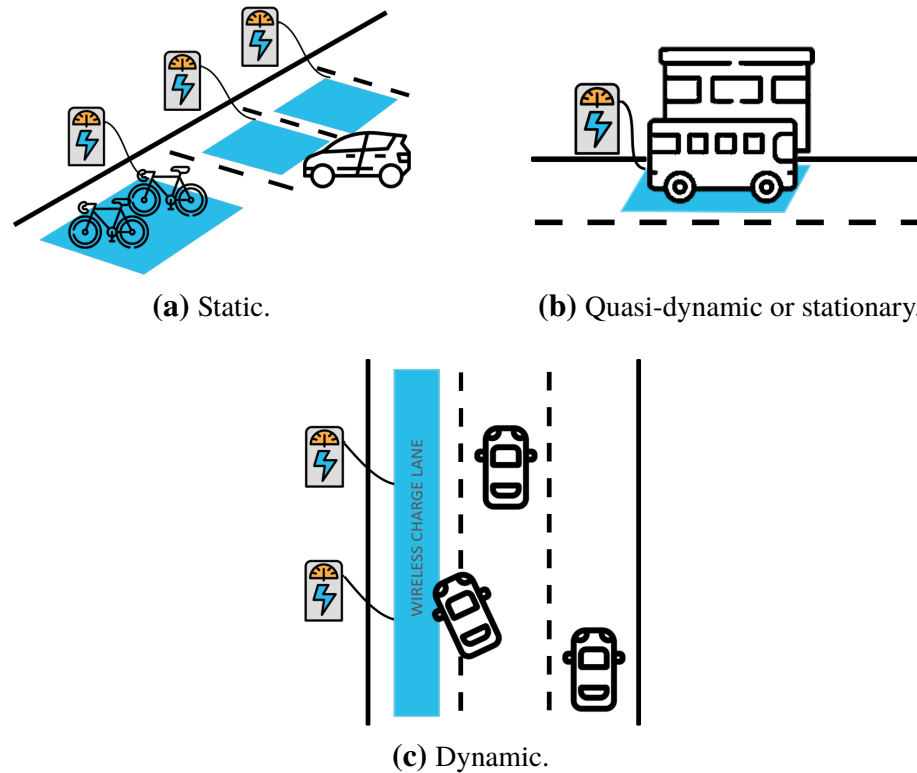


**Figure 2.10:** WPT operation modes.

considered together in a process that begins with the definition of the specifications, and continues with the design of the different components and the control system, the simulations, the implementation and the experimental tests. Figure 2.11 shows a generic flowchart of the design process of a WPT system.

This section analyses the coils and the compensation system as the core of a magnetic-resonance charger, as well as the process required to correctly design these components.

## 2.2.1 Coils

Coils are a fundamental part of resonant magnetic chargers. Their function is to transmit power from the primary side, whose coil is located on the ground, to the secondary side, located on the underside of the vehicle, through an air gap coupling.

The behaviour of the coils is mainly related to the geometry and the construction materials. However, their design does not depend exclusively on electrical parameters. The economic factor is also important in this process, since the materials used for high frequency operation are expensive and the manufacturing cost will depend on the length and section of the cables.

The design of the coils directly affects the electrical parameters of the circuit. Firstly, they determine the configuration of the compensation systems, which are discussed in the

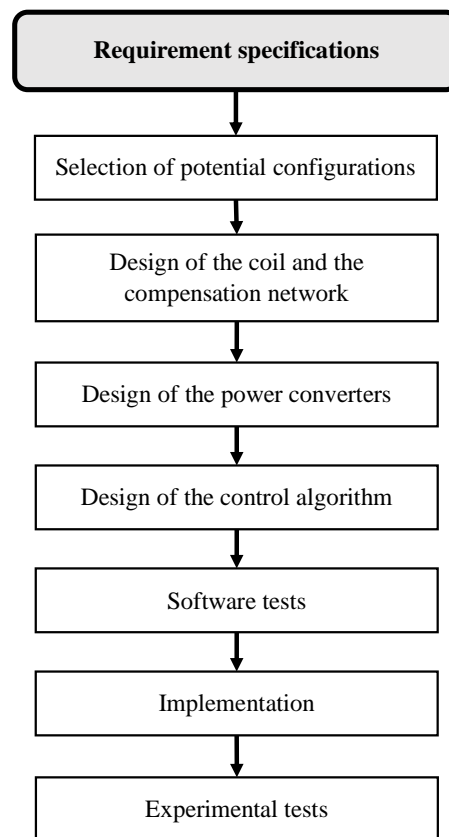


**Figure 2.11:** Generic flowchart for the design of a magnetic-resonance charger [14].

next subsection. They also define the ability of the chargers to deal with misalignments, which can be summarized as horizontal, vertical and angular, although this last option is not common in EVs.

The main coil designs opt for planar coils, as this type of design facilitates integration both in the vehicle and on the ground. The simplest structures are **circular** and **rectangular**, which are especially suitable for low-cost applications. The circular geometry presents higher self-inductance for the same cable length and greater mutual inductance than the rectangular structures when perfectly aligned [43]. However, rectangular geometry is more widely used due to its higher tolerance to misalignment.

Although these geometries continue to be used today, there are other more complex geometries that offer better resistance to misalignment [44]. The most commonly known are DD, DDQ and bipolar. **Double-D or DD** coils are composed of two rectangular coils that have the same dimensions and share one side. Although electrically both coils are in parallel, magnetically they behave like two coils in series since they concatenate the magnetic field. **DD quadrature or DDQ** coils are based on DD coils. This topology

is composed of a DD coil and a Q coil, which is placed over half the area of each DD subcoil. The Q coil is decoupled from the DD coil. The main advantage of DDQ coils over DD coils is in their improved behaviour in cases of misalignment, although in perfectly aligned systems the additional coil does not provide any advantage over the DD solution. **Bipolar** coils are also composed of two square or rectangular subcoils in which, unlike DD coils, one of them overlaps half the area of the other. This solution shows an intermediate performance between DD and DDQ, but bipolar coils successfully reduce the use of copper by 25% compared to DDQ [45].

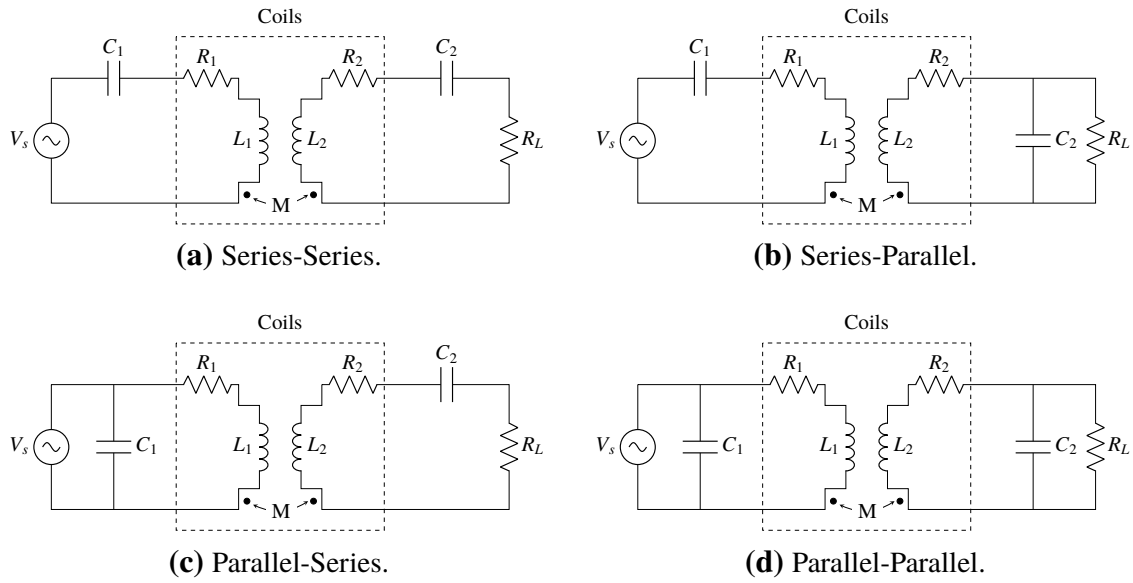
Static chargers use a single coil. However, dynamic chargers can use two solutions: lumped and stretched. The lumped or segmented structure is composed of a series of coils with similar dimensions to the secondary coil, while the stretched structure is a rail-based solution in which the longitudinal dimension is much greater than the width of the coil. This structure can be classified as E-type, U-type, W-type, I-type or S-type depending on the geometry of the ferromagnetic material. The stretched structure has some disadvantages in relation to lumped coils, such as higher installation and maintenance costs, higher losses and, therefore, lower efficiency [42].

## 2.2.2 Compensation networks

Compensation networks are installed on each side of the charger. The simplest structures, composed of a single capacitor connected in series or in parallel, are known as mono-resonant compensation topologies. They can be classified into SS, SP, PS and PP, which are represented in Figure 2.12. The primary series topologies have some disadvantages in comparison to primary parallel topologies because the input impedance phase angle is highly dependent on the load and coupling condition, and in the event that the receiver coil is absent the current that circulates through the transmitter coil must be controlled. However, the SS topology is the most widely used mono-resonant topology because it is less sensitive to misalignment and load variation. Table 2.1 includes equations to compute the capacitor values and the efficiency of each topology.

The coil design process and the compensation system are directly related. The compensation topology affects parameters such as the number of turns, dimensions and section of the coil conductors. At the same time, the design of the coil must take into account the current and voltage limitations of the compensation system, in addition to avoiding the bifurcation phenomenon.

The bifurcation phenomenon refers to the stability problems that a system can present when it has more than one Zero Phase Angle (ZPA). The effects of bifurcation can lead to very steep increases in current and voltage, with the associated risks. This phenomenon


**Figure 2.12:** Mono-resonant compensation topologies.

**Table 2.1:** Capacitor values and AC efficiency for mono-resonant compensation topologies [46].

Topology	$C_1$	$C_2$	Efficiency	$\vec{Z}_T$
<b>SS</b>	$\frac{1}{L_1\omega}$	$\frac{1}{L_2\omega}$	$\eta \cong \frac{R_L}{R_2+R_L}$	$\left(R_1 + j\left(L_1\omega - \frac{1}{C_1\omega}\right)\right) + \frac{\omega^2 M^2}{R_2 + R_L + j\left(L_2\omega - \frac{1}{C_2\omega}\right)}$
<b>SP</b>	$\frac{L_2^2 C_2}{L_1 L_2 - M^2}$	$\frac{1}{L_2\omega}$	$\eta \cong \frac{R_L}{R_2 + R_L + \frac{R_1 L_2^2}{M^2}}$	$\left(R_1 + j\left(L_1\omega - \frac{1}{C_1\omega}\right)\right) + \frac{\omega^2 M^2}{R_2 + jL_2\omega + \frac{R_L}{1 + jR_L C_2\omega}}$
<b>PS</b>	$\frac{L_2 C_2}{L_1 + \frac{M^4}{L_1 L_2 C_2 R_L^2}}$	$\frac{1}{L_2\omega}$	$\eta \cong \frac{R_L}{R_2 + R_L}$	$\frac{1}{R_1 + jL_1\omega + \frac{\omega^2 M^2}{R_2 + R_L + j\left(L_2\omega - \frac{1}{C_2\omega}\right)} + jC_1\omega}$
<b>PP</b>	$\frac{(L_1 L_2 - M^2) L_2^2 C_2}{\frac{M^4 R_L^2 C_2}{L_2} (L_1 L_2 - M^2)^2}$	$\frac{1}{L_2\omega}$	$\eta \cong \frac{R_L}{R_2 + R_L + \frac{R_1 L_2^2}{M^2}}$	$\frac{1}{R_1 + jL_1\omega + \frac{1}{\frac{\omega^2 M^2 (1 + jR_L C_2\omega)}{(R_L + (R_2 + jL_2\omega)(1 + jR_L C_2\omega))}} + jC_1\omega}$

depends on the compensation system, the values of the reactive components and the loading condition. However, stability can be guaranteed by maintaining a connection between the quality factors of the primary ( $q_1$ ) and secondary ( $q_2$ ) coils, which depends on the compensation system used.

There are also more complex structures, composed of several elements such as coils as well as capacitors, which are known as multi-resonant compensation topologies. These structures are widely used on the primary side of the WPT system. LCL and, in particular, LCC topologies are the most popular multi-resonant compensation topologies. The advantages of these topologies over mono-resonant ones are the absence of the bifurcation phenomenon and a more constant power profile under misalignment [47].

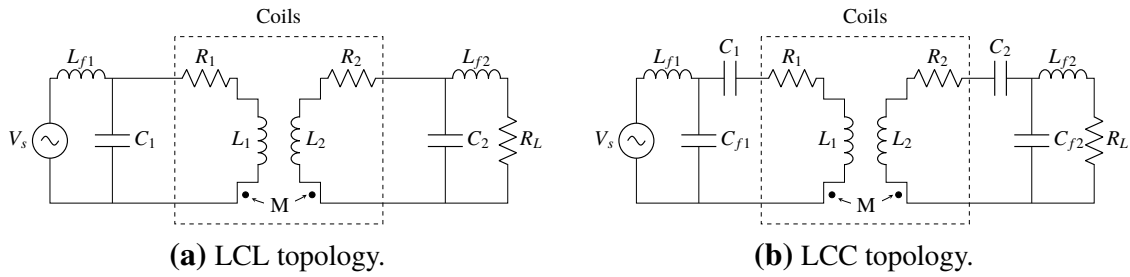


**Figure 2.13:** Multi-resonant compensation topologies.

## 2.2.3 Misalignment

As commented in Section 2.2.1, misalignment is one of the most common contingencies in wireless charging. Although there are alignment and positioning systems [48, 49, 50] that reduce the effects of misalignment in dynamic and static charging operations, their implementation is complex and expensive.

However, the misalignment of the coils in static charging is expected to be very low. In these circumstances, the SS topology is the most commonly used because it does not have to deal with large misalignments and can take better advantage of its higher efficiency due to the fewer number of components compared to multi-resonant solutions.

Despite the small misalignments of the load, their effects on the SS compensation systems must be studied and monitored by the control system. The primary current is the parameter most affected by horizontal misalignments and the increase in the gap between the coils. As shown in Figure 2.14a, which analyses changes in the primary current under horizontal and vertical misalignments in a 3.7-kW prototype, the primary current doubles when there is a misalignment corresponding to half the length of the primary coil. Figure 2.14b shows the effect of misalignment on the AC efficiency of the system, although this effect is more pronounced in the DC efficiency due to losses in the power electronics. In addition to these higher losses, the increase in current can cause irreparable damage to the system, so monitoring the effects of misalignment in real time is essential when operating any WPT system.

Dynamic charging is associated with greater difficulty in aligning both coils as long as the vehicle is not guided by a rail system. Multiresonant systems are more stable in these situations as they do not have the drawbacks experienced with uniresonant compensation. In [47], the authors analyse an LCC compensation system on the primary side of a dynamic charger with circular coils. A direct comparison between the SS compensation and the LCC-S shows that the latter is able to maintain the charging power above 80% of the nominal value within almost 200% of coupling factor variation, keeping the efficiency almost constant throughout the range. The study highlights that these conclusions can be

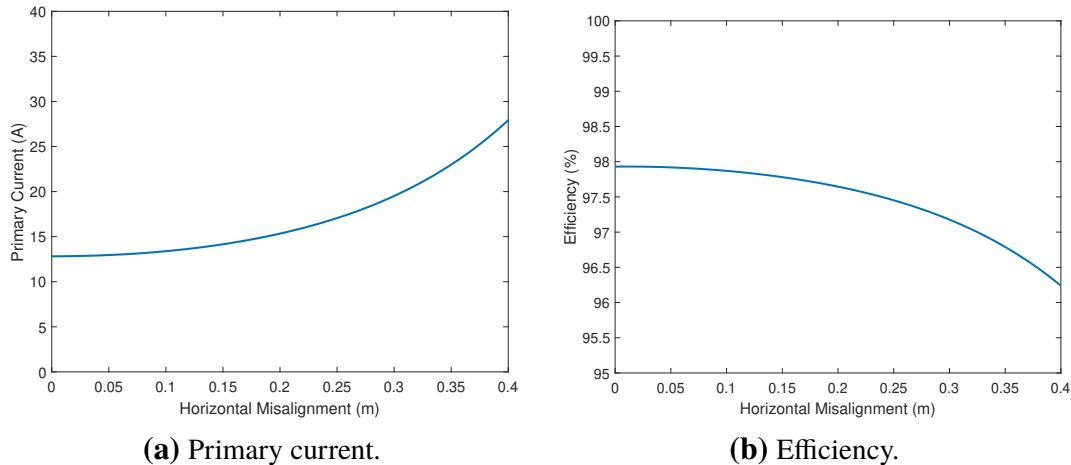


**Figure 2.14:** Effects of horizontal misalignment in both axes and a distance between the coils of 0.25 m [51].

applied to an optimal tuning of the compensation system, since otherwise the results could be similar to the SS compensation. The research developed in [52, 53] also reaches similar conclusions for a double-side LCC system.

It is also possible to combine two compensation topologies on each side of the charger to take advantage of each. This type of solution requires coils with three terminals, such as bipolar coils. The authors of [54] propose a hybrid structure that combines the LCC topology with the SS for a V2G system. The main advantage of this proposal over previous solutions is that the system is capable of keeping the charging power constant while maintaining efficiency with large 3-D pad misalignments. This study also includes an exhaustive analysis of the currents and voltages that circulate through the system, which do not show relevant variations except within the compensation system.

## 2.2.4 Design procedure

The design of the coils and the compensation system mainly depends on **requirement specifications**. These are decided based on the specific use intended for the WPT system. The most relevant specifications that are defined in this first phase are:

- **Charging power.** This is usually adapted to the power classes defined in the regulations.
- **Battery nominal current and voltage.** These values depend on the vehicle manufacturer, but the system can be designed to maximize compatibility.
- **Charging strategy.** Most known strategies are Constant Current (CC), Constant Voltage (CV) and Constant Current-Constant Voltage (CC/CV).

- **Operation mode.**, Static, stationary or dynamic charging.
- **Dimension restriction.** This applies to both primary and secondary sides.
- **Weight restriction.** Along with the dimension restriction, this is particularly relevant for small vehicles such as bicycles. The weight also influences the vehicle's consumption.
- **Cost.** Minimizing cost is always a goal of any design, but it needs to be balanced against other goals such as maximizing efficiency or misalignment performance.

There are other specification requirements, such as operating frequency or electromagnetic emissions, but these are regulated by international standards.

Defining specifications makes it possible to select **potential configurations** that meet these requirements. At this stage, the coil topologies and the compensation system are decided, which depends on the charger's specific use. For example, for a static charger with small misalignment, the rectangular or DD coils with SS compensation perform well, while for a dynamic system, the DDQ coils and LCC compensation will give a better performance.

The selected potential configurations are analysed in the design phase of the coils and the compensation system. This process is carried out using an iterative algorithm such as the one described in the flowchart in Figure 2.15. The algorithm calculates the characteristics of the coils and compensation from a set of possibilities, which include different sizes and number of turns ( $N_1$ ,  $N_2$ ) of the coils and sections of the conductors. The algorithm verifies that each solution meets the requirements for stable operation. These requirements are related to bifurcation, maximum currents, efficiency, or transmitted power. The final configuration is chosen from among the valid options, mainly according to cost effectiveness.

## 2.3 Power electronics in WPT

Power electronics are a core element of EV chargers, as it is necessary to convert the AC from the grid to the requirements of the chargers with maximum efficiency. These requirements are not limited to using a suitable charging voltage/current to comply with the battery charging specifications: it is also necessary to operate with a high frequency in wireless chargers. Please note that the induced voltage is proportional to the changes in the magnetic flux so it is of interest to generate a magnetic field with a high variability, i.e. with a high frequency.

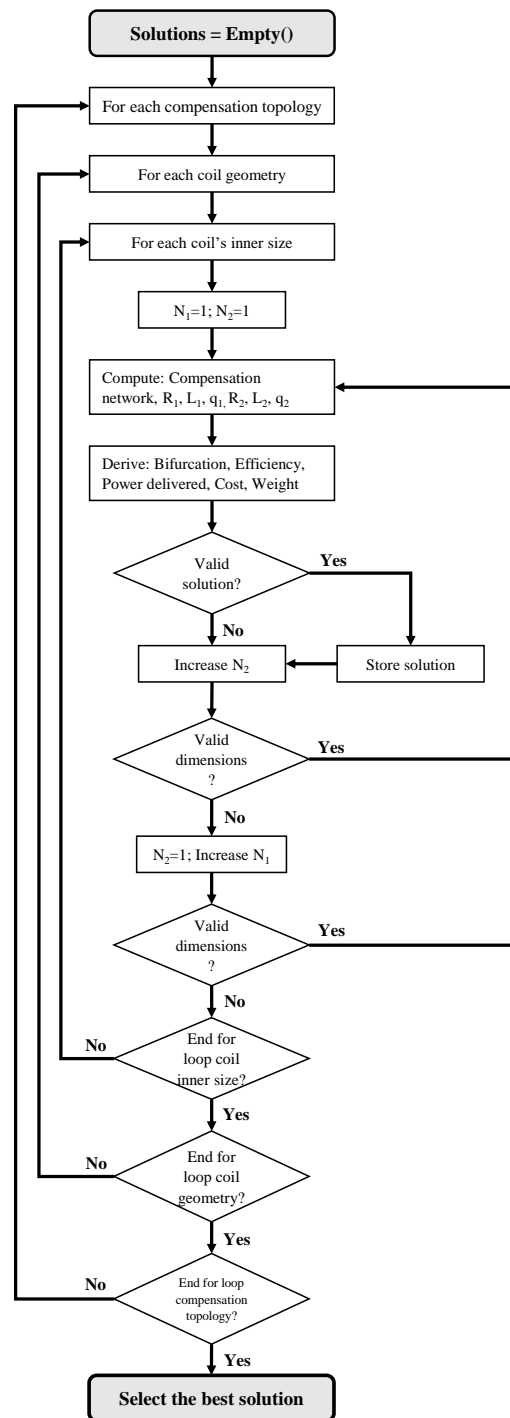


**Figure 2.15:** Flowchart of the iterative algorithm used to design the coils and the compensation system [14].

The conventional topology of a wireless charger begins with a rectification of the AC of the grid. This signal is converted to DC in order to be converted later to a high-frequency current using an inverter. This current flows through the primary coil, which generates a magnetic field that passes through the secondary coil and induces a high-frequency elec-



tromotive force (emf) in it. Since the battery is charged at DC, it is necessary to perform a final conversion step using a rectifier. Optionally, it is possible to use a DC/DC converter on the secondary side to regulate the charging voltage or as an impedance adapter. Figure 2.16 shows a schematic of this process.

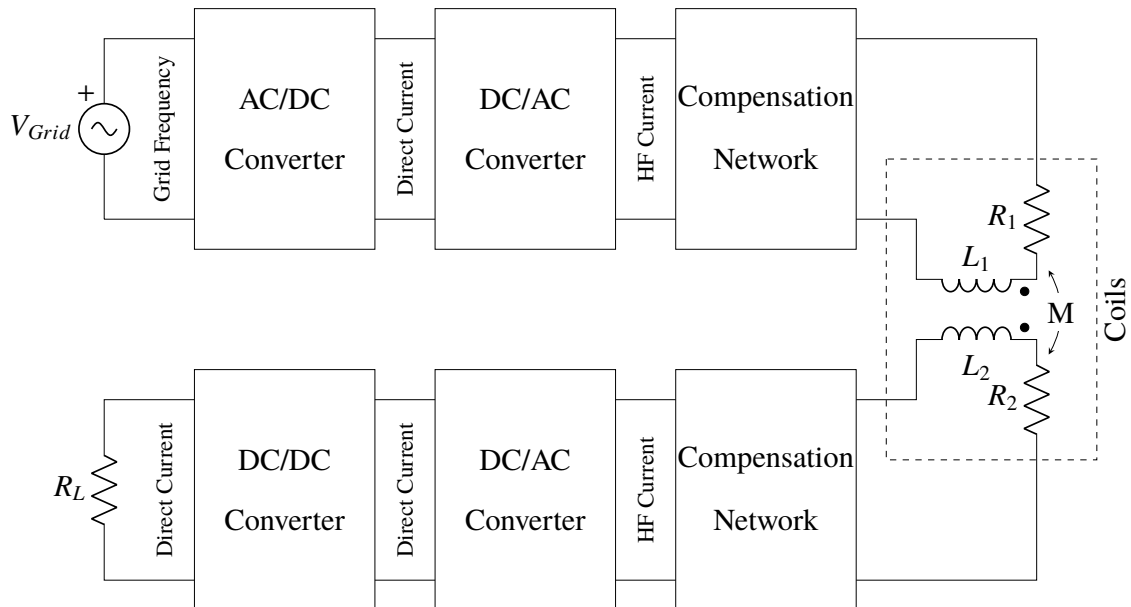


**Figure 2.16:** Generic structure of a magnetic resonance wireless charger.

Power converters are composed of switches and other electronic components. Switches must operate at high frequency, meaning that this task can only be performed by semiconductor devices. Current rectification can be carried out using uncontrolled semiconductors, such as diodes, but other conversion tasks require controlled semiconductors, such as thyristors, IGBTs, or MOSFETs. These components are mainly selected based on the supported power and the switching frequency. Figure 2.17 classifies different types of controlled semiconductor devices according to these parameters.

IGBTs are the main controlled semiconductors used in conversion tasks thanks to their strong price–performance ratio. These features meant that the first prototypes of wireless chargers used this technology to convert the grid frequency to that of the charger’s operation. However, these prototypes operated at a frequency of about 20 kHz [55, 56]. The operating frequency currently used, set at 85 kHz, makes IGBTs unviable because their efficiency greatly decreases and cooling requirements increase significantly. MOSFETs are devices enabled to operate at this frequency range, but the supported power does not make them suitable for this task either.

The trade-off is found in SiC technology. This Wide BandGap (WBG) material [57] presents four main superior properties [58]:

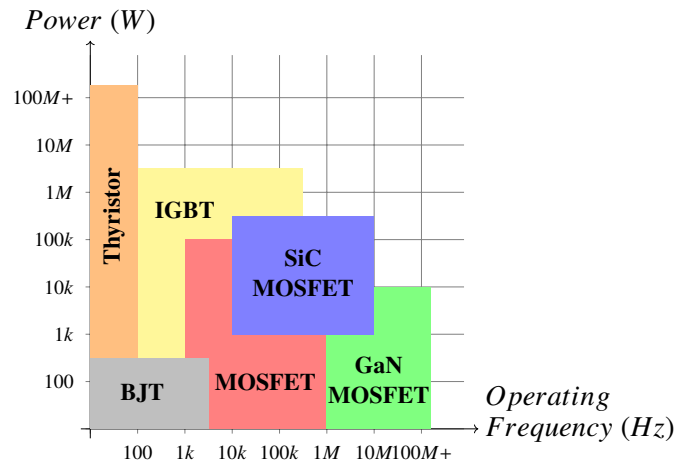


**Figure 2.17:** Power/operating frequency regions of the main controllable semiconductor devices.

1. **Higher breakdown voltage.** It increases the operating voltage range without damaging the semiconductor.
2. **Lower leakage currents.** Lower losses than with silicon semiconductors.
3. **Higher thermal conductivity.** Better heat dissipation performance and less cooling needs.
4. **Lower on-state resistance.** This implies lower losses when the device is active.

Although SiC technology has been applied to various types of semiconductors, its use is more widespread in MOSFETs. SiC MOSFETs are widely used in current prototypes of EV wireless chargers. They are part of the inverter and are also highly recommended in diodes for rectification tasks, as they have lower forward resistance and low recovery charge.

As well as selecting the semiconductor devices, another important decision that must be taken in the design process of the power converters is their topologies. Power conversion can be performed using different converter topologies, in which the arrangement and number of switches and analog components vary. The choice of each topology depends on the characteristics of cost, efficiency, weight, supported power, electromagnetic emissions and type of control. The following subsections discuss different converter topologies used in the related literature for each of the charger conversion stages.

### 2.3.1 Grid rectifier

Grid rectifiers are the systems responsible for converting the AC voltage from the grid to DC. Despite being a fundamental part of the process, these components are not usually

studied when computing the efficiency of the WPT systems. This simplification is mainly due to the fact that their function is limited to rectifying a 50 Hz signal with very mature techniques and components, which do not imply large losses in the system.

Depending on the nominal power of the charger, either single-phase or three-phase rectifiers are used. Single-phase rectifiers are normally used in the home environment for powers below 3.7 kW, whereas three-phase chargers are used for higher powers, particularly greater than 7.4 kW.

The simplest topology for single-phase rectification is the half-bridge rectifier, which is composed of a single diode that extracts energy from the positive semi-cycle of the AC. This topology is not commonly used for charging EVs as it is not suitable for high power applications due to its low efficiency. Alternatively, the simplest and most effective solution for single-phase chargers is the full-bridge rectifier, which uses a solution composed of four diodes. With this structure two diodes are always activated so that the rectifier is able to rectify both the positive and negative semi-cycles of the signal.

With regard to three-phase rectifiers, the simplest topology is the half-bridge rectifier, which is connected to the grid in a Y-connection using three diodes for the rectification task. Specifically, only one of them is activated at a time. Despite the simplicity of the half-bridge, the full-bridge topology is more widely used, since its output voltage is higher, it has less ripple and does not require a neutral point in its connection to the grid. It is composed of 6 diodes, with 2 of them conducting at any given time. As a result, the full-bridge rectifier provides a higher output voltage and less ripple.

All of these rectifier outputs result in a signal that is far from being continuous/constant. Thus, it is necessary to use an output filter to remove some of the ripple and provide a signal that is close to DC. The simplest filter consists of a single capacitor between the output terminals. Its capacitance is directly related to the voltage ripple. This value in particular can be calculated using the following equation:

$$V_0 = \frac{I}{fC} \quad (2.3)$$

where  $V_0$  is the output ripple voltage,  $I$  is the intensity of the DC,  $f$  is the ripple frequency and  $C$  is the capacitance of the capacitor in this filter. This capacitor filter is commonly referred to as the DC link.

The filter capacitor is charged only when the AC voltage is higher than that of the capacitor. This occurs for short periods of time, which causes the current consumed from the grid to experience peaks. These peaks increase the harmonic content and electromagnetic emissions, which, in turn, decreases the power factor. Power Factor Correction (PFC) systems can be included to overcome these problems. These systems can be classified as follows:

- **Passive PFC:** These are composed of reactive elements capable of attenuating the harmonic content of the input current. They mainly use various LC-type filter topologies, in which the inductor can be placed in series with the input or with the load.
- **Active PFC:** These use an additional power converter. Although this solution requires a control system, it provides a greater number of advantages over passive solutions, with less bulky components and the possibility of regulating the output voltage. It can be implemented in a single-stage or a two-stage approach. The latter option consists in installing a DC/DC converter, as a boost, between the primary rectifier and the primary inverter. This is the most common topology due to its greater simplicity.

### 2.3.2 Primary inverter

The inverter, also known as a DC/AC converter, is responsible for generating the high-frequency current that flows through the primary coil. Due to the high switching frequency, semiconductors play an important role in both the efficiency of the system and its cooling needs.

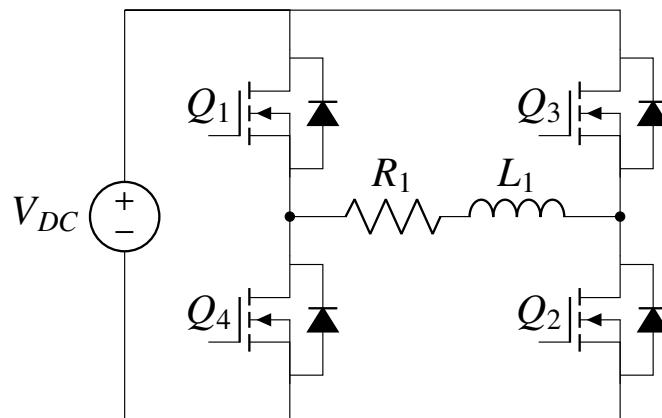


**Figure 2.18:** Topology of a full-bridge inverter.

The most widely used topology in the literature is the full-bridge inverter, since it is the most balanced in terms of efficiency, cost, weight and complexity. Its structure is presented in Figure 2.18. This topology is made up of 4 switches divided into 2 for each leg of the inverter. Each of these legs is configured to activate no more than one transistor, since the activation of both would produce a short circuit that would damage or destroy the components. The output voltage depends on the pair of transistors that is active, so that the possible outputs are:

- **Interval  $0 \leq t \leq T/2$ , Q1 and Q2 activated.** The current flows from the left to the right leg and  $V_{out}$  is  $V_{DC}$ .

- **Interval  $T/2 \leq t \leq T$ , Q3 and Q4 activated.** The current flows from the right to the left leg and  $V_{out}$  is  $-V_{DC}$ .

These two states allow us to derive that the output voltage is a square signal oscillating between  $V_{DC}$  and  $-V_{DC}$ . The theoretical analysis of a system with this topology is carried out with the first harmonic of the voltage, following the first harmonic approximation. For a square-wave, the first harmonic corresponds with the following expression:

$$V_{out} = \frac{4V_{DC}}{\sqrt{2} \pi} \quad (2.4)$$

Although the full-bridge inverter is the most widely used topology, other solutions are also used in the literature. The simplest proposal is the topology with a class-E inverter, which uses a single switch connected to a DC feed inductance and a shunt capacitor. Class  $\phi_2$  inverter, single-ended quasi-resonant inverter, half-bridge inverters and class-D inverters are also a simple solution since they are composed of two switches. All these proposals are recommended only for low-power appliances because the current flowing through their switches is higher than in the full-bridge topology.

Multilevel inverters can also be a suitable solution for high powers [59], as they are composed of several full-bridge inverters so that the power supported by each switching device is diminished. However, this topology is not common in these systems due to its greater cost, weight and complexity of control.

### 2.3.3 Secondary rectifier

The secondary rectifier or AC/DC converter is used to convert the high frequency current that is induced in the secondary coil to DC, as this is required by the battery.

The most commonly used topologies in the bibliography are the uncontrolled type, specifically the full-bridge rectifier. An explanation of how this converter operates has already been given in section 2.3.1. Unlike grid rectifiers, these rectifiers work at a much higher frequency, so it is necessary to use diodes with low recovery charge. SiC-technology is suitable to avoid significant losses. Despite the high operating frequency, the use of output filters is also recommended, although the capacities required for the capacitors are lower.

The battery resistance cannot be included in the AC analysis with its nominal value because the rectifier is a non-linear device which acts as an impedance transformer [60]. Equation (2.5) includes the relation between the battery resistance ( $R_L$ ) and the equivalent resistance ( $R_{eq}$ ).

$$R_{eq} = \frac{V_{ac,rms}}{I_{ac,rms}} = \frac{8}{\pi^2} \frac{V_L}{I_L} = \frac{8}{\pi^2} R_L \quad (2.5)$$

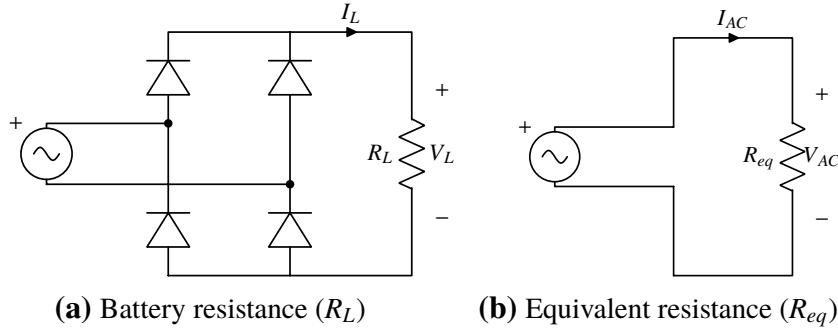


**Figure 2.19:** Comparison between battery resistance and equivalent resistance.

Controlled rectifiers are an increasingly popular option despite the higher cost and complexity of control. This is due to the advantages they have over traditional diode rectifiers. Specifically, controlled rectifiers have the following benefits:

- Direct voltage conversion without a DC/DC converter.
- Higher efficiency than non-controlled rectifiers due to the lower voltage drop.
- Fewer elements than in solutions that use a DC/DC converter, which results in lower losses.
- The reactive power of the AC circuit can be controlled.
- The converter can also operate as an inverter, providing bidirectional capability.

There are different topologies for controlled rectifiers depending on the arrangement of the actively controlled switches. Fig. 2.20a shows a single switch semi-active bridge rectifier [61] in which one switch replaces a bottom diode from the traditional diode full-bridge rectifier. Fig. 2.20b shows a symmetrical bridgeless active rectifier [62] in which each of the rectifier legs includes a diode and a switch. The asymmetrical bridgeless rectifier is shown in Fig. 2.20c, where one leg is composed of two switches, while the second leg contains only two diodes. Finally, a full-bridge controlled rectifier [63] is presented in Fig. 2.20d, which requires four switches to operate.

### 2.3.4 Secondary DC/DC converter

Secondary DC/DC converters are used in some WPT topologies. Their use is only required when it is necessary to control the charge on the secondary side, when the previous stage is an uncontrolled rectifier.

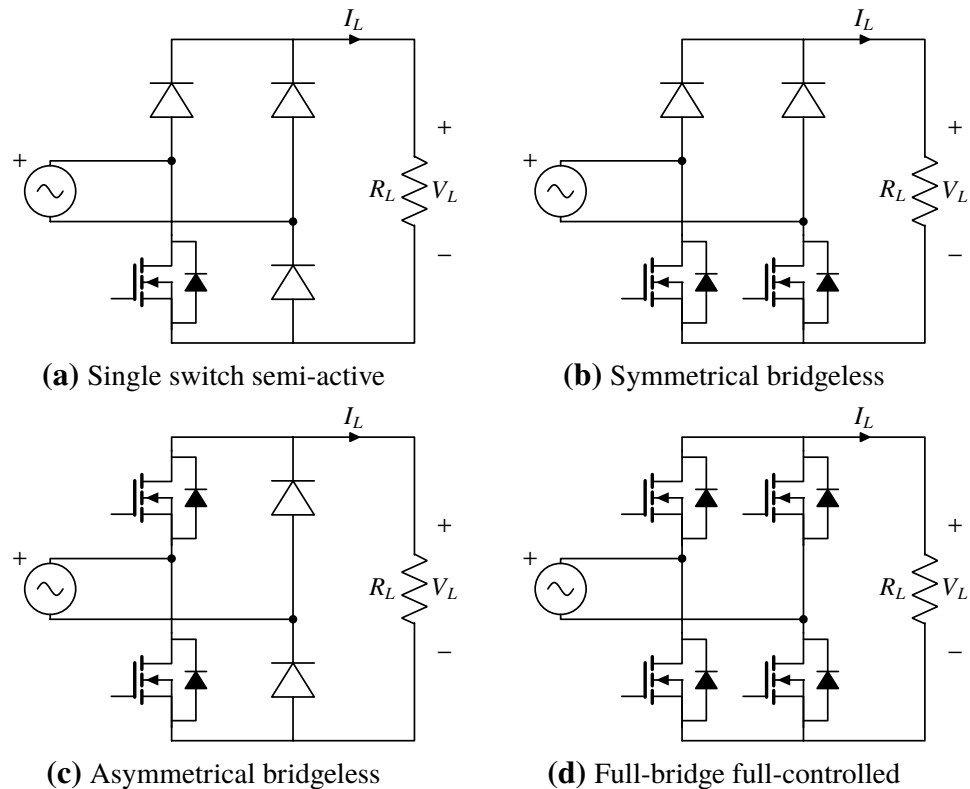


**Figure 2.20:** Single-phase active rectifiers.

The main advantage these converters have over controlled rectifiers is their simplified control, since they are usually composed of a single switch that works directly on the rectified DC signal. Thus, it is not necessary to operate the converter at the same operating frequency as the magnetic field or to sample the AC signal induced in the secondary coil. This advantage does not affect the compatibility between different chargers and vehicles, which is guaranteed as long as the type of converter chosen operates in the range of working voltages. These ranges are not only selected based on the operating voltages of the batteries: it is also necessary to consider the voltage variations on the DC bus due to possible misalignments.

There are several topologies for performing a DC/DC conversion. The most commonly known topologies are the boost converter, when the battery voltage is higher than that of the secondary DC bus, and also the buck converter [64, 65]. Their popularity is based on the simple structure of the converters, since only an active switch is used, and on their control, which adjusts the converters by modifying the switching duty cycle ( $D$ ). The authors of [66] present a complementary solution to the boost converter, which moves the inductor from the converter to the AC circuit. This variation makes the inductor perform a double function, storing energy for the DC/DC conversion, and creating a LCL compensation system on the secondary side, which reduces the reactive power in the circuit and improves

efficiency.

Both converters present voltage restrictions that can be solved using a different topology, such as the buck/boost converter, which is also composed of a single active switch regulated by its duty cycle. This solution allows the voltage to be increased or decreased, depending on the value of the duty cycle. However, the design process must take into account the fact that the output voltage is negative with respect to the input voltage. Moreover, this technology not only maximizes compatibility between different chargers and batteries, but it also deals better with voltage variations caused by misalignments.

Cuk converters and Single-Ended Primary-Inductor Converters (SEPIC) [67] are solutions that also have the ability to work over the full voltage range, but offer less ripple in the output signal [68]. Additionally, the SEPIC converter does not have the output voltage inverted with respect to the input voltage.

The following table summarizes the different types of DC/DC converters used in the literature, as well as the relationship between the input and output voltage ( $V_{in}$  and  $V_{out}$  respectively).

## 2.4 Control in WPT

Control in WPT is an essential aspect of regulating the power flow, i.e. the charging power. Traditional charging strategies try to optimize fast charging, controlling the rate at which the battery degrades and ensuring that the process is safe.

The most commonly known battery charging strategy is the CC/CV pattern. It involves charging the battery at a CC until the battery reaches the maximum voltage recommended by the manufacturer. From that moment on, the control regulates the charging current so that the battery voltage remains constant at the maximum value. Figure 2.21 depicts the different stages of the CC/CV process during the charging time ( $t_{charge}$ ).

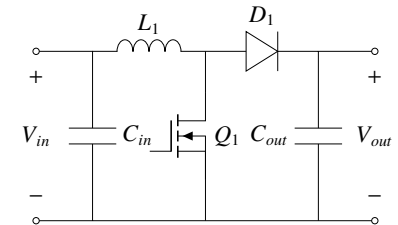
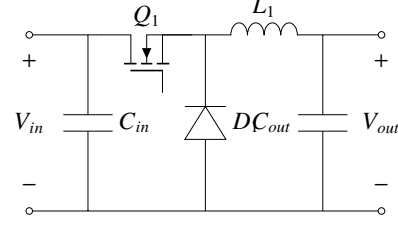
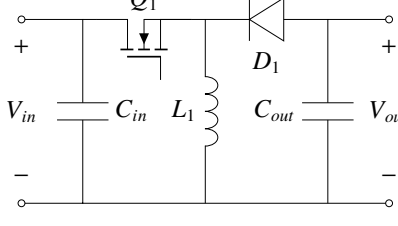
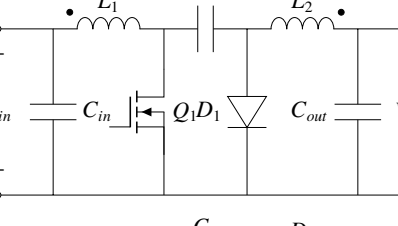
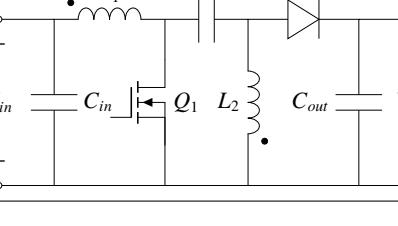
Charging strategies can serve several goals, such as maximum efficiency or maximum charging power. Depending on which converter the control operates, it can be classified into: primary-side, secondary-side and dual-side control. The following subsections develop the related literature with regard to each type of control. They analyse which converter is operated by the control and which strategy has been implemented. Figure 2.22 shows the classification and describes the main strategies applied to each power converter.

### 2.4.1 Primary-side control

In primary-side control, the regulation takes place in the power converters on the primary side. The main advantage of this approach is that the complexity, cost and weight on the



**Table 2.2:** Common DC/DC converters and the relationship between the input and output voltage.

Type	Diagram	$V_{out}$
Boost		$V_{out} = \frac{1}{1-D} V_{in}$
Buck		$V_{out} = D V_{in}$
Buck/Boost		$V_{out} = -\frac{D}{1-D} V_{in}$
Ćuk		$V_{out} = -\frac{D}{1-D} V_{in}$
SEPIC		$V_{out} = \frac{D}{1-D} V_{in}$

secondary side are minimized. Most strategies require measurements from the secondary side to implement a feedback control system. In order to send this information to the primary side, wireless communications are essential. Alternatively, other proposals avoid wireless channels to ease control or for security reasons. If no information from the secondary side is provided, some values must be computed, such as the charging current, the charging voltage or the mutual inductance. This last parameter can be estimated using different methods [65, 69, 70].

Primary-side controls can be further classified into two main categories: the primary

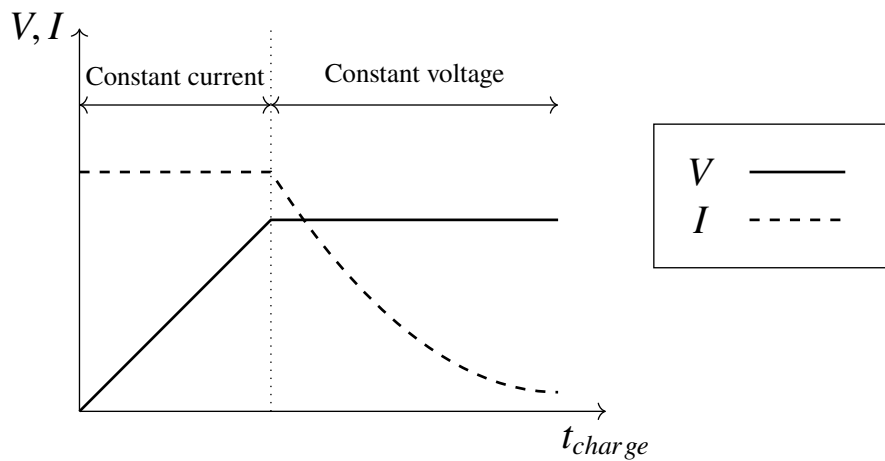


**Figure 2.21:** CC/CV battery charging process.

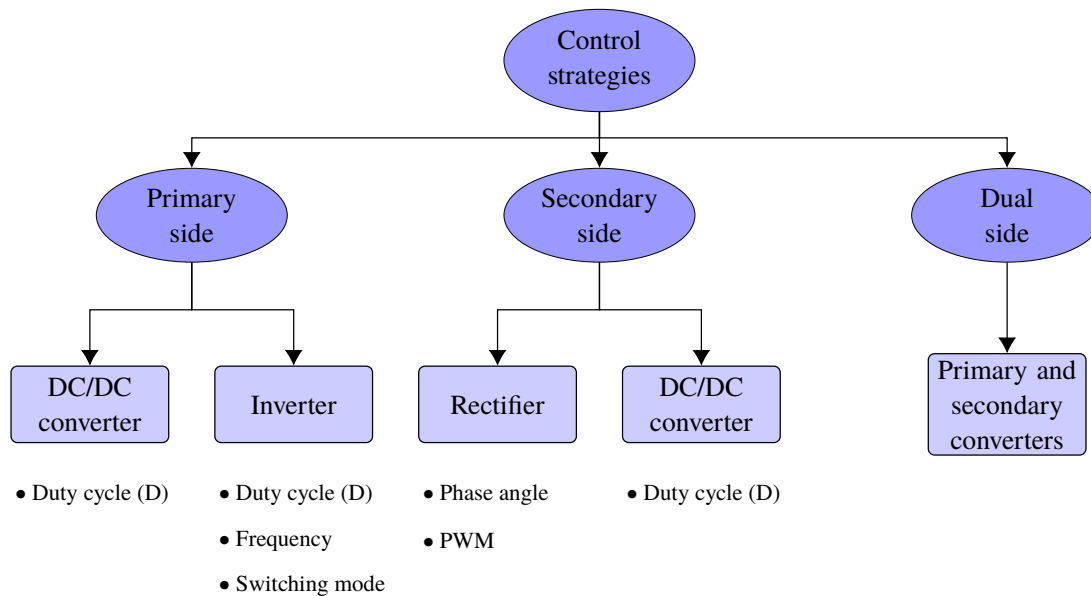


**Figure 2.22:** Classification of controls according to the converter they operate.

DC/DC converter and the primary inverter.

## Primary DC/DC converter

Solutions with a DC/DC converter on the primary side are less frequent than those that only include a primary inverter, since they require an additional converter to be installed. As multi-resonant compensation topologies have developed, this converter has become more popular given that inverter control techniques such as phase-shifting introduce harmonics into the AC circuit, reducing its effectiveness.

This option is also preferred in solutions in which a PFC is used for the rectification process of the grid current. In [71] a DC/DC converter is included to work as a PFC. It

regulates the battery charge by applying a CC/CV strategy. Inverter control is achieved by means of a decoupled control strategy, which ensures ZVS operation. The authors of [72] propose an alternative solution for a buck converter, which follows a novel control strategy combining One Cycle Control and Proportional Differential control (OCC-PD). Finally, the work presented in [73] includes a proposal for regulating the charge without communicating with the secondary side, monitoring the current and voltage solely on the primary side.

## Primary inverter

Primary-side control on a primary inverter is the preferred option in the literature. The reason is that this topology minimizes and simplifies the required components, since it only uses the inverter as a controlled converter. In the same way, the secondary side is also simplified, with only an uncontrolled rectifier. Both the primary and secondary DC/DC converters are not required for this strategy.

Phase-shifting control is a common method for adjusting the charging power from the primary inverter. As explained in Section 2.3.2, the full-bridge inverter operates with an output voltage that can reach  $V_{DC}$  and  $-V_{DC}$ . Phase-shifting adds a new potential level with 0 V when the transistors Q1 and Q3 or the pair Q2 and Q4 are activated. Thus, the operation of an inverter with phase shifting has the following phases:

- **Interval  $0 \leq t \leq D$ , Q1 and Q2 activated.** The current flows from the left to the right leg and  $V_{out}$  is  $V_{DC}$ .
- **Interval  $D \leq t \leq D + \text{Delay}$ , Q1 and Q3 activated.** Both terminals of the load are connected to the positive side, so the voltage is zero and no current flows.
- **Interval  $D + \text{Delay} \leq t \leq T - \text{Delay}$ , Q3 and Q4 activated.** The current flows from the right to the left leg and  $V_{out}$  is  $-V_{DC}$ .
- **Interval  $T - \text{Delay} \leq t \leq T$ , Q2 and Q4 activated.** Similarly to the second state, both terminals are connected to the negative side and no current flows through the load.

These phases are depicted in Figure 2.23, while the output voltage and activation signals are presented in Figure 2.24.

The analysis of the output voltage yields to the following expression:

$$V_{out}(t) = \sum_{n=1}^{\infty} \frac{4V_{DC}}{n\pi} \sin(n\pi D) \sin(n\omega t) \quad (2.6)$$

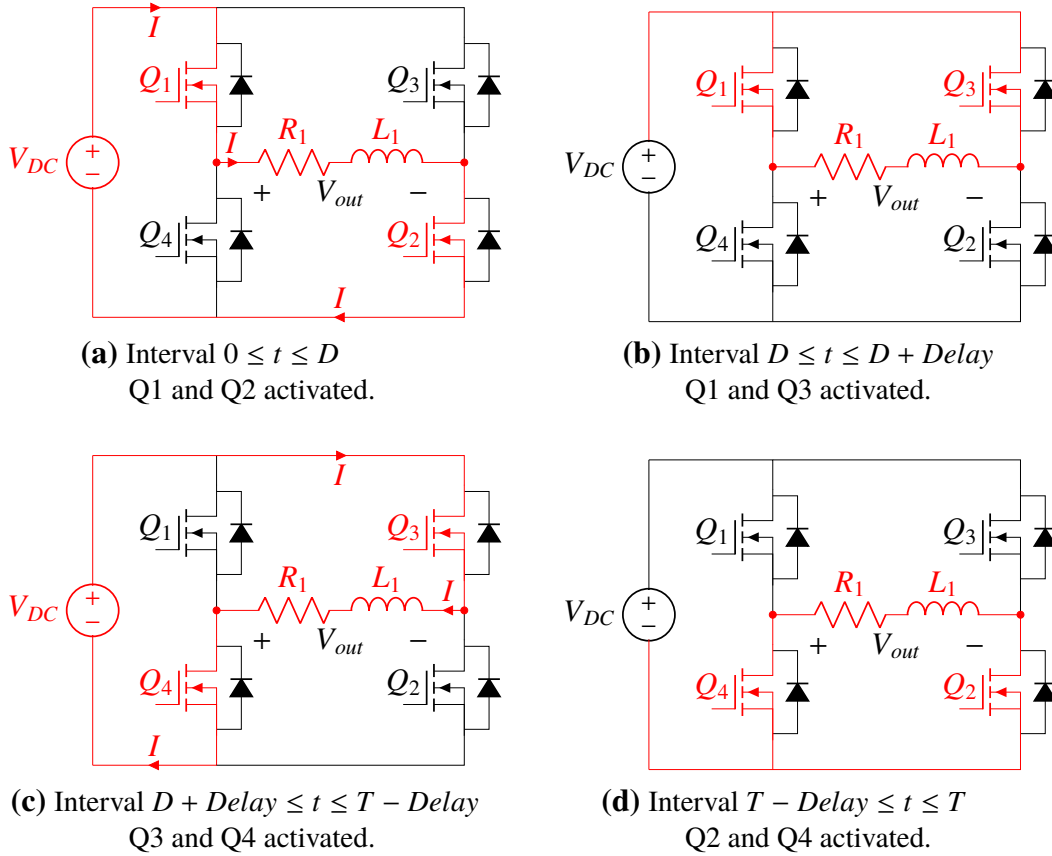


**Figure 2.23:** Operation of phase-shifting technique in a full-bridge inverter.

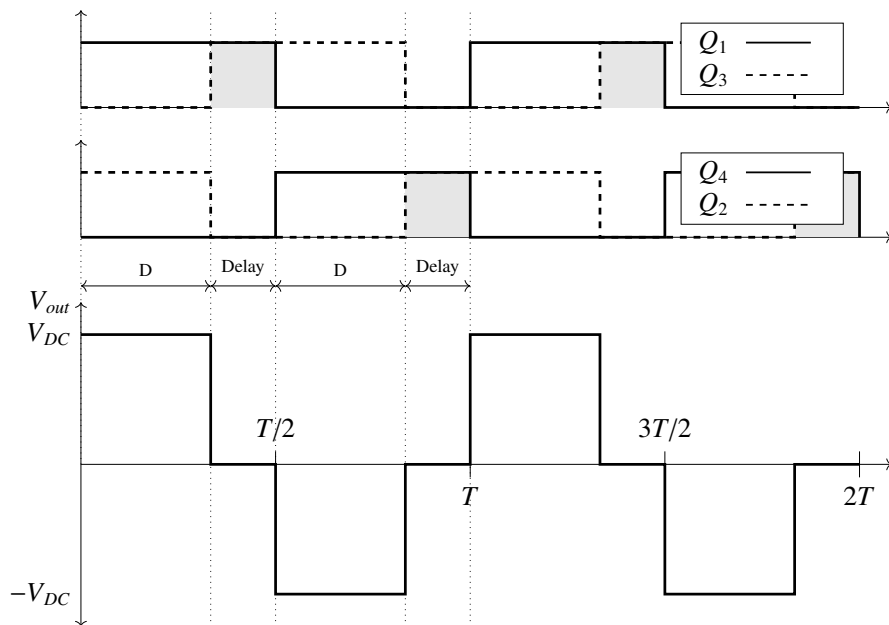


**Figure 2.24:** Voltages in a full-bridge inverter with an square-wave activation and phase-shifting.

where  $n$  is the harmonic number and  $\omega$  is the angular frequency.

As can be observed, the first harmonic is reduced according to parameter  $\sin(n\pi D)$ . The maximum amplitude for every harmonic component is  $4V_{DC}/n\pi$  and it is reached when this parameter is equal to 1.

This control technique is applied in several works. The simplest solution is to control the charging current and voltage using a Proportional–Integral–Derivative (PID) control. The work in [74] presents a different implementation based on the estimation of the mutual inductance to compute the phase angle for constant power. Authors in [75] present the same solution adapted to a dynamic system controlling both the charging power and the primary current. In both approaches, estimating the mutual inductance requires taking some measurements on the secondary side and transmitting them to the primary side.

The authors in [76] propose a solution that avoids communications, estimating the charging voltage with primary voltage and current measurements. A similar approach is presented in [77], but allows CC/CV charging. Both these strategies that dispense with communications share the same problem: they cannot deal with misalignment. In [78], a solution is proposed that resolves this issue. The control performs an estimation of the mutual inductance based solely on the measurements of the primary side.

The inverter operating frequency can also be used to regulate the battery charge. Unlike other control strategies, this does not modify the inverter output voltage, which remains constant, but rather plays with the transformation ratio of the coupled coils. By performing a mesh analysis of the generic diagram for inductive wireless chargers presented in Figure 2.3, Eq. (2.7) and (2.8) can be defined. These equations show how the frequency affects the secondary current and therefore the secondary voltage.

$$\vec{V}_1 = j\omega L_1 \vec{I}_1 - j\omega M \vec{I}_2 \quad (2.7)$$

$$j\omega M \vec{I}_1 = j\omega L_1 \vec{I}_2 + R_L \vec{I}_2 \quad (2.8)$$

Although frequency regulation is a viable option, international standards for wireless chargers limit the range of the operating frequency as seen below. Consequently, the frequency restriction also limits the range of secondary voltages. Another drawback of this control strategy is found in the bifurcation problem, which is especially present in mono-resonant compensation topologies.

Despite these restrictions, there are some authors who opt for this solution because it improves efficiency: finely adjusting the frequency can make the system operate in resonance, reducing the reactive in the circuit and the losses. However, it is not common to find this type of strategy in systems with multi-resonant compensation networks because

it is difficult to achieve resonance.

In [79], the authors follow this approach, designing a maximum efficiency strategy for a system with series compensation on the primary side and parallel compensation on the secondary side. The key to this improved efficiency lies in the inverter's ZPA operation, which reduces losses. It is implemented using a Phase Locked Loop (PLL) system, which analyses the phase difference between voltage and current. The PLL then adjusts the operating frequency taking into account the allowed limits and the instabilities created by the bifurcation phenomenon.

Some authors have combined these two control strategies for the primary inverter. They can therefore take advantage of the regulation of the charging power achieved by the phase-shifting, and they can also improve efficiency by adjusting the frequency. This is seen in the solutions presented in [80, 81, 82].

## 2.4.2 Secondary-side control

The most simple secondary-side topology is the full-bridge diode rectifier. This type of converter does not contain active switches, so it is not a controllable power converter and therefore does not allow any charging regulation on the secondary side. Although secondary-side control requires more complex solutions for power electronics because they include controlled components, the control strategies are easier to implement due to the absence of communications. Not relying on a data transmission also provides greater robustness. Moreover, by measuring all values directly on the secondary side, the system is able to deal with coil misalignment.

Secondary-side control can be performed adjusting the operation of two power converters: secondary DC/DC converter and secondary controlled rectifier.

### Secondary DC/DC converter

The secondary DC/DC converter was the preferred solution when magnetic resonance charging was first developed. The reason is that it is very simple, since it uses widely analysed technology. In addition, the previous stage can be an uncontrolled rectifier, which does not require any communication with the primary side of the charger.

The control of the DC/DC converters is generally less complex, since they act on a single (or dual) switch and their operation is decoupled from the high frequency signal of the charger. This means that the converter can operate at a different frequency than that of the magnetic field. The related literature contains some examples illustrating the difference in this operating frequency. In [83], the DC/DC converter operates at 10 kHz versus 100 kHz in the inductive system, and in [64], the authors also resort to 10 kHz

versus 38.4 kHz for the wireless charging system.

The output voltage of a DC/DC converter is regulated with the duty cycle. This parameter is regulated by standard control methods using a PID controller that computes the error between the measured charging current or voltage and the setpoint. This control strategy can be easily adapted to variations in the mutual inductance (i.e. misalignment) as long as the input voltage values are within the design limits of the drive.

In addition to the controllers that regulate the charging current or voltage, the bibliography includes other proposals with more ambitious objectives. One of these solutions is found in [84], in which the authors propose a Maximum Power Point Tracking (MPPT) method for a buck converter. The algorithm computes the optimal duty cycle for maximum power transfer using the coil coupling coefficient, the operating frequency, coil resistance, charging resistance and input voltage values. As the coupling coefficient of the coils is measured in the system, the algorithm is also robust under misalignment, assuming that the charger operates in resonance. The work in [85] also presents a MPPT solution with a perturb-and-observe strategy. These types of solutions have a slow response and are not concerned with efficiency. Alternatively, a maximum efficiency control for dynamic charging is proposed in [83]. This method can also deal with misalignment since it is based on a real-time coupling coefficient estimation.

## Secondary controlled rectifier

Secondary controlled rectifiers are designed to control the charge from the secondary side in a single stage. They are the most complicated converters to use because they must operate at the charger's frequency, normally set at 85 kHz. However, the main difficulty is not the frequency value but the fact that the switches must operate in synchronization with the voltage induced in the secondary coil. It is therefore necessary to use drivers with a very low response time.

The related work includes only a few secondary controlled rectifier solutions because, as we shall see later, this controller is normally used in dual-side mechanisms. One of these proposals is found in [86], in which the authors present a symmetrical bridgeless active rectifier solution. The rectifier is operated using Pulse Density Modulation (PDM). The objective of the control is to achieve soft switching even in cases of misalignment. The work in [87] proposes a solution that is similar but adapted to dynamic chargers.

Another symmetrical bridgeless active rectifier solution is presented in [88]. The converter is controlled using a phase-shifted Pulse-Width Modulation (PWM) signal. The rectifier control bases its operation on two main variables: the phase controller angle ( $\alpha$ ), which indicates the period of time between the rising edge of the rectifier voltage and the decreasing edge of the primary resonant tank voltage, and the conduction angle ( $\beta$ ), which

determines the output voltage. These values are obtained from the operating frequency of the system, the phase difference between the voltage and current of the secondary coil, the coupling coefficient factor and the equivalent resistance of the battery. A PI controller adjusts the output voltage working simultaneously with the computed control variables. Finally, the authors in [62] propose a solution to control the phase angle in the AC circuit in order to reduce losses due to reactive power.

### 2.4.3 Dual-side control

Dual side control is the most difficult scheme because one controller is installed on each side of the charger and they have to work simultaneously in a coordinated way. The main advantage of this control is the flexibility that it provides to implement more complex strategies.

In order to perform this task, wireless communications are normally used, as it is the only way to share data between the two controllers. However, some authors have also implemented dual-side strategies without communications. The work carried out in [89] is an example of this. The authors propose a topology that includes a DC/DC converter on the secondary side, which regulates the battery charging voltage using a hysteresis control. The regulation on the primary side is performed in the inverter using the phase-shifting technique, in which the system tries to minimize input power, thus maximizing transfer efficiency. Although this control operates robustly, the lack of communications affects response times and its effectiveness.

The maximum efficiency strategies are undoubtedly the most widely established goal in dual-side control. The main differences between the existing proposals in the bibliography are found in the converters on which the control acts. DC/DC converters are the easiest to control, since they are usually composed of a single switch that controls the voltage by adjusting the duty cycle. The authors of [90] opt for such a solution, in which the secondary DC/DC converter acts as an impedance adapter while the primary converter adjusts the load voltage. The control adjusts these parameters using a perturb-and-observe strategy which, as mentioned above, has slow response times. The operating frequency remains fixed throughout the charging process, although it is set at the beginning so that the system operates in resonance.

The work presented in [91] was undertaken with the aim of eliminating the perturb-and-observe strategy and its drawbacks. The proposed control method is based on the estimation of the coil coupling coefficient, using the primary and secondary voltage and current measurements. This estimation is used to compute the optimal duty cycle of the impedance adapter with which the maximum efficiency is achieved. The charging voltage



is regulated with the primary DC/DC converter, using a closed-loop control. This solution is also compatible with dynamic chargers since the mutual inductance is estimated dynamically.

Using a DC/DC converter on the primary side means that an additional converter needs to be installed, with the increased cost that this entails. The voltage on the primary side can also be regulated by the inverter. In [92] the authors implement a maximum efficiency solution with a perturb-and-observe strategy, which adjusts the phase-shift angle of the inverter and the duty cycle of the secondary DC/DC converter.

The authors in [93] propose a solution that adjusts the phase-shift angle of the inverter, the duty cycle of the secondary DC/DC converter and the operating frequency of the system. The solution to control the three parameters is found in a perturb-and-observe strategy with a double loop, in which the first loop makes small variations in the frequency while the second phase makes these variations to the phase-shift angle and the duty cycle. The number of iterations of this proposal is much higher compared to a simple perturb-and-observe algorithm, which makes response times even slower.

It is also possible to implement the control in a controlled rectifier instead of a secondary DC/DC converter. This is a more complex and expensive solution. The bidirectional nature of this converter makes it especially suitable for V2G systems. In [94], the authors offer a solution that includes a full-bridge rectifier controlled on the secondary side. Both the primary inverter and the secondary rectifier are operated following the Pulse Density Modulation (PDM) technique. The main objective of the proposal is to ensure the soft switching operation, for which a ZVS branch is included. The branch is composed of a coil and a capacitor, which are connected between both legs of the inverter to provide a ZVS current.

Another full-bridge controlled rectifier is presented in [95]. The authors propose a semi-impedance-matching method based on a careful selection between full-bridge and half-bridge modes of the inverter and rectifier. When deciding the type of converter, the control calculates which of the two converters provides better transmission efficiency based on an estimation of the mutual inductance. This is needed to make the system compatible in cases of misalignment. The LCC-S topology chosen for compensation ensures the CV load. Finally, the authors of [96] implement a ZVS solution of maximum efficiency with a CC/CV load. The primary inverter adjusts the optimal load impedance by modifying the operating mode between full bridge, full-half bridge and half bridge, while a semi-bridgeless rectifier regulates the battery charge using a phase locked method.

## 2.4.4 Control summary

Table 2.3 includes a summary of the control strategies described in this section.

**Table 2.3:** Control strategies summary.

Ref	Type	Controlled variable	Controlled component	Type of control
[71]	Static	Duty cycle (D)	Primary DC/DC	CC/CV
[72]	Static	Duty cycle (D)	Primary DC/DC	CC/CV
[74]	Static	Duty cycle (D)	Primary inverter	CP
[75]	Dynamic	Duty cycle (D)	Primary inverter	CP
[76]	Static	Duty cycle (D)	Primary inverter	CV
[77]	Static	Duty cycle (D)	Primary inverter	CC/CV
[78]	Static	Duty cycle (D)	Primary inverter	CC/CV
[79]	Static / Dynamic	Inverter frequency	Primary inverter	CP with ZPA
[80]	Static	Inverter frequency and duty cycle (D)	Primary inverter	Maximum efficiency
[81]	Static	Inverter frequency and duty cycle (D)	Primary inverter	Maximum efficiency CC
[82]	Static	Inverter frequency and duty cycle (D)	Primary inverter	Maximum efficiency CC
[83]	Dynamic	Duty cycle (D)	Secondary DC/DC	Maximum efficiency
[84]	Static	Duty cycle (D)	Secondary DC/DC	Maximum power transfer
[85]	Static	Duty cycle (D)	Secondary DC/DC	Maximum power transfer
[86]	Static	Pulse Density Modu- lation (PDM)	Secondary rectifier	CV with soft switch- ing
[87]	Dynamic	Pulse Density Modu- lation (PDM)	Secondary rectifier	CV with ZVS and ZCS

Continued on the next page

**Table 2.3:** Control strategies summary (continued)

Ref	Type	Controlled variable	Controlled component	Type of control
[88]	Static	Phase controller angle ( $\alpha$ ) and conduction angle ( $\beta$ )	Secondary rectifier	CV
[62]	Static	Phase angle	Secondary rectifier	-
[89]	Static	Primary inverter phase-shift and secondary hysteresis control	Primary inverter and Secondary DC/DC	Maximum efficiency CV
[90]	Static	Frequency and Duty cycle (D)	Primary and Secondary DC/DC	Maximum efficiency CV
[91]	Static / Dynamic	Frequency and Duty cycle (D)	Primary and Secondary DC/DC	Maximum efficiency CV
[92]	Static	Phase-shift and Duty cycle (D)	Primary inverter and Secondary DC/DC	Maximum efficiency CV
[93]	Static	Frequency, Phase-shift and Duty cycle (D)	Primary inverter and Secondary DC/DC	Maximum efficiency CC/CV
[94]	Static	Pulse Density Modulated (PDM) and its Duty cycle (D)	Primary inverter and Secondary rectifier	ZVS
[95]	Static	Full-bridge or half-bridge operation mode selection	Primary inverter and Secondary rectifier	Maximum efficiency CV
[96]	Static	Inverter operation mode and rectifier duty cycle and phase difference	Primary inverter and Secondary rectifier	Maximum efficiency CC/CV

## 2.5 Standards for EV wireless chargers

Wireless charging of EVs is regulated by three international standards: SAE J2954 [12], IEC 61980 [97, 98, 99] and ISO 19363 [100].

The **SAE J2954** standard, defined by the Society of Automotive Engineers (SAE), is the most widely known specification in the international industry. This specification seeks to ensure the interoperability of light-duty vehicles with different universal wireless chargers in static charge. Specifically, this standard is focused on magnetic resonance WPT.

The standard document is entitled “Wireless Power Transfer for Light-Duty Plug-In/Electric Vehicles and Alignment Methodology” and its most recent version was published in 2020. This specification regulates only light vehicles, but SAE is working towards a new standard for heavy vehicles. The standard classifies chargers into 4 fundamental types based on their charging power, which are defined in Table 2.4 with their minimum levels of efficiency.

**Table 2.4:** WPT power classifications for light-duty vehicles.

	WPT Power Class			
	WPT1	WPT2	WPT3	WPT4
Maximum input Volts Amps	3.7 kVA	7.7 kVA	11.1 kVA	22 kVA
Minimum target efficiency at nominal x,y alignment	>85%	>85%	>85%	TBD <sup>1</sup>
Minimum target efficiency at offset position	>80%	>80%	>80%	TBD <sup>1</sup>

<sup>1</sup> TBD: To be defined.

The interoperability of the chargers depends on the above classification. Table 2.5 summarizes the interoperability requirements. Primary and secondary coils of types WPT1 and WPT2 must be able to operate with each other, while primary coils of type WPT3 only have to guarantee operation with secondary coils of type WPT2. The WPT4 classification has not yet been defined in this specification.

The gap between coils is also defined in the standard as Vehicle Assembly (VA) coil ground clearance. Depending on the gap, SAE J2954 defines three types of operation called Z-classes:

- **Z1-class:** gap between 100 and 150 mm.

**Table 2.5:** Interoperability by Power Class.

		Secondary Coils			
		WPT1	WPT2	WPT3	WPT4
Primary Coils	WPT1	<i>Required</i>	<i>Required</i>	Optional	Optional
	WPT2	<i>Required</i>	<i>Required</i>	Optional	Optional
	WPT3	Optional	<i>Required</i>	<i>Required</i>	Optional
	WPT4	Optional	Optional	Optional	<i>Required</i>

- **Z2-class:** gap between 140 and 210 mm.
- **Z3-class:** gap between 170 and 250 mm.

The document also defines the operational parameters. One of these parameters is the frequency, which has an established nominal value of 85 kHz, but can range from 81.38 to 90 kHz. With regard to misalignment, the system must tolerate an offset positioning while maintaining the minimum levels of efficiency indicated above. The misalignment tolerance requirements are defined in Table 2.6. In addition to these offsets between coils, chargers must also ensure operation when a Roll of up to  $\pm 2\%$ , a Pitch of up to  $\pm 2\%$  and Yaw of up to  $\pm 10\%$  occur simultaneously.

**Table 2.6:** Positioning tolerance requirements for Test Stand VAs and Product VAs.

Offset Direction	Value (mm)
$\Delta X$	$\pm 75$
$\Delta Y$	$\pm 100$
$\Delta Z$	$Z_{nom} - \Delta_{low} - > Z_{nom} - \Delta_{high}$

The SAE J2954 document does not include any reference to communications between the wireless charger and the EV. SAE J2847/6 establishes minimum requirements for communication between them. Concerning the protocol, JSON is recommended and the communication channel must be on IEEE 802.11n (Wi-Fi).

**IEC 61980** is the standard defined by the International Electrotechnical Commission (IEC) that regulates EV WPT systems. This document is divided into three main parts:

**Part 1: General requirements** This part covers general aspects such as the characteristics and operating conditions of a supply device, the specification for the required level of electrical safety in a supply device, communication between EV and wireless charger, efficiency and alignment of systems, and specific EMC requirements.

Its most recent publication in 2020 reorganized the content in order to make it compatible with other wireless technologies.

**Part 2: Specific requirements for communication between electric road vehicle (EV) and infrastructure** This document defines the specifications for operational and functional characteristics of the WPT communication subsystem. Communication requirements for dynamic charging, for two- and three-wheel vehicles, and for bidirectional power transfer are also being considered for future releases.

**Part 3: Specific requirements for the magnetic field wireless power transfer systems.** This document only applies to magnetic resonance wireless chargers, as it defines the requirements of the generated magnetic field. The operating frequency for passenger cars and light duty vehicles is also established in the 81.38-90 kHz range, with a nominal value of 85 kHz.

Finally, the **ISO 19363** standard was defined by the International Organization for Standardization (ISO) under the title “Electrically propelled road vehicles — Magnetic field wireless power transfer — Safety and interoperability requirements”. The document addresses several aspects in a similar way to the previous standards. It sets safety requirements, transferred power and power transfer efficiency, ground clearance of the EV device, functionality with associated off-board systems under various conditions and independence of manufacturer and test procedures. This standard is compatible with IEC 61980, so devices developed with any of these standards fulfil the requirements of each one.

Although these standards regulate most aspects of wireless vehicle chargers, electromagnetic emission restrictions are governed by other more general regulations. These restrictions are necessary for health and safety reasons. The International Commission on Non-Ionizing Radiation Protection (ICNIRP) has published guidelines for limiting exposure to time-varying electric and magnetic fields. Specifically, the document [39] regulates the magnetic fields of wireless chargers since their nominal frequency is established at 85 kHz. The imposed restrictions are summarized in Table 2.7.

**Table 2.7:** Electromagnetic restrictions set by ICNIRP in the 3 kHz-10 MHz range.

Public	E-field strength E ( $kVm^{-1}$ )	Magnetic field strength H ( $Am^{-1}$ )	Magnetic flux density B (T)
<b>Occupational</b>	$1.7 \cdot 10^{-1}$	80	$1 \cdot 10^{-4}$
<b>General</b>	$8.3 \cdot 10^{-2}$	21	$2.7 \cdot 10^{-5}$

## 2.6 Market perspectives

Future prospects for EV wireless chargers are unclear due to the market challenges they face, such as the current low market share of EVs, the higher cost of implementing this technology compared to conductive ones and the lower charging speeds. However, these complications do not seem to be affecting the growth of this technology, given that it is in a developmental stage and provides a number of advantages such as the non-intervention of users, improved safety in the charging process, and dynamic charging thanks to the elimination of cables.

The wireless charger industry for EVs currently has a global turnover of about \$16 million [101], which is an excessively low value considering that the market gives priority to this technology. However, the rapid growth forecast for EV sales and the support of different market players mean that the market for Wireless EV Charging is expected to grow at a Compound Annual Growth Rate (CAGR) of between 30-50% from 2020 to 2025 [102, 103]. As a result, EVs worth a total of \$250 million are expected to be in use by 2025.

The global wireless charging market is dominated by Europe, which had a 41% share of the market in 2019 [102] due to the presence of major players in this region. Europe is expected to maintain its dominant position, led by the UK, France and, especially, Germany, which has taken advantage of its position as an automotive manufacturing hub. Projects such as STILLE [104], which is funded by the German Federal Ministry for Economic Affairs and Energy and in which various car manufacturers collaborate, will also contribute to Germany's role as a leader.

The growth of this technology will also be partly based on direct support from EV manufacturers. Some of these manufacturers have already confirmed that they will adopt this technology, including:

**Audi.** One of Audi's objectives is to launch the e-tron model with the possibility of wireless charging, using a charging station with a 90x70 cm<sup>2</sup> coil, while the vehicle uses a 60x60 cm<sup>2</sup> plate. This system is expected to be capable of recharging the 95 kWh battery from 10 per cent to 80 per cent capacity in 12 hours.

**BMW.** The manufacturer first implemented this technology in the 530e iPerformance plug-in hybrid sedan models, albeit restricted to Germany with plans to expand into other markets. The BMW wireless charger includes a 3.2-kW ground pad that allows the 9.2 kWh battery to be charged in under 3 hours.

**Hyundai-KIA.** The Hyundai group, which also includes the Kia Motors brand, has only put forward concepts so far, of which the "Automated Valet Parking System (AVPS)"

stands out: it is a system that combines wireless charging with autonomous parking. This prototype is expected to be capable of charging at 10 kW with an efficiency greater than 85%.

**Mercedes-Benz.** The German manufacturer was expected to implement a 3.6 kW wireless charging system in its S550e Plug-In Hybrid model. However, despite having been announced, this system has not yet been seen in any of its models.

Other wireless EV charger providers have also deployed this technology. These companies are summarized below:

**EFACEC.** The multinational EFACEC works on wireless chargers under the Qualcomm Halo license, which is explained below.

**HEVO Inc.** The Brooklyn-based startup, with just 10 employees, has its chargers in low-volume production. Their wireless chargers will provide a charging power of 8 kW and an efficiency of around 91%. The cost of the secondary coil is estimated at around \$500, while the primary coil, which includes the associated electronics, will cost \$2,500 [105].

**Momentum Dynamics Corporation.** Momentum Dynamics is an American company whose product portfolio include solutions of up to 75 kW for light-duty vehicles, up to 150 kW for delivery vans and 450 kW for public transport. One of their most ambitious projects is Link Transit [106], in which they have installed four 50-kW chargers at a transit stop at Columbia Station in Wenatchee, WA, where multiple transit vehicles arrive hourly. A charge of between 7 and 10 minutes every hour is enough to keep the bus batteries charged at 75%, enough to complete the trips.

**Plugless Power.** Plugless power is one of the few manufacturers that has domestic commercial solutions for sale. Its product portfolio includes Wireless EV Charging Stations of 3.3 and 7.2 kW for BMW i3 and Tesla Model S.

**Qualcomm.** Qualcomm acquired Halo wireless charging technology along with the Australian company HaloIPT in 2011. In the Halo portfolio there are charging solutions from 3.3 to 20 kW with an efficiency greater than 90%. This technology has been used in the world of car racing, where it was responsible for charging the Formula E Safety Car. In 2019, Witricity acquired Halo technology from Qualcomm, including the more than 1,500 patents related to this technology.

**WiTricity.** WiTricity is an MIT spinout which was founded in 2007. The founders' vision included not only the charging of EVs but also domestic applications. This



company is one of the leaders in the sector, as demonstrated by its contribution to the development of the SAE J2954 standard, as well as its collaboration with large car manufacturers such as Toyota and Mitsubishi. This position has been reinforced with the company's acquisition of Halo technology from Qualcomm. Their portfolio includes wireless chargers with charging powers between 3.6 and 11 kW and with an efficiency of 90-93%.

The transition from traditional conductive charging to wireless charging is going to be a gradual process, in which both technologies will have to coexist simultaneously [107]. An example of this is the collaboration carried out between Momentum Dynamics and Jaguar Land Rover [108], where a 50-kW inductive charger system has been installed in the Jaguar I-PACE model for Cabonline, the largest taxi network in Norway. This installation has been carried out in parallel with the vehicle's 11-kW on-board conductive charger, so none of the components of the two systems has been shared, increasing both the cost of the system and the weight of the vehicle.

The companies' objective is to find configurations for vehicles that allow compatibility between both technologies, simplifying the electronics used and reducing the costs of including both technologies. This creates a new concept called **hybrid charger**. In [109], authors discuss the integration of WPT in EVs, offering new operational concepts but without referring to the topologies that make these concepts possible. In this sense, both Tesla and Toyota have registered patents [110, 111] of systems that hybridize part of the electronics. The proposals include similar concepts in which both chargers share an on-board DC/DC converter.

There are also some academic proposals for hybrid charging, although they are mainly focused on sharing off-board components rather than on-board components. The authors in [112] propose a solution in which the integrated boost converter of the traction drive system rectifies the AC voltage of conductive and inductive charging. However, the main development of this prototype is the sharing of off-board components, where the grid rectifier, the high frequency full-bridge inverter and the transformer are used for both conductive and inductive loads. The output of the high frequency transformer can be connected to the on-board rectifier for conductive charging or to the primary coil for inductive charging. A 7.7-kW prototype was tested with 85% and 84% efficiencies for the inductive and the conductive charger respectively. [113] also defines a hybrid solution with a similar approach. Although these solutions simplify the power electronics, they do not address the on-board components, which are the most critical for weight and, therefore, consumption and autonomy.



# Chapter 3

## Contributions

---

Over the course of the doctoral program, multiple lines of research have been developed and concluded with published results. In total, the publications consist of three conference articles, seven journal articles, and a book published by Springer.

The most relevant publications in prestigious journals are listed below:

**Contribution 1** A. Triviño-Cabrera, J. Aguado and J. González (2017), "Analytical characterisation of magnetic field generated by ICPT wireless charger," *Electronic Letters*, vol. 53, pp. 871-873, 2017. doi: 10.1049/el.2017.0968. **JCR Impact Factor (2017): 1.232 (Q3)**. The doctoral student has contributed to the review of the state-of-art, formal analysis, validation, writing—original draft preparation.

**Contribution 2** B. Vu, J. M. Gonzalez-Gonzalez, V. Pickert, M. Dahidah and A. Trivino, "A hybrid charger of conductive and inductive modes for Electric Vehicles," *IEEE Transactions on Industrial Electronics*, Early Access, 2020. doi: 10.1109/TIE.2020.3042162. **JCR Impact Factor (2019): 7.515 (Q1)**. The doctoral student has contributed to the review of the state-of-art, formal analysis, methodology, writing—original draft preparation and review of the final manuscript.

**Contribution 3** "Design and implementation of a cost-effective wireless charger for an electric bicycle", *IEEE Access*, vol. 9, pp. 85277-85288, 2021, doi: 10.1109/ACCESS.2021.3084802. **JCR Impact Factor (2019): 3.745 (Q1)**. The doctoral student has contributed to the review of the state-of-art, formal analysis, methodology,

physical implementation, validation, writing—original draft preparation and review of the final manuscript.

**Contribution 4** J.M. González-González, A. Triviño-Cabrera and J.A. Aguado, “Design and Validation of a Control Algorithm for a SAE J2954-Compliant Wireless Charger to Guarantee the Operational Electrical Constraints,” *Energies*, vol. 11, no. 3, pp. 604, 2018. doi: 10.3390/en11030604. **JCR Impact Factor (2017): 2.707 (Q3).**

**Contribution 5** J. M. Gonzalez-Gonzalez, A. Trivino and J. A. Aguado, "Model Predictive Control to Maximize the Efficiency in EV Wireless Chargers," *IEEE Transactions on Industrial Electronics*, Early Access, 2020. doi: 10.1109/TIE.2021.3057006. **JCR Impact Factor (2019): 7.515 (Q1).**

The order of the contributions does not correspond to the temporal order of publication, but to the research process carried out throughout the period. These publications are summarized and presented below.

## 3.1 Analytical characterisation of magnetic field generated by ICPT wireless charger

WPT magnetic resonance technology bases its operation on magnetic fields. These must be controlled to avoid posing a risk to people and other electronic devices. As explained in Chapter 2, the frequency of the magnetic field is regulated by international wireless charging standards, while the limits for human exposure to magnetic fields are regulated by ICNIRP.

The characterization of the magnetic field is a fundamental tool when designing inductive charger coils. Although this task can be carried out using expensive and complex software based on the finite element method (e.g. ANSYS Maxwell), this software does not allow a quick analysis of the multiple possibilities for coil design. This proposal is designed to overcome the limitations of these programs, obtaining a method that can be implemented with simple scripts to conduct studies.

This analytical characterization was developed by focusing on rectangular coils. Although circular coils are more efficient under ideal conditions, rectangular coils outperform them in cases of misalignment, which makes them one of the most frequently used structures in practice.

The proposed solution has a series of advantages over others in the literature, such as the possibility of obtaining the value of the magnetic field at any point, the non-use of magnetic dipoles and the ease of incorporating shielding or ferromagnetic elements into the model by modifying the equivalent electrical parameters.

The calculation methodology is based on the relationship between the static magnetic field ( $\overline{B}_s$ ) and the magnetic potential vector ( $\overline{A}$ ), which is defined in equation (3.1). The two components of the magnetic potential vector are computed by applying the Biot-Savart law. The final magnetic field is calculated by multiplying the resulting static magnetic field by the number of turns and a time-dependent factor.

$$\overline{B}_s = \nabla_x \overline{A} \quad (3.1)$$

The magnetic field generated by magnetic resonant chargers must include the effects of both coils, but if we assume that they operate in a linear medium, this value can be computed by adding the contributions of the magnetic field generated by primary coil and that created by the secondary coil. For each coil, the basic magnetic field is computed for one loop. Then, the number of loops is used as a proportional constant of the derived magnetic field.

Since misalignment also impacts the current phase of the system, the equations have

considered this phenomenon by including the terms  $\varphi_1$  and  $\varphi_2$ . All these effects are included in the analytical expression:

$$B_{ICPT} = N_1 B_S(0, 0, 0, I_1) \sin(\omega t + \varphi_1) + N_2 B_S(x, y, gap, I_2) \sin(\omega t + \varphi_2) \quad (3.2)$$

The proposed characterisation has been verified with the laboratory prototype using an auxiliary coil to measure the magnetic field in a wide set of configurations for different misalignment conditions. The comparison between measurements and theoretical results concludes with a mean error of 8% and a standard deviation equal to 6.5%.

Pages 61-62 are hidden due to copyright. They contain the following paper:

A. Triviño-Cabrera, J. Aguado and J. González (2017), "Analytical characterisation of magnetic field generated by ICPT wireless charger," *Electronic Letters*, vol. 53, pp. 871-873, 2017. doi: 10.1049/el.2017.0968.

## 3.2 A hybrid charger of conductive and inductive modes for electric vehicles

Despite the advantages that wireless chargers have over conductive ones, their implementation will be a slow process in which both technologies will probably coexist simultaneously to take advantage of the existing conductive charging infrastructure. When both charging technologies are implemented, the system is referred to as hybrid.

EVs can be charged with both external and internal chargers. External chargers are related to DC chargers because they perform power conversion with power electronics located in an external device. These chargers are not used in domestic environments because they are dangerous and require high power and available space. On the other hand, on-board chargers are integrated on the vehicle and can be directly connected to the grid.

The hybridization of chargers is not a widely studied topic. The bibliography is scarce with a limited number of works and just two patents from Tesla and Toyota as described in Section 2.6. The proposal made by these manufacturers is to share the DC/DC converter of the secondary side between both technologies.

This work aims to take advantage of the on-board power electronics responsible for battery charging in current EVs so that the wireless and the conductive chargers share more components than those proposed in the patents. This will reduce the weight and cost of the vehicle.

To that end, this work proposes a novel charging concept in which the transformer used to isolate the vehicle from the grid is replaced by two coils built with Litz Wire which, in turn, are used by the wireless system as receiving coils. The rectifier installed in the vehicle can therefore be shared by both technologies. This change is significant because the electronic components must be capable of working at high frequency. The frequency of the grid current also has to be incremented in order for this concept to be viable. This process can also be used to regulate the charging power, which could simplify other stages of a traditional on-board charger.

One of the main challenges of this work is the design of the coils, which has been carried out using a finite element method conducted in ANSYS Maxwell 3D. On the one hand, both coils installed in the vehicle must have specifications that make it possible to regulate the charging power and isolate the vehicle from the grid, while on the other hand they must also act as receiving coils for wireless charging, which requires them to have a very small gap between the two and to be the same size. The difference in the gap between the two coils poses a problem for inductive charging since the mutual inductance with the primary coil is different and this produces a circulating current that increases system



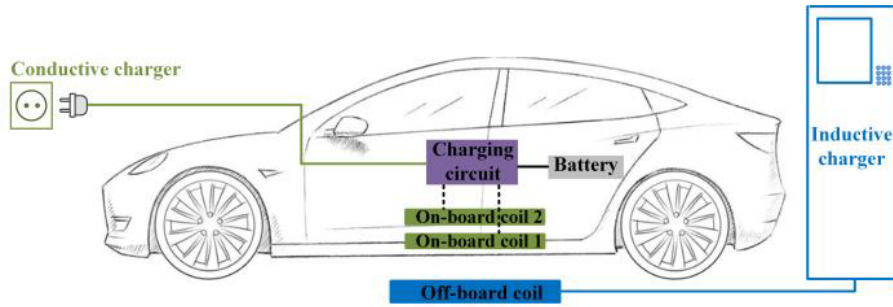


**Figure 3.1:** Proposed concept of inductive and conductive EV hybrid charger [114].

losses. Minimizing this gap is therefore essential to improve the efficiency of the system.

Both charging modes work with a CC/CV profile. The wireless charging of the vehicle is performed thanks to an off-board primary inverter that converts the grid current to a high-frequency current of 85 kHz. This current feeds the primary coil, which includes an LCC resonant tank to improve misalignment efficiency. The magnetic field generated passes through the two coils installed in the vehicle and induces a high-frequency voltage, which is rectified using an uncontrolled rectifier and the anti-parallel diodes of the on-board inverter. Therefore, there are two ways by which the current flows to the battery, shown in the schema of Figure 3.2. Load regulation is carried out by phase-shifting technique in the primary inverter.

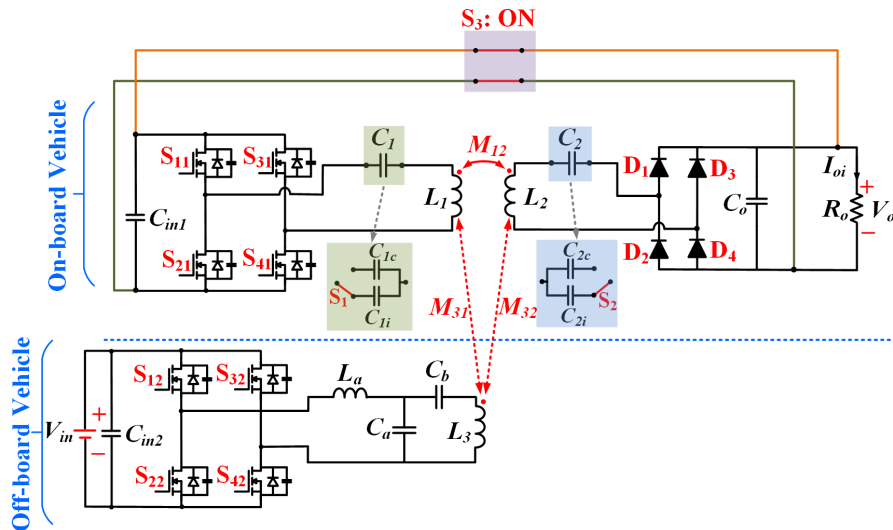


**Figure 3.2:** The proposed hybrid charger with inductive mode configuration [114].

Conductive charging uses only the two coils installed in the vehicle in a similar process to wireless charging. In this case, an on-board inverter generates the high-frequency current necessary for the transfer. The charging power is regulated using a frequency control

that operates in the range between 100 and 140 kHz.

The proposal has been implemented in a 3-kW hybrid charger prototype with proven feasibility. The results show that the system operation is valid throughout the range of battery loads, with efficiencies higher than 93% in conductive mode and 87% in inductive mode. These efficiency levels are reached because the system operates in ZVS when the phase angle of the input impedance is high, although it increases the reactive power in the circuit. Efficiency is also analysed under misalignment with an equivalent resistance of 53.3  $\Omega$ , reaching values greater than 90% with 15 cm of misalignment and greater than 80% with 30 cm. Finally, it has been verified that the prototype complies with the limits for electromagnetic emissions.

Pages 66-78 are hidden due to copyright. They contain the following paper:

B. Vu, J. M. Gonzalez-Gonzalez, V. Pickert, M. Dahidah and A. Trivino, "A hybrid charger of conductive and inductive modes for Electric Vehicles," *IEEE Transactions on Industrial Electronics*, Early Access, 2020. doi: 10.1109/TIE.2020.3042162.

### 3.3 Design and implementation of a cost-effective wireless charger for an electric bicycle

Wireless vehicle charging is traditionally associated with cars. However, this technology is also compatible with other types of vehicles, such as buses, motorcycles, drones and e-bikes. Developing a prototype for any vehicle is always a challenge, as its design must be adapted to its technical requirements. Larger vehicles usually include large-capacity batteries, so their chargers must be able to operate at high power so that the process does not take an excessive length of time. In addition, these batteries operate with high voltages that require adequate power electronics for these levels. However, the requirements for lighter vehicles are different: the charging power is no longer a determining factor because it is limited by the C-rate of their batteries. The priority of these systems is to find a solution that is compact enough so that it can be installed in the vehicle while maintaining a low cost so that its implementation is attractive to users.

This contribution aims to develop an 84-W prototype for charging a Torrot City Surfer e-bike, including designing and implementing all the charger components, as well as the control system, which regulates the battery charge in a simple and robust way.



**Figure 3.3:** Picture of e-bike wireless charger prototype.

The prototype design process begins with the transmission coils, which have been designed using a circular structure. This type of coil has a lower tolerance to misalignment than rectangular coils. However, for this application, it has been installed on a physical

support that guarantees its alignment with the secondary coil. Under these circumstances, circular coils provide better efficiency than rectangular coils. The design was finally implemented using Litz wire, which reduces the Skin effect and therefore the losses.

Testing the prototype in a real vehicle poses additional challenges when designing the coils, as the working conditions are no longer ideal. One of the main difficulties is the effect that the metallic parts of the vehicle have on the magnetic field. In the analysis carried out in the laboratory, we observed that the surrounding conductive materials affect the equivalent circuit of the charger. The interfering materials can be modelled by adding a third mesh composed of an inductor and a resistor ( $L_3$  and  $R_3$  respectively). Figure 3.4a shows the equivalent circuit with the three meshes where the primary side is composed of the primary coil and compensation network capacitor and the secondary side is composed of the secondary coil and the compensation network capacitor. In order to simplify the analysis, we propose a solution that makes it possible to reduce the circuit to a two-mesh equivalent topology. The effects of the surrounding interfering materials are incorporated by modifying the values of the inductances and the resistances. The scheme of this proposal is shown in Figure 3.4b.

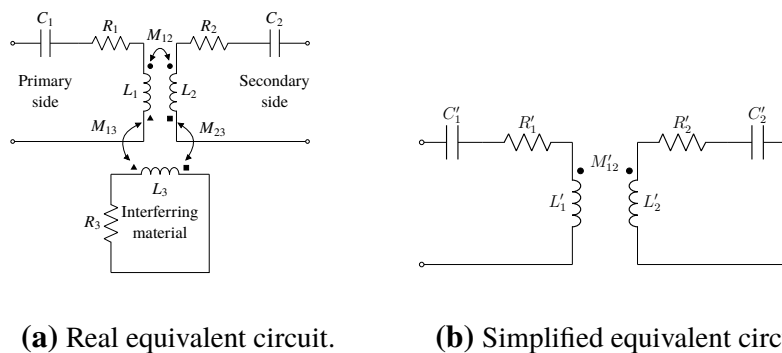


**Figure 3.4:** Model of the magnetic coupling of the e-bike and the surrounding interfering materials.

The final positioning of the coils has been decided based on the experimental analysis of the three positions described in Figure 3.5. The front area of the bike (position A and B) has a negative effect on the efficiency, since the spokes of the wheel, fork and braking system are made of steel. This effect is even more significant in position B due to the inclination of the fork and the closer proximity to the bike frame. In contrast, position C achieves a good level of efficiency thanks to the low metal content of the seat. Both the frame — because it incorporates the battery inside — and the rear wheel — due to the amount of metal in the gear system — were discarded from the analysis as it was not feasible to incorporate the coil in those positions.

The design process for the charger also includes compensation system sizing and power electronics topology. The compensation network has been implemented using a SS struc-

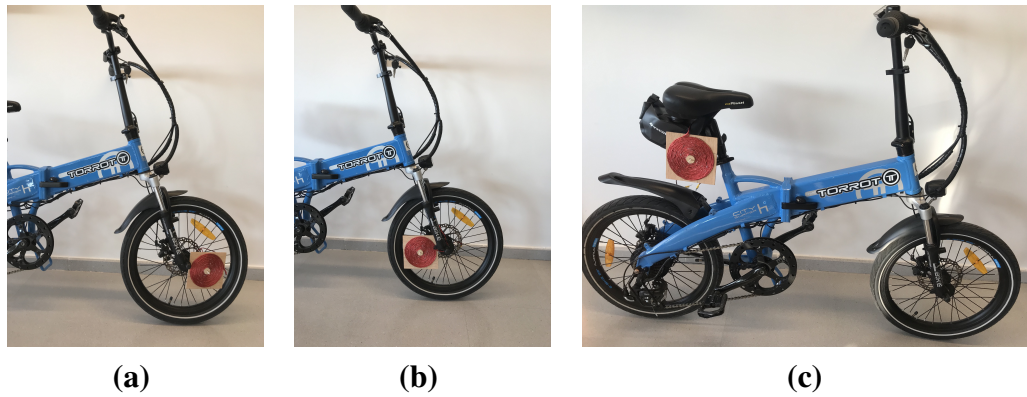


**Figure 3.5:** Tested positions of the secondary coils.

ture, which achieves good performance. These structures are composed of polypropylene capacitors as the only component. The high frequency signal is generated by a full-bridge inverter that integrates SiC MOSFETs. This inverter is also in charge of regulating the flow of transmitted energy. The full-bridge topology is also used for the secondary rectifier, which is composed of SiC diodes to reduce losses.

Another challenge when implementing a prototype in a real system lies in the bicycle battery. In laboratory setups, a resistance that maintains its constant value is used to emulate the battery. However, the behavior of the batteries evolves during the charging process, that is, as the State-Of-Charge (SOC) increases. This effect has to be considered by the control system. We have implemented a simple but robust CC/CV charging algorithm that sets the battery charging current at 2 A until the maximum battery voltage (42 V) is reached. When this happens, the charging current is regulated to prevent the voltage from exceeding the maximum value. Figure 3.6 shows a schematic of the implemented algorithm.

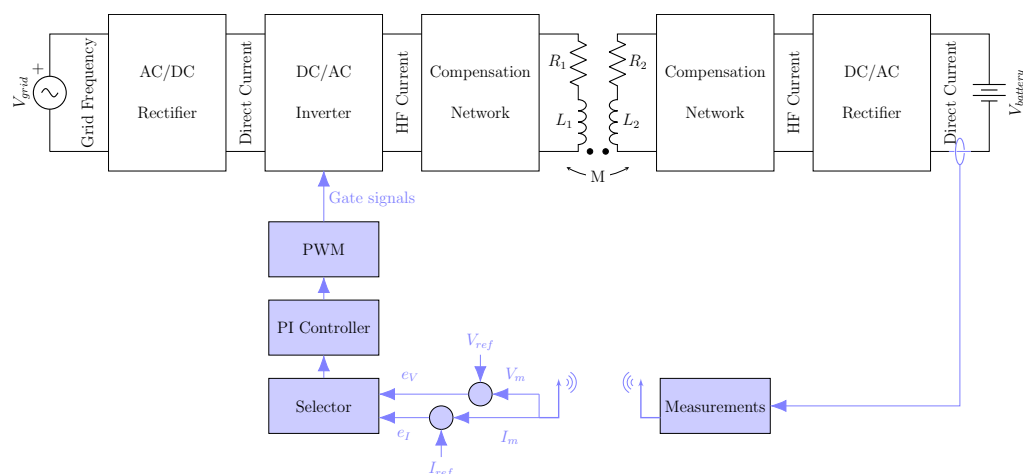


**Figure 3.6:** Proposed prototype and control schemes.

The experimental results have shown how the position of the coils greatly affects the efficiency of the system, obtaining 92% when it is in position C compared to approximately 80% achieved in the other two positions. The charging process, regulated by the CC/CV control, has also been validated. It has been observed that the efficiency decreases when the battery SOC increases. These results conclude that both coil position and control algorithm must be carefully selected during the design process in real prototypes because they affect the efficiency and, therefore, the viability of a wireless charger.



# Design and implementation of a cost-effective wireless charger for an electric bicycle

A. TRIVIÑO<sup>1</sup>, J.M GONZÁLEZ-GONZÁLEZ<sup>1</sup>, J.A. AGUADO<sup>1</sup>, (Member, IEEE)

<sup>1</sup>Escuela de Ingenierías Industriales, Universidad de Málaga, Spain.

Corresponding author: Alicia Triviño (e-mail: atc@uma.es).

“Funding for this project was partially provided by the Spanish Ministerio de Ciencia e Innovacion (MICINN) project PID2019-110531-RA-I00 from the "Proyectos de I+D+i - RTI Tipo A" program and by the II Plan Propio Smart-Campus by the University of Malaga.”

**ABSTRACT** Wireless charging is a convenient method of charging Electric Vehicles (EVs). Its application has been widely studied for electric cars but so far there have been limited experiments for electric bicycles (e-bikes). This paper addresses the design process and implementation details related to a wireless charger for a specific e-bike. Some issues such as the position of the secondary coil or the control algorithm prove to be crucial to the performance of the wireless transfer. Concerning the placement of the secondary coil, the paper proposes and validates a theoretical model to quantify the effects of the surrounding interfering materials. A CC-CV (Constant Current - Constant Voltage) control algorithm has been implemented to validate the theoretical results in these two charging phases. The control, the coils and the compensation networks have been designed to be simple and robust. The theoretical model, the charger and its control have proven to be effective in a real 84-W e-bike.

**INDEX TERMS** Control, Coil position, Electric bicycle, Wireless charger.

## I. INTRODUCTION

**E**LECTRIC Vehicles (EV) constitute a sustainable mode of transport to cope with the greenhouse emissions generated by fuel-based vehicles. Of all electric vehicles, electric bicycles (e-bikes) are considered to be the most convenient form of transportation in the Smart City due to their low cost and maintenance, capability to operate in crowded environments and the fact that there is no need for licences or road taxes [1]. These advantages are helping to expand the e-bike market. In fact, it is expected to number up to 6.8 million units in 2024, which represents a 8.2% annual growth rate from 2016 [2]. The European region accounted for 20.12% of the global market, with the fastest growth occurring during the forecast period.

Wireless Power Transfer (WPT) can be foreseen as a suitable technology to promote the use of Electric Vehicles [3]. In the case of e-bikes in particular, WPT eases their charge process, makes the operation safer [4] and also broadens the scenarios in which the vehicle can be charged (even while moving) [5]. Although there are multiple technologies associated with WPT, the technology used most extensively

for Electric Vehicles is inductive resonant WPT [3]. The basis of resonant WPT consists of two coupled coils referred to as the primary and the secondary coil. The primary coil is connected to the grid and, when powered, generates a time-varying magnetic field. The secondary coil must be placed so that it concatenates some of the generated magnetic field. This field will then induce a voltage on the secondary coil. As the secondary coil is connected to the EV battery, this component can be charged. More complex structures have been proposed with three [6]–[8] or four coils [9]. The power transfer is clearly affected by the relative position or misalignment between the primary and the secondary coils.

The use of inductive WPT in electric cars has already been tested in some prototypes and experiments, so we can conclude that they have reached a mature status [10]. However, so far a limited number of experiments have been conducted with other types of vehicles such as e-bikes. The application of this technology to e-bikes is not straightforward if we only consider the knowledge acquired in the context of electric cars. Firstly, weight and physical stability are critical in an e-bike. These two conditions can be compromised with the



incorporation of bulky and heavy power components for the wireless charge. Secondly, the costs need to be much lower than for a car. The maintainability must also be minimized in order not to lose the advantages of this kind of transportation. With these requirements in mind, the design of these systems focuses on the particular features of an e-bike battery. Currently, the most popular types of batteries in e-bikes are the Li-Ion batteries [1]. These batteries are charged in a two-phase sequence. During the first phase, the battery is charged at a Constant Current (CC) until the battery reaches a voltage level. In the second phase, the battery is charged with the reached/Constant Voltage (CV) level until the current decreases to a predetermined threshold. The equivalent resistance of the battery during the process also varies. Moreover, the predefined current in the CC mode and the regulated voltage in the CV mode must be guaranteed even when the system suffers from a deviation from its standard operating conditions [11].

Thus, the key design steps of an e-bike wireless charger are the definition and position of the coils, the matching networks, the control strategy and the operational frequency. The main approaches to these subsystems are described next.

A core element in the wireless charger is the coupled coils. In electric cars, the secondary coil is placed underneath the chassis so that this element minimizes electromagnetic emissions inside the vehicle. The position of the secondary coil is more or less fixed and there has been no debate on this point. Indeed, there are new standards that fix the coil in the aforementioned position [10]. However, other vehicles do not have this metallic structure and therefore the position of the secondary coil may be arbitrary. This is the case with e-bikes. The authors in [12] presents the design of two complex pairs of coils to be placed in the kickstand for a single or double support. The coils rely on ferromagnetic materials to improve the power transfer, which makes the charger more expensive than when using simple coils. Interference with other materials of the e-bike has not been considered, as the prototype does not include this type of vehicle. A series-resonant inductive system is proposed in [13] for a wireless charger. It also suffers from the same inconvenience as the previous approach because it includes an E-shape coil with ferromagnetic material. Alternatively, a bulky coil is placed in the base of the rear wheel in [5]. The volume and position of the secondary coil may restrict its applicability. The work in [14] proposes the placement of the secondary coil in a salient pole of the charging structure. The pole is inserted in the bicycle armature to increase the efficiency of the WPT while avoiding coil misalignment. Although the coupling coefficient is increased, this solution demands a structure for the charging station, which may also be prone to damage. A three-layer coil for the primary side and some switched capacitors are proposed in [15] to change from the CC to the CV mode. The work in [8] implements the power transmitter as two coils. One of the coils is only connected for the CV mode. As can be observed, these experiments rely on complex structures for the coils and have not addressed the

most convenient position for these components.

Wireless chargers count on matching networks to make the system operate at resonance. The most simple topology is the Series-Series, as used in [13], but there are other multi-resonant approaches. The work in [16] proposes the use of switched capacitors and coils on the secondary side to have a different circuit when the battery is charged in CC or CV mode. In [4], the authors propose a S-LCC topology for the control of the CC-CV charging. On the primary side, there is a switch that activates/deactivates one capacitor for each mode. On the secondary side, a reactive network with two capacitors is implemented. As concluded in [17], [18], the Series-Series is the most cost-effective solution. The authors in [6] opt for two different capacitors in a Series-Series topology. One of the capacitors on the primary side is used for the CC mode and another for the CV mode.

Control algorithms are necessary to ensure a correct wireless power transfer under misalignment or different battery status. The work in [11] presents a control algorithm, which is tested in a real e-bike. The designed control sets the voltage output at 48 V so it does not implement the CC mode. The experiments, which were conducted for a linear load instead of a battery, show a low efficiency. The authors have not carried out an analysis of the best position for the secondary coil. In fact, the efficiency of their charge is very low (25-80 % for a coil gap of 0-10 cm), which could be derived from a magnetic leakage on the components of the bicycle due to the position selected for the secondary coil. Alternatively, the work in [17] varies the current according to the relative position of the coils. To extend the durability of the battery, it is preferable to perform the charge in a CC-CV mode. In addition, the work in [17] concludes that a cost-effective control algorithm should be preferred for e-bikes. The work in [6] uses some switches and two coils on the primary side to change the circuit process for a CC and a CV mode. In order to identify when to set the corresponding operation mode, the equivalent resistance of the battery is estimated. A perfectly-tuned Series-Series compensation network is assumed for this estimation.

As we have previously stated, it is important to reduce the costs and weight of the secondary side to make a commercial-grade e-bike charger appealing. Thus, the secondary structure should be reduced. This implies minimizing the additional components (coils and matching networks) and implementing a simple control algorithm for the CC and CV charging modes. Taking into account these requirements, we design, implement and test a wireless charger for a specific e-bike. The contributions of this work are twofold:

- Providing the details required for effective implementation of a wireless charger for an e-bike. In contrast to some previous works [4], [6], [7], [12], [13], [16], [17], the design has taken into account the impact of mounting the secondary coil on the vehicle. With this goal in mind, we propose a theoretical model, which includes the effects of the surrounding interfering materials. For some measurements, the model has been vali-

dated and tested on an e-bike instead of in a laboratory setting. As demonstrated theoretically and experimentally, the position of the secondary coil clearly affects the electromagnetic emissions and, in turn, the losses [19]. In contrast to [18], this work has evaluated the most convenient position of the secondary coil while keeping in mind its usability. The experimental results have revealed the impact of the position of the secondary coil on the system efficiency, temperature risks and electromagnetic emissions.

- Designing a low-cost and reliable secondary-side charger with a simple but effective control that manages the CC and the CV charging modes to illustrate the performance of the WPT system and compare it with the theoretical results derived from the proposed model. The defined control strategy does not rely on additional reactive components. A simple Series-Series compensation topology is used as in [8], but the CC and the CV charging modes are implemented as recommended for the Li-Ion batteries [1]. With this approach, the costs of the charger in the bicycle are reduced while its reliability is improved.

The remainder of the paper is structured as follows. Section 2 describes the equivalent circuit of the charger and presents the theoretical model used to quantify the losses caused by the surrounding interfering materials. This description is necessary for the design, as shown in Section 3, which addresses the implementation issues of this charger. In particular, it focuses on the three potential positions of the secondary coil and validates the theoretical model developed previously. Section 4 describes some related work on control algorithms for e-bikes and presents a simple but effective control algorithm, which will be used to validate the model. Section 5 presents the experimental characterization of the wireless charger when installed on the e-bike for the three positions analyzed. Finally, Section 6 summarizes the main conclusions of this paper.

## II. THEORETICAL ANALYSIS

For our design proposal, we aim to use a simple but controllable wireless charger. We opted for one of the most simple structures of an EV wireless charger, as depicted in Figure 1. It does not include any DC/DC converter on the secondary side, which eases its implementation and control [11], [18].

This diagram is usually modelled as an electric circuit as shown in Figure 2. In this circuit, we have two coupled coils ( $L_1$  and  $L_2$ ) and their parasitic resistances ( $R_1$  and  $R_2$ ).  $M$  corresponds to the mutual inductance between the transmitter and the receiver. The matching networks follow a simple but effective Series-Series topology as in [13]. They are composed of capacitors  $C_1$  and  $C_2$ . Although there are complex matching networks [16], the Series-Series compensation network has shown its effectiveness in coping with coil misalignment at a low cost [11].

In this simplification, the output inverter  $V_1$  is a sinusoidal wave assuming a first harmonic approximation. The

impedance of the battery at the input of the secondary rectifier is modelled as the resistance  $R_L$  (referred to as the equivalent load resistance). The relationship between the internal resistance of the battery  $R_{Bat}$  and  $R_L$  is expressed as follows:

$$R_L = \frac{8R_{Bat}}{\pi^2} \quad (1)$$

With a mesh-based analysis, we can state that:

$$\vec{V}_1 = \left( R_1 + j\omega L_1 + \frac{1}{j\omega C_1} \right) \vec{I}_1 - j\omega M \vec{I}_2 \quad (2)$$

$$\vec{V}_2 = \left[ (R_2 + j\omega L_2) \vec{I}_2 - j\omega M \vec{I}_1 \right] = \left( R_L + \frac{1}{j\omega C_2} \right) \vec{I}_2 \quad (3)$$

From the two previous equations, we can infer the input impedance  $Z_{in}$  as follows:

$$Z_{in} = \frac{\vec{V}_1}{\vec{I}_1} = R_1 + j \left( \omega L_1 - \frac{1}{\omega C_1} \right) + \frac{\omega^2 M^2}{Z_{22}} \quad (4)$$

where  $Z_{22} = (R_2 + R_L) + j \left( \omega L_2 - \frac{1}{\omega C_2} \right)$

In order to have a purely ohmic input impedance, the reactive term must be null. This condition is expressed with the following equation:

$$\omega L_1 - \frac{1}{\omega C_1} = -Imag \left( \frac{\omega^2 M^2}{(R_2 + R_L) + j \left( \omega L_2 - \frac{1}{\omega C_2} \right)} \right) \quad (5)$$

After developing this further, we obtain:

$$\omega L_1 - \frac{1}{\omega C_1} = \frac{\omega^2 M^2 \left( \omega L_2 - \frac{1}{\omega C_2} \right)}{(R_2 + R_L)^2 + j \left( \omega L_2 - \frac{1}{\omega C_2} \right)^2} \quad (6)$$

This last equation is verified when the two pairs of coils and their corresponding capacitor constitute two independent resonant tanks at the same operational frequency ( $\omega_0$ ).

$$\omega_0 = \frac{1}{\sqrt{L_1 C_1}} = \frac{1}{\sqrt{L_2 C_2}} \quad (7)$$

Thus, to design an SS compensation network, the capacitors can be defined with their corresponding coils once the frequency is set according to the application specifications.

The system efficiency is defined as the ratio between the active power delivered to the load and the active power generated by the source. This parameter can be formally expressed as:

$$\eta = \frac{R_L I_2^2}{R_1 I_1^2 + R_2 I_2^2 + R_L I_2^2} = \frac{R_L}{\frac{R_1 I_1^2}{I_2^2} + R_2 + R_L} \quad (8)$$

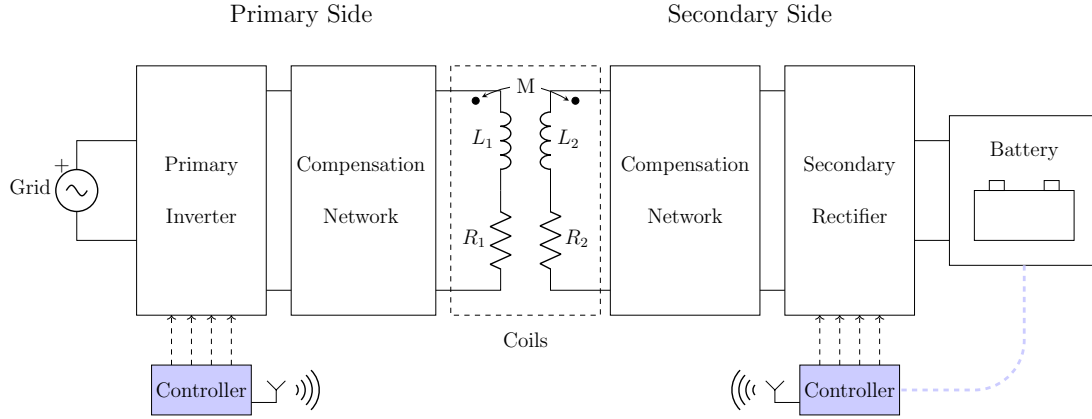


FIGURE 1. Generic diagram for magnetic resonance wireless chargers with compensation networks.

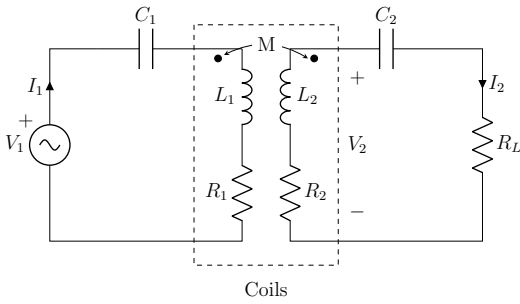


FIGURE 2. Core structure of a wireless charger with Series-Series compensation network.

From Equation (3), we can infer the relationship between the modules of the  $I_1$  and  $I_2$  currents.

$$\left| \frac{I_1}{I_2} \right| = \frac{R_2 + R_L}{\omega_0 M} \quad (9)$$

So that the system efficiency is equal to:

$$\eta = \frac{R_L}{R_1 \left( \frac{R_2 + R_L}{\omega_0 M} \right)^2 + R_2 + R_L} \quad (10)$$

In order to maximize the efficiency, the denominator of the previous expression should be minimized. This implies that:

$$\frac{R_2 + R_L}{\omega_0 M} \ll 1 \quad (11)$$

Thus,

$$\omega_0 \gg \frac{R_2 + R_L}{M} \quad (12)$$

If the relationship in Equation (12) holds, the efficiency corresponds to:

$$\eta \cong \frac{R_L}{R_2 + R_L} \quad (13)$$

As a conclusion, we can state that a perfectly-tuned Series-Series system keeps its efficiency in a wide range of gaps.

For an efficient power transfer, it is desirable to minimize the ratio  $R_2/R_L$ .

However, the coils will not be isolated in a real prototype. In fact, there will be other conductive materials of the vehicle surrounding the coils, which will alter the equivalent circuit. In this paper, we model their effects in the circuit analysis by incorporating only one additional mesh. This model represents an application of the approach derived in [20], where two additional meshes were incorporated to model the two types of shielding materials. In our model, we mainly have one single interfering material so we modified the previous model to adapt to this condition. This new mesh is composed of a resistance ( $R_3$ ) and an inductor ( $L_3$ ), with the latter element coupled with the primary and the secondary coils. This effect is illustrated in Figure 3.

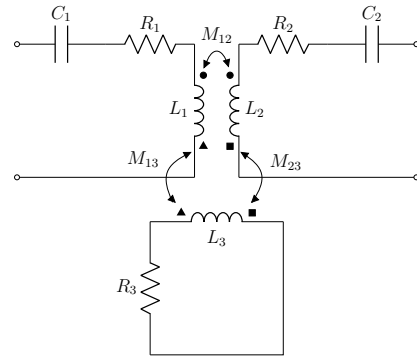


FIGURE 3. Model of the core structure of the e-bike and the surrounding interfering materials.

$R_3$  and  $L_3$  model the losses caused by the interfering materials. In particular,  $R_3$  models the conductive losses. As presented in [20], the resistance of a plate can be approximated to:

$$R_3 \propto \sqrt{\rho f \mu} \quad (14)$$

where  $\rho$  and  $\mu$  are the resistivity and the permeability of the interfering material respectively.

With circuitual simplifications, it is possible to derive the equivalent coupler in Figure 4.

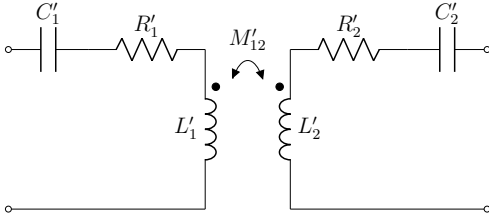


FIGURE 4. Simplified equivalent circuit of a coupler with surrounding (ferromagnetic and metallic) materials.

The values of these components in the simplified model are:

$$Z'_{11} = Z_{11} + \frac{\omega^2 M_{13}^2}{Z_{33}} \quad (15)$$

$$Z'_{22} = Z_{22} + \frac{\omega^2 M_{23}^2}{Z_{33}} \quad (16)$$

$$M'_{12} = M_{12} \left( 1 - \frac{K_{13} K_{32}}{K_{12}} \right) \quad (17)$$

where  $Z_{33} = j\omega L_3 + R_3$ ,  $Z_{11} = j\omega L_1 + \frac{1}{j\omega C_1} + R_1$ ,  $Z_{22} = j\omega L_2 + \frac{1}{j\omega C_2} + R_2 + R_L$  and  $K_{12}$ ,  $K_{13}$  and  $K_{32}$  are the coupling coefficients associated to  $M_{12}$ ,  $M_{13}$  and  $M_{32}$  respectively.

If we further analyse this last expression, we can derive that:

$$\text{Real}(Z'_{11}) = R'_1 = R_1 + \frac{\omega^2 M_{13}^2}{|Z_{33}|^2} * R_3 \quad (18)$$

$$L'_1 = L_1 - \frac{\omega^2 M_{13}^2}{|Z_{33}|^2} * L_3 \quad (19)$$

$$\text{Real}(Z'_{22}) = R'_2 = R_2 + \frac{\omega^2 M_{32}^2}{|Z_{33}|^2} * R_3 \quad (20)$$

$$L'_2 = L_2 - \frac{\omega^2 M_{32}^2}{|Z_{33}|^2} * L_3 \quad (21)$$

Thus, the self-inductances and the new mutual inductance of the equivalent coupler are lower than in the configuration of the original coils without the conductive materials [21]. As for the resistances, they are increased. In the particular case of the e-bike, the effects are expected to be more severe on the secondary side due to its proximity to the interfering material, so the parameters of the equivalent secondary side will change more noticeably. With regard to Equation (10), the efficiency will also be reduced as the new  $R_2$  will be higher. The system in a real bicycle will also experience a lower output power as the equivalent mutual inductance decreases. Since the value of  $R'_2$  is dependent on  $R_3$  as expressed in Equation (20), the greater the resistance of the

interfering materials and their size, the greater the increase of  $R_2$ . Thus,  $R'_2$  is dependent on the interfering materials, i.e. on the position of the secondary coil. The efficiency and the power transfer are both affected by the placement of this component in a real e-bike. This effect is not reflected in the experiments conducted without a real vehicle.

When connected to the battery, we can work with the input impedance of the wireless charging coupler. In a real vehicle, the input impedance is equal to:

$$Z'_{in} = \frac{\vec{V}_1}{\vec{I}_1} = Z'_{11} - \frac{\omega^2 M_{12}^2}{Z'_{22}} \quad (22)$$

Different positions of the secondary coil are associated with a different distribution of the surrounding materials. Thus, they will experiment different input impedances.

So far, we have described the efficiency related to the coupler, but a real prototype will also be affected by the efficiency of the power converters, as we will explain in Section 5.

### III. COIL DESIGN AND PLACEMENT

Similarly to the approach proposed in [3], we first list the requirements imposed on the WPT charger for an e-bike. The identified requirements are:

- Low cost
- Low weight
- Avoiding the heating of some metallic structures of the bicycles due to the magnetic field. This could affect the safety of the charge and affect the users' health.

One of the key phases in the design of the wireless charger is the coil design. In this particular case, misalignment may not be so severe, as the bicycle can be supported by an auxiliary platform that can guarantee the position of the vehicle during the charge process (e.g. Daymak drive system). Due to their simplicity, the topologies analysed for the e-bike coils were the square and circular ones without additional ferromagnetic materials, to obtain low-cost components. Alternative options such as DD or DDQ were discarded as they result in more expensive coils [3].

For the e-bike in question (Torrot City Surfer), we designed two circular coils with the following features:

TABLE 1. Parameters of the developed coils.

Primary coil		Secondary coil	
$L_1$	150.47 $\mu\text{H}$	$L_2$	27.08 $\mu\text{H}$
$R_1$	195.01 m $\Omega$	$R_2$	22.89 m $\Omega$
$r_{1,in}$	5 cm	$r_{2,in}$	1.5 cm
$r_{1,out}$	11 cm	$r_{2,out}$	7 cm
$N_1$	28	$N_2$	20
M		13.04 $\mu\text{H}$	

where  $r_{1,in}$  and  $r_{2,in}$  are the internal radius of the primary and the secondary coil respectively. The variables  $r_{1,out}$  and  $r_{2,out}$  are the external radius of the primary and the secondary coil and  $N_1$  and  $N_2$  are the number of turns of both coils. For a separation of 7 cm, the mutual inductance is 13.1  $\mu\text{H}$ . These



dimensions have been carefully selected to represent: (i) a negligible additional weight in comparison with the e-bike (21 kg) and (ii) an element that could be easily inserted in the bicycle wheel. The next image shows the implementation of the coils. The coils are built with Litz-wire in order to reduce the skin effect at the operating frequency.

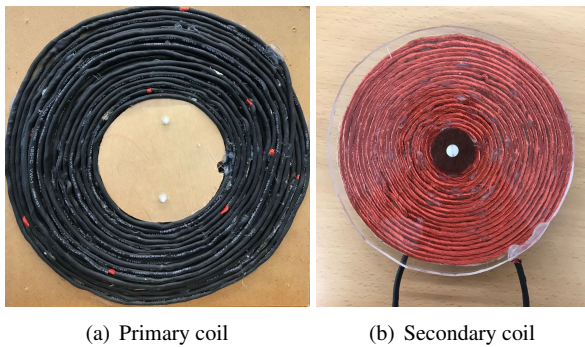


FIGURE 5. Implementation of the coils

The operating frequency is selected as 85 kHz. In this way, the charger can comply with international recommendations for EV chargers, in case e-bikes are included in the future [10]. As mentioned in Section II, the prototype has been designed following a Series-Series topology as it allows for simple control. This topology uses one capacitor in series with the coil on each side of the charger. Their capacitance value depends on the self-inductance of the coils and is computed using (7). For the coils defined in Table 1, the capacitance values for the matching network are:

TABLE 2. Parameters of the matching network.

Capacitor	Theoretical value [nF]	Measured value [nF]
$C_1$	24.43	24.85
$C_2$	135.83	145.52

The matching network has been made using polypropylene capacitors because their good performance under high frequencies makes them suitable for this prototype.

One of the goals of the paper is to evaluate the ideal position of the coils in a real bicycle, which could differ from what is expected. In fact, the positioning of the coils constitutes one of the main difficulties with this kind of EV wireless charger. In electric cars, the position of the secondary coil is not a concern as it is always installed under the chassis of the vehicle. In contrast, there is no fixed position for the secondary coil on e-bikes. Moreover, its placement will impact on the bike's stability, the charger efficiency and even the feasibility of using the bike immediately after the charging process because of derived heat problems. As presented in the previous section, the surrounding materials alter the equivalent resistance of the developed model and, in turn, other performance metrics are also altered. In order to validate the previous model, we have set three tentative positions for the coil on the e-bike taking into account the

quantity of interfering materials found nearby. In particular, we have studied the materials used in the Torrot City Surfer e-bike. There are two representative placements on the front wheel, and one close to the seat. The proportion of the surrounding materials is similar on the back wheel, and so the effects are assumed to be alike to those obtained in two of the positions tested. The alternative position on the bicycle frame was ruled out, as initial tests showed that the battery suffered from a noticeable increase in temperature, which may cause some damage. Other complex placements, which were not feasible in a pre-built bicycle, were also omitted. Thus, the positions analysed are:

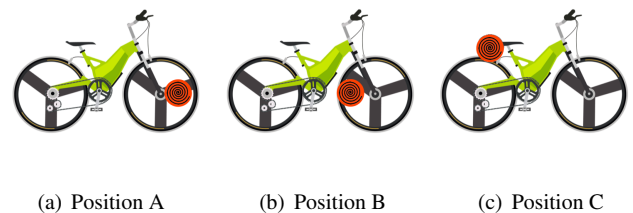


FIGURE 6. Coil positions analysed.

For the tentative positions, we have derived the percentage of interfering material in a circular area with a diameter equal to twice the radius of the secondary coil. Through an image analysis, we have quantified the number of pixels associated to the interfering materials, i.e. air, aluminum and plastic. Please note that the magnetic properties of these materials are quite different. The results are summarized in Table 3.

TABLE 3. Percentage of surrounding materials for the positions analysed.

Pos.	Air [%] $\mu: 1.25 \cdot 10^{-6}$ $\rho: 1.3 \cdot 10^{16}$	Plastic [%] $\mu: -$ $\rho: 10 \cdot 10^{20}$	Aluminium [%] $\mu: 1.25 \cdot 10^{-6}$ $\rho: 3.9 \cdot 10^{-8}$
A	46	23	31
B	43	25	32
C	40	60	0

Units:  $\mu[H/m]$ ,  $\rho[\Omega m]$

According to Equation (21), the input impedance of the positions is affected by the way in which the interfering materials modify the parameters of the equivalent circuit in Figure 4. We have conducted multiple tests to validate this model. In particular, for the three tested positions we have measured the relationship between the input voltage and the input current. From these measurements, we have derived a linear relationship. The proportional constant is a complex number, which represents the input impedance. The next Figure reflects the module of the input impedance for the three positions tested and for the situation in which the coils are not mounted on a vehicle.

The variation of the input impedance is a consequence of modifying the parameters in the model presented in Figure 3. Table 5 reflects this effect for the three positions tested in a real e-bike. In particular, the Torrot City Surfer has

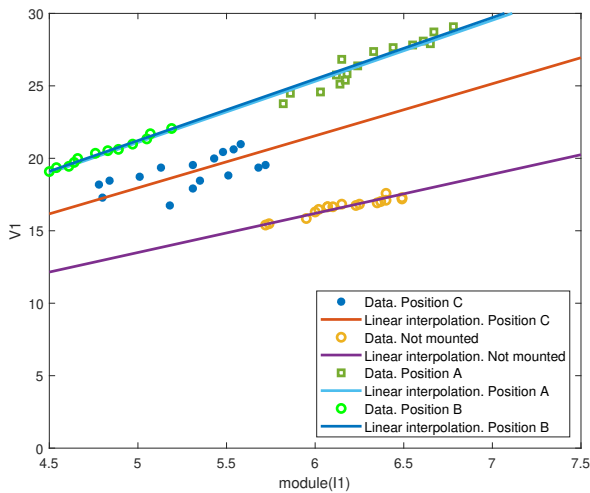


FIGURE 7. Linear interpolation of the measurements as an input impedance.

TABLE 4. Modelled input impedance

Position	Module [ $\Omega$ ]	Angle [rad]
Not mounted	2.69	0.45
A	4.218	0.47
B	4.24	0.18
C	3.59	0.19

been used for these experiments, along with an LCR meter. There are notable changes in the measured resistance of the secondary coil for each of the three positions. As predicted by the model, the resistance levels of the coils increase when they are surrounded by interfering materials (Equations (18) and (20)), whereas the inductances decrease (Equations(17) , (19) and (21) ).

TABLE 5. LCR measurements.

	L1[ $\mu H$ ]	R1[ $m\Omega$ ]	L2[ $\mu H$ ]	R2[ $m\Omega$ ]	M[ $\mu H$ ]
Not mounted	150.47	195.01	27.07	22.89	13.04
A	147.72	452.70	26.74	58.20	11.45
B	148.76	189.50	26.93	492.01	12.02
C	150.33	206.50	26.86	22.71	12.82

An alternative to this model is Finite Element Analysis (FEA) software. However, this software tool requires some expertise on how to proceed with the surface triangle mesh, which may not be easily acquired. In addition, FEA simulations are computer-based and time-consuming, which may delay the design process considerably.

#### IV. PROPOSED ROBUST AND SIMPLE CONTROL

To extend the durability of lithium-ion batteries, they must be charged with a two-phase method referred to as CC/CV [3]. This strategy consists in charging the battery at constant current until the maximum battery voltage recommended by the battery manufacturer is reached. When this happens, the charge is regulated so that the voltage is kept constant. The

value of the charging current is also chosen based on the characteristics of the battery, although values lower than the recommended maximum help to extend the battery lifespan.

One of the goals of this paper is to evaluate the developed model to determine the effects of the interfering materials on a complete CC-CV charge. The following figure shows an example of a theoretical CC/CV charging application for the battery used in the prototype. It has a first constant-current stage at 2 A in which the voltage increases, followed by a constant-voltage stage at 42 V in which the charging current gradually decreases. During the charge process, the equivalent resistance of the battery changes with an increasing non-linear function.

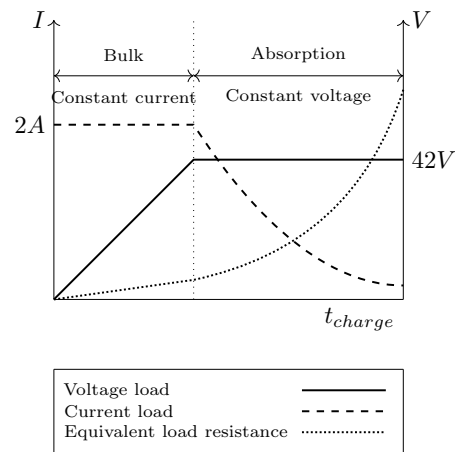


FIGURE 8. CC/CV charge.

This control technique has been applied in the literature for generic EV wireless chargers using several strategies. The variants mainly depend on the converter in which they operate and the communication systems used. In addition, the proposal in [22] modifies the topology to include switches to commute the devices operating in each phase. Apart from the bulky switches, this proposal presents a main limitation as it is not able to regulate the charging current or voltage. This shortcoming restricts the compatibility between different devices. In the field of power electronics design, it also presents other drawbacks, such as greater design complexity and an increased number of components. It results in a higher cost and weight in a system that seeks to reduce both of these to a minimum. The authors in [23] also apply a strategy in which the charger topology is modified. Specifically, they opt for a dual full-bridge inverter and a PI control, which makes the system more complex.

Conversely to what is observed when switches are added, options based solely on adjusting the operation of the converters result in simpler systems, which are more convenient for an e-bike charger [24]. Relying on communications between primary and secondary sides allows for the application of simpler and equally robust control strategies, as shown in [23]. The authors use a dual parallel PI controller installed on the primary side. There are two PI controllers: one for the

current regulation and another for the voltage regulation. A selector forces only one controller to be active depending on the charging mode. Cascade PID controller solutions improve the transition between both charging modes. This solution is applied in [25], but the controller adjusts the grid controlled rectifier instead of the primary inverter. As a consequence, it is necessary to incorporate a Phase Locked Loop (PLL).

Our proposal opts for a simplified approach, as shown in [26] but with two main simplifications. Firstly, there is no need to use intermediate coils, which means that the design process and its implementation are easier in comparison with [26]. Secondly, we include an automation for the selector, which avoids the manual switching for the two charging phases. These modifications ensure the proper application of the two-phase charging while minimizing the required computational resources. This simplification could report in a reduction of the controller. The control scheme is depicted in Fig. 9. As can be observed, only one PI controller is included.

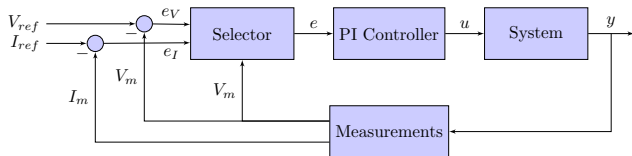


FIGURE 9. Control scheme for CC/CV charging.

The control works as follows. Firstly, the current and the voltage ( $I_m$  and  $V_m$ ) are acquired from the battery connection and sent to the primary side via a wireless communication channel. On the primary side, the measurements are received and processed. The primary control includes two comparison blocks, a selector and a PI controller. During the first charging phase, the charger must operate in the CC mode. The selector has been automated so that the controller receives the current error ( $I_{ref} - I_m$ ) as long as the voltage is lower than  $V_{ref}$ .  $V_{ref}$  corresponds to the maximum indicated by the battery manufacturer. When reached, it means that the CV phase should start. If this occurs, the controller receives the voltage error. It is important to highlight the fact that compatibility with other bikes is ensured as the charging references and the selector’s decision are based on the battery parameters sent by the secondary controller. For our particular e-bike,  $V_{ref}$  and  $I_{ref}$  are 42 V and 2 A respectively, as shown in Figure 8.

Once the selector has chosen the proper error that must be considered, it transfers this data to the PI controller. The PI controller then adjusts the phase switching to apply to the primary inverter. Phase-shifting modifies the output voltage of the primary inverter, thereby regulating the battery charge.

Both the control and the wireless communications have been implemented in a Raspberry Pi, a small single-board computer with Bluetooth and IEEE 802.11 as wireless technologies. More specifically, a Raspberry Pi 4 has been used for the primary controller, while the Raspberry Pi Zero W

has been used for the secondary controller. The choice of a different controller for the secondary side is due to the fact that, despite its lower processing capacity, it has very reduced energy consumption and size. As presented in the requirement lists, these two features must prevail in the e-bike wireless charger.

To comply with the CC/CV charging strategy of the proposed control, the secondary current and voltage measurements are required. The measurements are taken by the Raspberry Pi Zero W, which uses the I2C protocol to communicate with an Analog to Digital Converter (ADC) that converts the analog voltage and current measurements to digital form. These data are sent to the primary controller using a Bluetooth communication.

## V. EXPERIMENTAL EVALUATION

An important goal of our work was to evaluate the performance of the potential configurations of the wireless charger and the control design in a real e-bike. The wireless charger was designed and implemented for an e-bike manufactured by Torrot, in the City Surfer model. In addition to the coils, the compensation networks and the controllers, we also included the power electronics necessary to generate the 85-kHz magnetic field as recommended by SAE J2954. The schematic is illustrated in Figure 10.

One of the biggest challenges for power electronics is the high switching frequency, which can lead to excessively high losses and temperature problems in converters. SiC MOSFETs are suitable switches for these converters, since their low drain-to-source ON-resistance makes it possible to reach high frequencies while maintaining reduced dissipation needs. Specifically, the full-bridge inverter has been implemented using two evaluation boards model KIT8020-CRD-8FF1217P-1 from CREE. This board includes two SiC MOSFET to constitute each of the inverter’s legs. Figure 11 is an image of the primary side equipment. The full-bridge topology has been selected over the half-bridge even though it requires two additional MOSFETs. This is done for reliability purposes, as the current flowing through the converter is halved, which will lead to reduced losses and cooling needs in the conversion stage. This current also affects the losses in the coils. The secondary side includes a full-bridge rectifier composed of SiC diodes.

Figure 12 shows the designed pole for the primary coil, which also has some wooden rails to reduce the misalignment effects. The three positions evaluated for the secondary coil are illustrated in Figure 13 for the secondary coil.

For these three positions, we have measured the rectifier input power and the inverter output power. From these two measurements, we have computed the efficiency of the charger as summarized in Table 6. The inverter and the rectifier currents and the rectifier input voltage are rms values. The experimental efficiencies are measured between the rectifier input and the inverter output, as performed in the theoretical analysis in Section 2. No control has been applied in these tests. For illustrative purposes, we have included two scopes



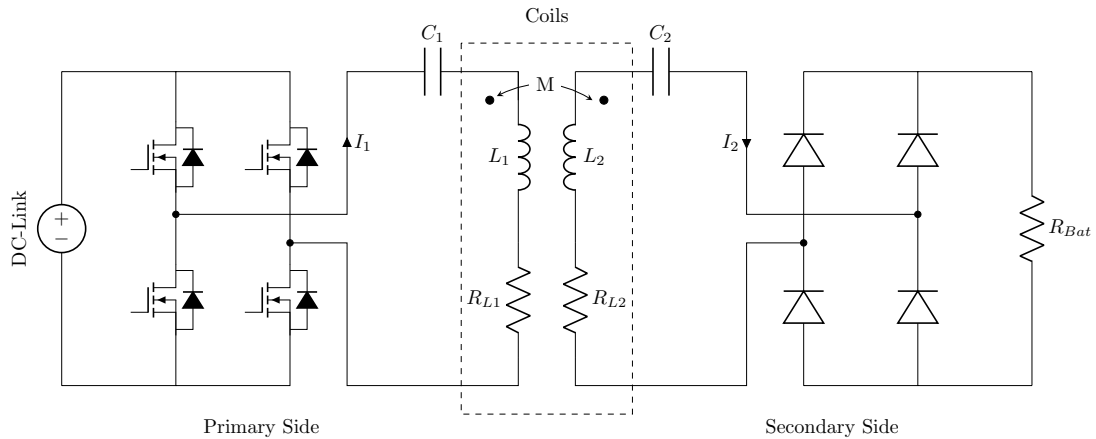


FIGURE 10. Scheme of the proposed charger topology.

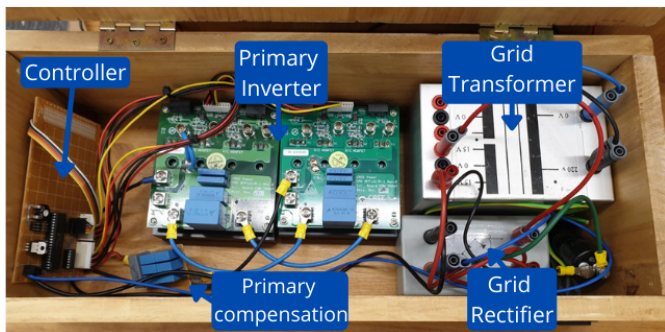


FIGURE 11. Picture of the primary side charger.



(a) Position A. (b) Position B.

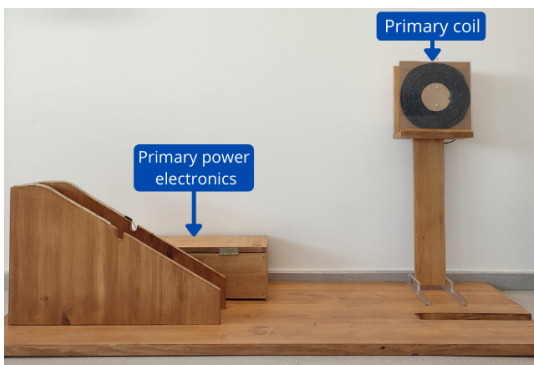


FIGURE 12. Picture of the pole with the primary coil.



(c) Position C.

FIGURE 13. Tested positions of the secondary coils

of the rectifier input and the inverter output for position C in Figures 14 and 15 respectively.

As explained in Section 2, efficiency is affected by the modified resistances of the secondary and primary coils once the surrounding elements are taken into account. Based on Equation (10), the efficiency is computed with these new parameters leading to the modelled efficiencies. It can be observed that positions A and B are associated to similar efficiencies, which is consistent with the type of surrounding materials. Position C, which has fewer interfering objects

around the secondary coil, leads to a more efficient performance, even when close to the limit situation in which the coils are not mounted on the vehicle.

If we look closely at these results, we can conclude that the position of the coil (even though it is the same secondary coil) has a strong impact on the system efficiency for an e-bike charger. In particular, position C is the most efficient, and it approximates the state in which no other conducting material interferes (not mounted). This convenience can be predicted from the measured resistances presented in Table 5. This suitability can also be seen in the heating of the



TABLE 6. Performance evaluation for the tested positions of the secondary coil.

Parameter	Not mounted	Pos. A	Pos. B	Pos. C
Inverter output voltage	18.6 V	22.3 V	20.4 V	20.5 V
Inverter output current	6.5 A	6.78 A	6.7 A	6.36 A
Inverter power factor	0.978	0.894	0.987	0.893
Rectifier input voltage	44.5 V	44.5 V	44.8 V	43.9 V
Rectifier input current	2.48 A	2.58 A	2.51 A	2.22 A
Rectifier power factor	0.998	0.998	0.998	0.998
Experimental efficiency	93.17 %	84.79 %	83.17%	92.6 %
Modelled efficiency	93.28 %	82.02 %	81.51 %	92.7 %

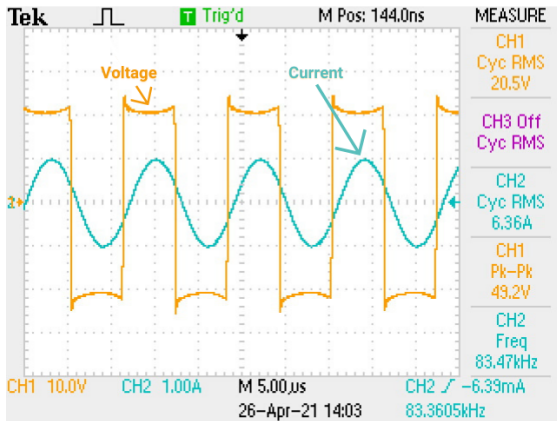


FIGURE 14. Voltage and current at primary inverter output (Position C).

bicycle structure. With a thermal camera, we measured the temperature of the bicycle chassis. The results obtained are shown in Figure 16. As can be observed, position C reaches a lower temperature (approximately 22 °C) in the bicycle material in comparison with the other two positions tested (37.4 °C for position A and 27.2 °C for position B).

Thus, we can conclude that position C is most suitable for our e-bike. For the selected position, we have verified the efficiency of the power converters. From Table 6, we obtained 7.01 W of losses associated to the coupler. For this operation, the inverter and the rectifier losses were 4.32 W

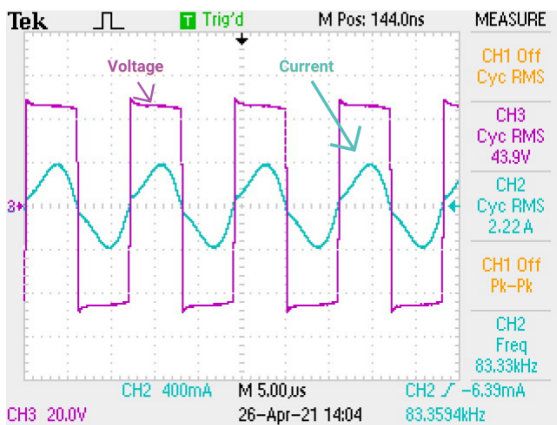


FIGURE 15. Voltage and current at secondary rectifier input (Position C).

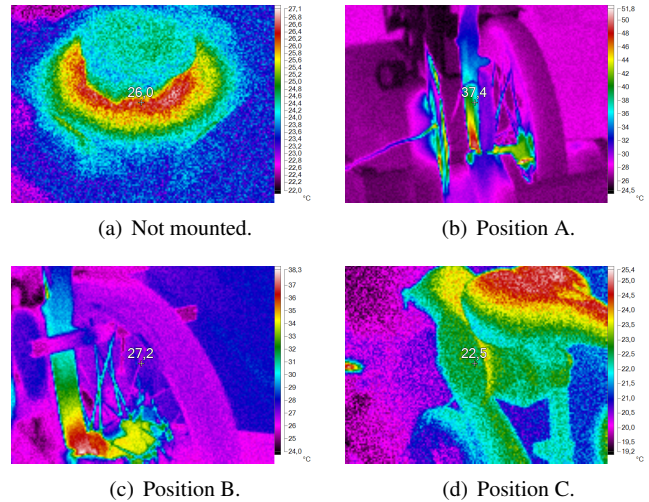


FIGURE 16. Temperature measurements in the wireless power transfer for the three tested positions.

and 3.62 W respectively.

In addition, we have checked that the control algorithm implemented in the controller works appropriately. For the specific e-bike model, the battery must be charged at 42 V when a constant-voltage phase is applied and 2 A for a constant-current phase. In Figure 17, the evolution of the charging current and voltage versus the battery equivalent resistance is plotted. The CV phase is shown as the second charging interval and starts with an equivalent resistance value of 21 Ω. The equivalent resistance of a conventional battery varies during the CC-CV charge process with a non-proportional relationship. Thus, the first interval of charge (the CC phase) occurs with low variations on the load resistance. In order to correctly evaluate the CC phase and make a correct graphical representation, it is necessary to establish more measurements for lower battery resistance values and plot them separately. A zoomed image is plotted in Figure 18 for lower values of equivalent resistances and the system working in the CC mode. It can be observed how the CC phase keeps a 2 A constant as the current charge while the voltage increases. Alternatively, the CV phase keeps a voltage constant to 42 V during the charge and the current gradually decreases.

During the charge process, the efficiency of the system varies slightly, as shown in Figure 19. In this figure, we have plotted the efficiencies computed from experimental measurements for different load resistances. Please note that the battery resistance increases during the charge in a non-proportional way. We have also included some theoretical efficiencies, which are derived from Equation (10) and the model parameters in Table 5. There is a notable similarity between both data sets.

To complete the performance evaluation of the prototype, we have included the measurement of the magnetic field for the three positions tested. The graph in Figure 20 shows how this parameter evolves with the distance  $d$  from the edge of

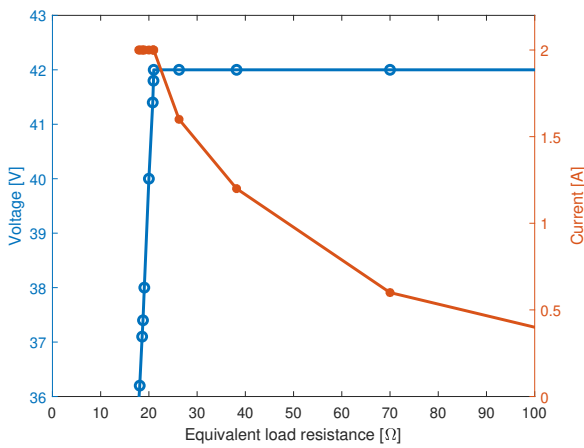


FIGURE 17. Evolution of the charging current and voltage versus battery equivalent resistance in the CV phase

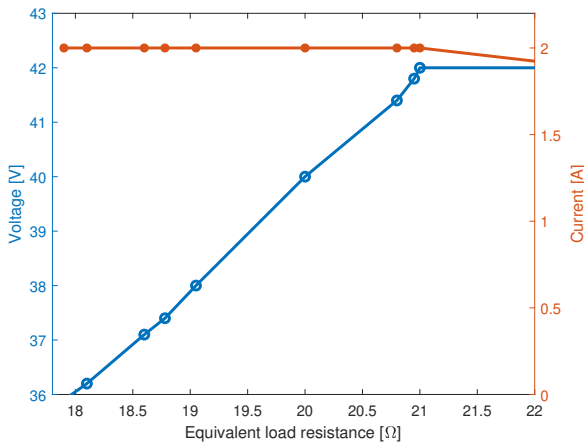


FIGURE 18. Evolution of the charging current and voltage versus battery equivalent resistance in the CC phase

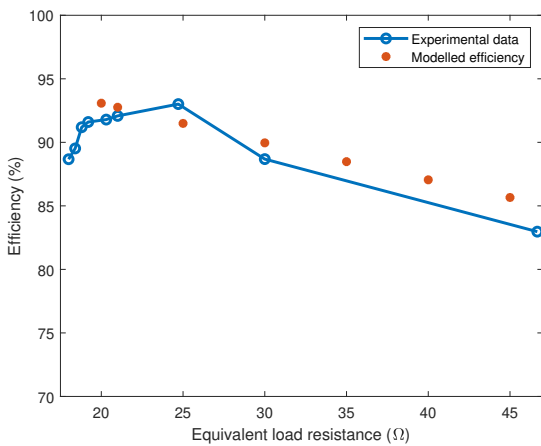


FIGURE 19. Evolution of the efficiency versus battery equivalent resistance.

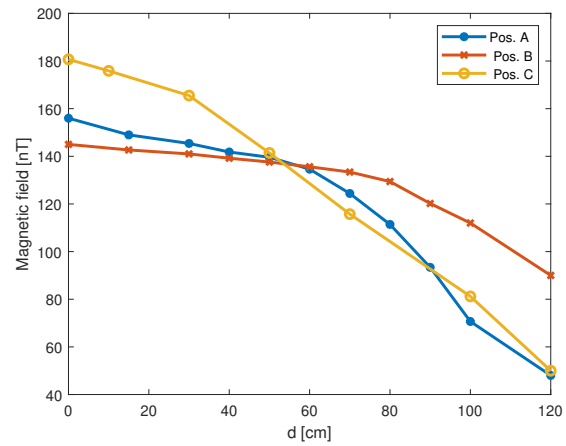


FIGURE 20. Magnetic field measured from the edge of the primary coil.

the primary coil.

It can be observed that the field is lower than  $27 \mu\text{T}$ , which is the maximum reference levels for the magnetic flux density for the frequency range between 3 kHz - 10 MHz for general public exposure established by the International Commission on Non-Ionizing Radiation Protection (ICNIRP).

## VI. CONCLUSIONS

E-bikes are foreseen as a convenient mode of transport for future smart cities due to their low cost and easy maintenance. Wireless chargers can encourage the acquisition of these EVs as they bring greater flexibility when charging the battery, which can even be programmable. E-bikes impose strong requirements concerning the weight, costs and size of the components of their wireless charger. These restrictions may be satisfied while achieving a good performance in terms of transfer efficiency and safety. This paper demonstrates the difficulty of resolving two important issues that must be addressed in real e-bikes prototypes. First, we have evaluated the position of the inductive components in the EV wireless charge on the secondary side and how these impact the system efficiency. A theoretical model has been developed and validated with experimental results. Secondly, we propose and evaluate a simple but robust control, particularly suitable for e-bike wireless chargers. With this control, we can conclude that interfering materials impact on the efficiency during the complete charge.

## ACKNOWLEDGEMENTS

Funding for this project was partially provided by the Spanish Ministerio de Ciencia e Innovacion (MICINN) project PID2019-110531-RA-I00 from the "Proyectos de I+D+i - RTI Tipo A" program and by the II Plan Propio Smart-Campus by the University of Malaga.

## REFERENCES

- [1] Nguyen Ba Hung and Ocktaeck Lim. A review of history, development, design and research of electric bicycles. *Applied Energy*, 260:114323, 2020.

- [2] Ryan Citron and John Gartner. Executive Summary: Electric Bicycles Li-Ion and SLA E-Bikes: Drivetrain, Motor, and Battery Technology Trends, Competitive Landscape, and Global Market Forecasts. Technical report, 2016.
- [3] Alicia Triviño-Cabrera, Jose M. Gonzalez-Gonzalez, and José. A. Aguado. Wireless power transfer for electric vehicles : foundations and design approach. Springer, 2020.
- [4] Ruikun Mai, Yang Chen, Yong Li, Youyuan Zhang, Guangzhong Cao, and Zhengyou He. Inductive Power Transfer for Massive Electric Bicycles Charging Based on Hybrid Topology Switching With a Single Inverter. *IEEE Transactions on Power Electronics*, 32(8):5897–5906, 8 2017.
- [5] L. A. Lisboa Cardoso, M. Comesaña Martínez, A. A. Nogueiras Meléndez, and João L. Afonso. Dynamic inductive power transfer lane design for E-Bikes. In *IEEE Conference on Intelligent Transportation Systems, Proceedings, ITSC*, pages 2307–2312. Institute of Electrical and Electronics Engineers Inc., 12 2016.
- [6] Sheng Liu, Xiaoming Li, and Lin Yang. Three-coil structure-based WPT system design for electric bike CC and CV charging without communication. *IET Electric Power Applications*, 13(9):1318–1327, 9 2019.
- [7] Hui Beh, Zhi Zak, Grant A. Covic, and John T. Boys. Wireless fleet charging system for electric bicycles. *IEEE Journal of Emerging and Selected Topics in Power Electronics*, 3(1):75–86, 3 2015.
- [8] Yang Chen, Naijian Yang, Bin Yang, Ruimin Dai, Zhengyou He, Ruikun Mai, and Shibin Gao. Two-/three-coil hybrid topology and coil design for WPT system charging electric bicycles. *IET Power Electronics*, 12(10):2501–2512, 8 2019.
- [9] Alicia Triviño-Cabrera and José Sánchez. A Review on the Fundamentals and Practical Implementation Details of Strongly Coupled Magnetic Resonant Technology for Wireless Power Transfer. *Energies*, 11(10):2844, 10 2018.
- [10] SAE International. *Wireless Power Transfer for Light-Duty Plug-In/Electric Vehicles and Alignment Methodology (SAE TIR J2954)*, 2019.
- [11] Peter K. Joseph, D. Elangovan, and G. Arunkumar. Linear control of wireless charging for electric bicycles. *Applied Energy*, 255:113898, 12 2019.
- [12] Hui Beh, Zhi Zak, Grant A. Covic, and John T. Boys. Investigation of magnetic couplers in bicycle kickstands for wireless charging of electric bicycles. *IEEE Journal of Emerging and Selected Topics in Power Electronics*, 3(1):87–100, 3 2015.
- [13] Diego Iannuzzi, Luigi Rubino, Luigi Pio Di Noia, Guido Rubino, and Pompeo Marino. Resonant inductive power transfer for an E-bike charging station. *Electric Power Systems Research*, 140:631–642, 11 2016.
- [14] Federico Genco, Michela Longo, Dario Zaninelli, Patrizia Livrieri, and Alicia Triviño. Wireless Power Transfer System Design for E-bikes Application. In *Proceedings of 2019 IEEE PES Innovative Smart Grid Technologies Europe, ISGT-Europe 2019*. Institute of Electrical and Electronics Engineers Inc., 9 2019.
- [15] Yong Li, Jiefeng Hu, Feibin Chen, Shunpan Liu, Zhaotian Yan, and Zhengyou He. A New-Variable-Coil-Structure-Based IPT System with Load-Independent Constant Output Current or Voltage for Charging Electric Bicycles. *IEEE Transactions on Power Electronics*, 33(10):8226–8230, 10 2018.
- [16] Yang Chen, Zhihao Kou, Youyuan Zhang, Zhengyou He, Ruikun Mai, and Guangzhong Cao. Hybrid Topology with Configurable Charge Current and Charge Voltage Output-Based WPT Charger for Massive Electric Bicycles. *IEEE Journal of Emerging and Selected Topics in Power Electronics*, 6(3):1581–1594, 9 2018.
- [17] Yang Chen, Mingxuan Li, Zhihao Kou, Zhengyou He, and Ruikun Mai. Cost-effective inductive power transfer charging system for electric bicycles with variable charging current using primary-side detuned series-series topology. *IET Electric Power Applications*, 13(9):1378–1386, 9 2019.
- [18] Peter K. Joseph, Devaraj Elangovan, and Padmanaban Sanjeevikumar. System Architecture, Design, and Optimization of a Flexible Wireless Charger for Renewable Energy-Powered Electric Bicycles. *IEEE Systems Journal*, pages 1–12, 6 2020.
- [19] Filippo Pellitteri, Massimo Caruso, Vincenzo Castiglia, Rosario Miceli, Ciro Spataro, and Fabio Viola. Experimental Investigation on Magnetic Field Effects of IPT for Electric Bikes. *Electric Power Components and Systems*, 46(2):125–134, 1 2018.
- [20] Mostak Mohammad, Eshet Tezera Wodajo, Seungdeog Choi, and Malik E. Elbuluk. Modeling and Design of Passive Shield to Limit EMF Emission and to Minimize Shield Loss in Unipolar Wireless Charging System for EV. *IEEE Transactions on Power Electronics*, 34(12):12235 – 12245, 12 2019.
- [21] Jiseong Kim, Jonghoon Kim, Sunkyu Kong, Hongseok Kim, In-Soo Suh, Nam Pyo Suh, Dong-Ho Cho, Joungho Kim, and Seungyoung Ahn. Coil Design and Shielding Methods for a Magnetic Resonant Wireless Power Transfer System. *Proceedings of the IEEE*, 101(6):1332–1342, 6 2013.
- [22] Yafei Chen, Hailong Zhang, Sung Jun Park, and Dong Hee Kim. A Switching Hybrid LCC-S Compensation Topology for Constant Current/Voltage EV Wireless Charging. *IEEE Access*, 7:133924–133935, 2019.
- [23] Hai Nam Vu and Woojin Choi. A Novel Dual Full-Bridge LLC Resonant Converter for CC and CV Charges of Batteries for Electric Vehicles. *IEEE Transactions on Industrial Electronics*, 65(3):2212–2225, 3 2018.
- [24] Fang Liu, Kainan Chen, Zhengming Zhao, Kai Li, and Liqiang Yuan. Transmitter-Side Control of Both the CC and CV Modes for the Wireless EV Charging System with the Weak Communication. *IEEE Journal of Emerging and Selected Topics in Power Electronics*, 6(2):955–965, 6 2018.
- [25] Wajahat Khan, Furkan Ahmad, and Mohammad Saad Alam. Fast EV charging station integration with grid ensuring optimal and quality power exchange. *Engineering Science and Technology, an International Journal*, 22(1):143–152, 2 2019.
- [26] Duc Hung Tran, Van Binh Vu, and Woojin Choi. Design of a High-Efficiency Wireless Power Transfer System with Intermediate Coils for the On-Board Chargers of Electric Vehicles. *IEEE Transactions on Power Electronics*, 33(1):175–187, 1 2018.



ALICIA TRIVIÑO-CABRERA was born in Málaga, Spain. She received the M. degree in telecommunication engineering and computer science engineering from University of Málaga, Spain in 2002 and 2008 respectively. Her Thesis, which was defended in 2007, focused on wireless networks.

She currently holds a position as an Associate Professor at the University of Málaga. Since 2011, her research activities focus on wireless power transfer. In the area related to Electric Vehicles wireless chargers, she has actively participated in the design and development of three prototypes including features as bi-directionality and dynamic charge.



JOSE M. GONZÁLEZ-GONZÁLEZ was born in Málaga, Spain. He received the M. degree in industrial engineering from University of Málaga, Spain in 2015.

He is currently working towards a Ph.D. on wireless power transfer in electric vehicles, focused on the design of a prototype with bidirectional features. He also has practical experience working on smart grids and renewable energy projects, with some publications on the integration of battery

energy storage.



JOSÉ A. AGUADO (M'01) was born in Málaga, Spain. He received the electrical engineer and Ph.D. degrees from the University of Málaga, Málaga, Spain, in 1997 and 2001, respectively.

He is a Full Professor and Head of the Electrical Engineering Department, University of Málaga, Spain. He has led more than 40 publicly funded research and consulting projects on the operation and planning of smart grids and wireless power transfer.

...

## 3.4 Design and validation of a control algorithm for a SAE J2954-compliant wireless charger to guarantee the operational electrical constraints

As presented in Chapter 2, multiple control strategies are available for EV wireless chargers. They mainly aim to adjust the charging power or maximize the efficiency. However, we observed a need to design and develop a control that combines the goal of providing the output power and protecting the system components. In a real prototype, capacitors and coils should be subject to current and voltage restrictions, because they may be damaged or destroyed if the manufacturer limits are exceeded. Although these restrictions may be considered in the design process and specific configuration, the real operation of the EV wireless chargers may lead to an increase in the voltage and/or current. This problem arises in particular when the charger does not operate with the nominal parameters considered in the design process. Three main eventualities may cause this: (i) coil misalignment; (ii) different values of equivalent resistance of the battery; and (iii) an operational frequency that differs from the nominal one. Since frequency is limited by regulations and the variations in the equivalent resistance are reduced, misalignment of the coils is the contingency that mostly affects the deviation of the system variables. In addition, coil misalignment is common in both static and dynamic charging for horizontal and/or vertical displacement.

In this paper, we have designed and developed a novel control system with the ability to regulate the charging power and operate the system in an adequate range of values for electrical variables. The control is also adapted to SAE J2954 specifications, which was recently approved.

The control is supported by a theoretical model of the effects of misalignment in a system with SS compensation. The complete formulation can be found in the published document. This model is validated in MATLAB to facilitate the analysis of the system performance for multiple variations of the mutual inductance (caused by misalignment). This analysis is performed with both vertical and horizontal misalignment, for which real values of mutual inductance measured in the laboratory are used. The results of this study show an increase in the current flowing through the primary coil for all cases of horizontal misalignment, while vertical misalignments increase the current only when the gap increases.

The results obtained in the analysis confirm the need to control the current parameters on the primary side of the charger to limit their value. For this reason, we have proposed



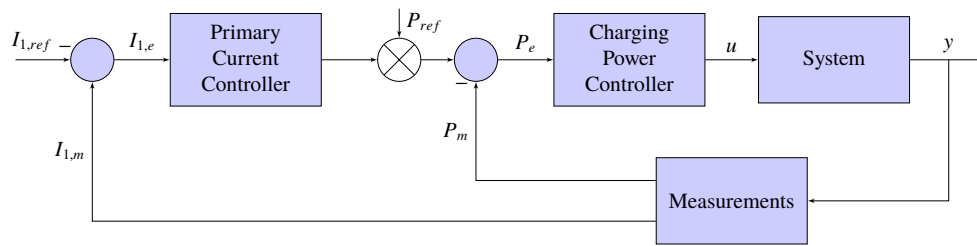


**Figure 3.7:** Scheme of the proposed control system.




a control that regulates the battery charging power and limits the current flowing through the primary side using the phase-shift technique. The main controller is located on the primary side of the charger and is responsible for applying the control strategy as well as measuring the current flowing through the primary side. As the control strategy requires measurements on the secondary side, it is necessary to install an auxiliary controller on this side that measures the charging current and battery voltage and sends the information to the main controller. This proposal includes a system composed of two PI controllers, in which one compares the measured charging power with the reference power, while the second controller limits the maximum current flowing through the primary side. The output of this system regulates the phase-shifting angle. It is then sent to a pulse generator that activates the MOSFETs of the primary inverter. Figure 3.7 depicts the scheme of the proposed control system.

The main difficulty with this controller lies in the tuning of its parameters, since an excessively fast action by one of them may cause the system to behave in an unstable way. This problem is exacerbated by delays in the analog-to-digital conversion and the communication delays between the primary and secondary sides. The configuration parameters have been carefully set to make the system regulate a sudden misalignment between coils in under one second.

The control is finally validated in the laboratory. It is implemented in a main Intel Edison Board that works in a coordinated way using Bluetooth technology with an auxiliary Intel Edison Board that is in charge of the measurements. The tests verify the conclusions derived in the theoretical analysis as the primary current increases when misalignment occurs. The control operates correctly and in a reasonable time to limit values higher than the recommended maximums. Despite satisfactory results, the phase-shifting technique produces a slight decrease in the system's efficiency due to the inclusion of additional harmonics.

Article

# Design and Validation of a Control Algorithm for a SAE J2954-Compliant Wireless Charger to Guarantee the Operational Electrical Constraints

José Manuel González-González \* , Alicia Triviño-Cabrera  and José Antonio Aguado 

Department of Electrical Engineering, Universidad de Málaga, 29016 Málaga, Spain; atc@uma.es (A.T.-C.); jaguado@uma.es (J.A.A.)

\* Correspondence: josemanuelgonzalez@uma.es; Tel.: +34-951-952548

Received: 30 December 2017; Accepted: 5 March 2018; Published: 9 March 2018

**Abstract:** Wireless power transfer is foreseen as a suitable technology to provide charge without cables to electric vehicles. This technology is mainly supported by two coupled coils, whose mutual inductance is sensitive to their relative positions. Variations on this coefficient greatly impact the electrical magnitudes of the wireless charger. The aim of this paper is the design and validation of a control algorithm for an Society of Automotive Engineers (SAE) J2954-compliant wireless charger to guarantee some operational and electrical constraints. These constraints are designed to prevent some components from being damaged by excessive voltage or current. This paper also presents the details for the design and implementation of the bidirectional charger topology in which the proposed controller is incorporated. The controller is installed on the primary and on the secondary side, given that wireless communication is necessary with the other side. The input data of the controller helps it decide about the phase shift required to apply in the DC/AC converter. The experimental results demonstrate how the system regulates the output voltage of the DC/AC converter so that some electrical magnitudes do not exceed predefined thresholds. The regulation, which has been tested when coil misalignments occur, is proven to be effective.

**Keywords:** inductive power transfer (IPT); wireless charger; control; electric vehicle; protection

## 1. Introduction

The popularity of Electric Vehicles (EV) is growing by the day. Nowadays, pollution and fuel cost volatility [1] are two main concerns that are encouraging both governments and manufacturers to make a strong commitment to EVs [2,3].

Despite the evolution that electric vehicles have experienced in recent years, this transportation mode is still associated with some disadvantages that need to be overcome. One of the most relevant issues concerns their autonomy, which fundamentally depends on the technology and capacity of the batteries. However, increasing the capacity of batteries requires a long development process. For this reason, researchers and industries are seeking other alternatives that ease the use of EVs while the battery technology evolves.

One possible solution relies on wireless chargers, which provide recharge for electric vehicles without the need for wires or user intervention. Moreover, as has been demonstrated recently, this technology allows electric vehicles to be recharged while they are moving [4,5], making this solution a feasible approach to increase their autonomy.

The wireless charge is produced by means of a high frequency alternating current that flows along a coil located on the floor (named the primary coil) and which, in turn, generates a magnetic field. This magnetic flux passes through a coil (referred to as the secondary coil) situated under the vehicle. This induces a voltage in the secondary coil and this is used to charge the battery.

The design of wireless charging systems for Electric Vehicles involves the determination of multiple parameters (mainly the coils topology and the power converters) to operate under specific conditions (e.g., distance between the coils, switching frequency). Any variation from the design conditions may negatively affect the charging process and the components of the system. These failures could be severe and may require the replacement of the component.

Moreover, the charge process of an EV wireless chargers has to be performed in a very specific way [6], as shown in Figure 1. As can be observed, there are two charging processes: the first with constant current and the second with constant voltage.

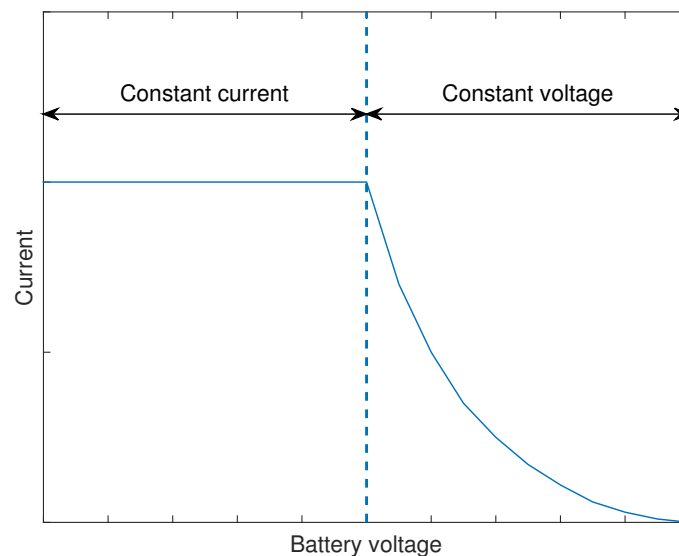


**Figure 1.** Processes of the charging process of a battery in an EV.

Following this charging scheme is not a trivial task because there are some time-varying conditions that affect the charge process. Thus, the power converters and the controllers become crucial as they are responsible for monitoring the voltage, the current and/or the power delivered to the battery so that they can adjust their operation by comparing the measurements with some established values. Several approaches related to the control for the EV wireless chargers have been proposed in the existing literature.

Some works focus on controlling the charging power by means of the electronics of the primary side [7]. Other proposals try to set the current either on the primary side, using a resonant inverter [8] or a DC converter [9]. The current on the secondary side can also be adjusted by regulating the inverter of the primary side [10]. Moreover, the voltage can also be controlled. For instance, Refs. [11–13] by regulating the primary voltage using different types of resonant inverters.

Despite controlling and monitoring a single variable, some of these methods are capable of working indistinctly with voltage or current to comply with the phases of the charging process. Ref. [14] presents an estimation method that prevents errors of weak communication with the capacity to control both variables. Alternatively, Ref. [15] shows a technique in which the adjustment of them is performed by a cascade buck and boost converter on the secondary side. Finally, other authors propose solutions to work with more than one variable. The goal of the control function is to achieve maximum efficiency. In this group, Ref. [16] proposes a scheme in which a primary-side-controlled charger is developed and uses a reactive power control to improve the efficiency of the system. On the other hand, Ref. [17] proposes a phase-frequency hybrid control strategy to operate at the resonant frequency.

Nevertheless, controller functions should not be limited to the discussed process as wireless chargers have to face with other potential adversities such as, for example, those derived from overpassing some electrical magnitudes. Some components are sensitive to overvoltages or overcurrents, which may cause interruptions, malfunctioning or even their destruction. These errors



could also provoke an incorrect or inefficient charge process. Thus, it is important that the controller also monitors the electrical state of the most relevant components of the wireless charger and not only the battery demands. Taking into account that coils and power converters are the components that make the wireless power transfer feasible, their electrical status should be considered by the controllers. On the one hand, the material from which the loosely coupled coils are built imposes some restrictions. These coils, which are the basis for the wireless power transfer, are usually made of Litz wire because this material minimizes the skin effect [18]. It is necessary to guarantee that the current along the wire does not exceed that allowed, as it could deteriorate the cable. It is important to note that the coils will dissipate heat that may alter other adjacent systems. On the other hand, the semiconductors of the power converters are also prone to deterioration when used incorrectly so they should operate under a range of current and/or voltage defined by their fabrication process.

Thus, the role of the controller should be an extension of those already proposed ones as it should take care of the battery and other components. This functionality is even more challenging as the electrical status of the components should be ensured even for some conditions that are not those considered in the design process. This is the case of the coil misalignment, which withstands those situations in which the relative distance between the structures of the coils differs from the one assumed in the design. As a consequence, the mutual inductance coefficient varies and the electrical magnitudes on the primary and/or secondary side are altered in comparison with the nominal ones.

From a theoretical study about the electrical consequences of the coil misalignments, this paper designs and implements a controller capable of adjusting the power transfer not only because of the requirements of the storage system, but also due to the technical constraints imposed by other components of the charger. A preliminary paper about this controller was presented in [19], but it omits the implementation concerns and the results in a real prototype.

The remainder of the paper is structured as follows. Section 2 defines the topology of the wireless charger to which we have applied the new controller. Section 3 studies the behavior of the system with different situations of coil misalignments in order to determine the most critical electrical parameter in the circuit. Section 4 presents the control technique that will be implemented in the physical controller. Section 5 shows the different components used in the laboratory and the evaluation of the proposal. Finally, Section 6 presents the main conclusions of our work.

## 2. Wireless Charger Topology

Wireless chargers for EVs are based on the Inductive Power Transfer (IPT) technology, which transfers the power through an air cored transformer. There is a reasonably large air gap between the primary coil, placed on the floor, and the secondary coil, located in the car. The coils counts on reactive structures known as compensation systems to operate under resonant conditions, which improve the power transfer. The magnetic field intensity and, in turn, the transferred power depend on the frequency of the current traversing the primary coil. Consequently, this technology relies on high frequency current to increase the charging power while maintaining the same primary voltage.

There are different proposals to generate this high frequency current on the primary side. The most popular solution is the full bridge inverter [8–10] due to its simplicity and its reliability. However, there are other options that lead to an improved performance at the expense of a greater complexity, such as, for example, multi-level inverters [13] or single-ended quasi-resonant converters [12]. For our design, we have opted for the full-bridge topology as it satisfies the power requirements easily. It is composed of four semiconductors (Q1, Q2, Q3 and Q4) working as switches. The reverse diodes are included to allow the current flow to the positive borne of the direct current (DC) source. In our case, the load corresponds to the coupled coils, the compensation topologies, the rectifier and the battery. Inverters require a DC source as its input. Thus, we have to use a rectifier connected to an alternating current (AC) source in the inverter input.

The generated alternating current flows through the primary coil, creating a magnetic field that mainly depends on the coil structures. As explained before, the intensity of the magnetic field

directly depends on the current and on its frequency. Between the inverter and the primary coil, a compensation system has been introduced to enable the operation under resonant conditions. For the physical implementation of this project, a series–series compensation topology has been selected due to its lower sensitivity to misalignment [20].

The magnetic field created by the primary coil passes through the secondary coil and induces an alternating voltage in it. When connected to the battery, there is an induced current. Finally, this current is converted to DC Current, which is appropriate for the battery. The conversion is performed by a rectifier, which usually is a full bridge rectifier composed of four diodes.

A similar topology can be used for bidirectional chargers or Vehicle to Grid (V2G) systems. In this case, when the system is discharging the battery and injecting power into the grid, the components are performing different functions. The secondary converter works as an inverter instead of working as a rectifier, while the primary converter works as a rectifier. Thus, bidirectional chargers require bidirectional power converters so that they can work as inverters or rectifiers depending on the direction of the power flow.

The control system is designed based on the bidirectional wireless charger topology presented in Figure 2. Nevertheless, the proposal could be extended to other schemes, for example when they include other components such as a Power Factor Corrector systems [21].

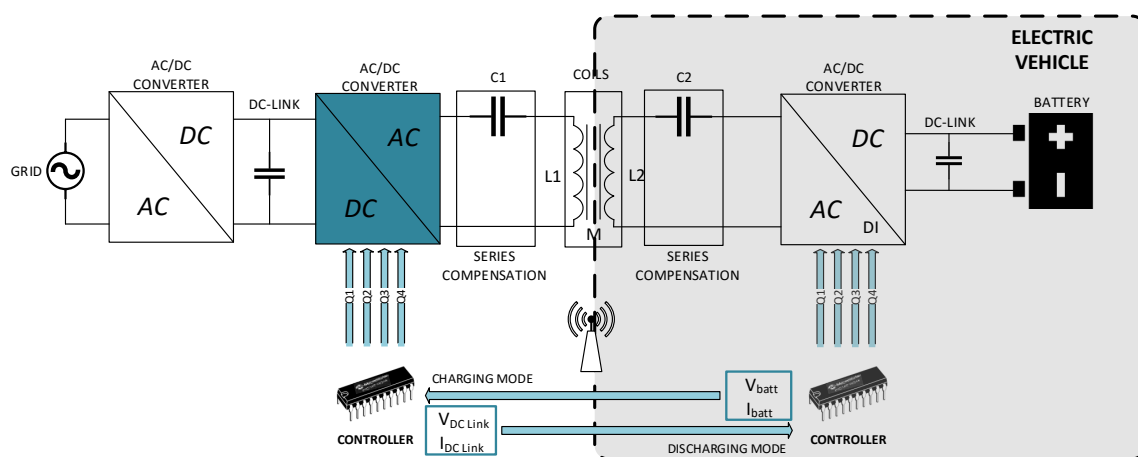


**Figure 2.** Topology adopted for the developed controller. This scheme is an adaptation of [19] for a bi-directional charger.

In addition to the mentioned structures, the systems include a wireless communication module so that the primary and the secondary side of the wireless charger can exchange information for the control. The control is executed in controllers that act on the switching devices of the power converters.

### 3. Effects of Coil Misalignments

For efficient charging, wireless EV chargers require primary and secondary coils alignment. This usually requires extra attention and time when parking.

Under realistic circumstances, the centers of the primary and secondary coils may be displaced a certain distance. This is the case of the horizontal misalignment,  $xm$ , as represented in Figure 3a. Horizontal misalignment could occur in both plane axes. The two coils could also be separated a certain distance ( $gap$ ) greater/lower than the one considered in the design process ( $gd$ ). When this happens, there is a vertical misalignment such as that shown in Figure 3b. It is usually caused by road conditions and vehicle weight. Finally, horizontal and vertical misalignment could both be present as shown in Figure 3c.

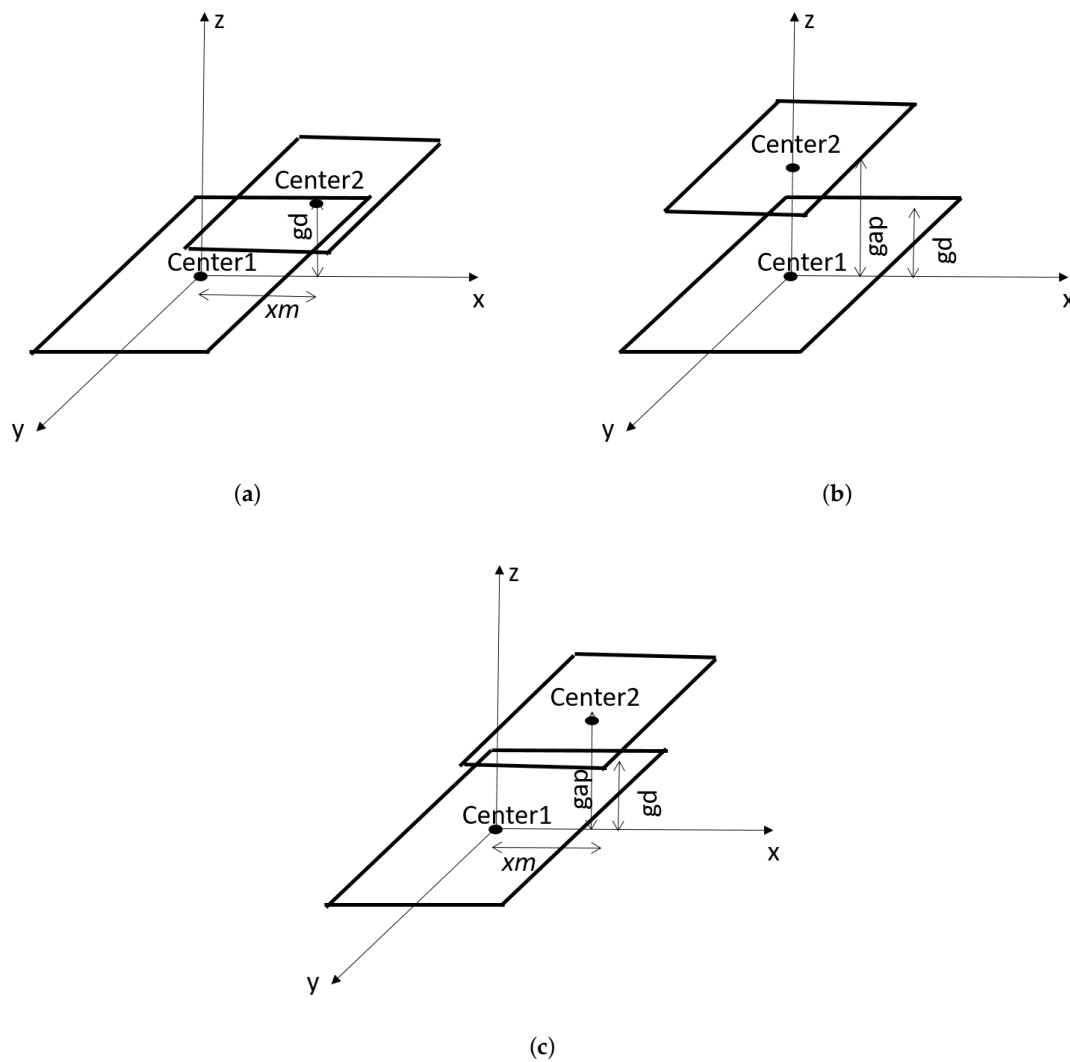


**Figure 3.** Types of coil misalignments. (a) horizontal misalignment with a  $x_m$  displacement; (b) vertical misalignment with a new  $gap$ ; and (c) horizontal and vertical misalignment simultaneously.

Coil misalignment impacts on magnetic and electrical magnitudes of the circuit. Specifically, coil misalignment alters the magnetic flux density traversing the secondary coil. This is modeled by the mutual inductance coefficient. The impedance reflected from the secondary side to the primary side depends on this parameter. As a consequence, variations in the mutual inductance coefficient implies changes in the voltages and currents in the system, included the primary side.

Next, we present a theoretical analysis of the equivalent circuit of a wireless charger. The equivalent circuit of an Inductively Coupled Power Transfer (ICPT) system with series-series compensation is presented in Figure 4.

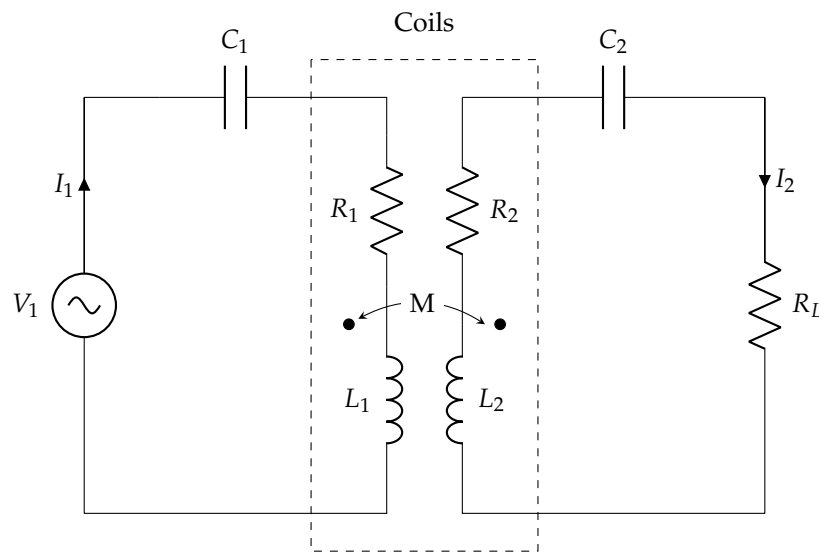


**Figure 4.** ICPT equivalent circuit with series-series compensation.

In this figure,  $L_1$ ,  $L_2$ ,  $R_1$  and  $R_2$  indicate the self-inductance and the resistance of primary and secondary coils, respectively. The capacitances of the compensation system of the primary and secondary side are  $C_1$  and  $C_2$ , respectively. The currents of the primary and secondary coils are  $\vec{I}_1$  and  $\vec{I}_2$ , respectively. The parameter  $M$  is the mutual inductance.

This compensation topology is better suited for the implementation of a control system in a bidirectional wireless charger. The capacitors are computed to force the system to operate under resonant conditions. Thus:

$$C_1 = \frac{1}{\omega^2 L_1'} \quad (1)$$

$$C_2 = \frac{1}{\omega^2 L_2'} \quad (2)$$

where  $\omega$  is the frequency of the current. The parasitic capacitances of the coils are not considered in this computation. As stated in [22], an accurate model for Litz-wire rectangular coils is exclusively composed of an internal resistance and their inductance when the operating frequency is below 600 kHz.

In this equivalent circuit,  $R_L$  represents the equivalent resistance of the battery considering the effects of a rectifier.

This circuit can be analyzed using Kirchhoff's second law, which results in the following equations:

$$\vec{V}_1 = [R_1 + j(L_1\omega - \frac{1}{C_1\omega})]\vec{I}_1 - j\omega M\vec{I}_2, \quad (3)$$

$$0 = [(R_2 + R_L) + j(L_2\omega - \frac{1}{C_2\omega})]\vec{I}_2 - j\omega M\vec{I}_1, \quad (4)$$

where  $\vec{V}_1$  is the voltage at the output of the DC/AC converter. When the output of the inverter is not sinusoidal, we can work with the first harmonic approximation to derive the magnitude of  $\vec{V}_1$ .

The compensation systems have been designed to allow the charger to operate at resonance. Under this assumption and with Equation (4), the relation between the primary and the secondary current is shown in Equation (5):

$$\left| \frac{I_1}{I_2} \right| = \frac{R_2 + R_L}{\omega M}. \quad (5)$$

As this equation states, the relation between the primary and the secondary current is directly affected by the value of  $M$ . This implies that the relationship between the active power at the load and the one provided by the inverter is:

$$\eta = \frac{R_L}{(R_L + R_2) \left(1 + \frac{R_1(R_2 + R_L)}{\omega^2 M^2}\right)} = \frac{R_L}{R_L + R_2 + R_1 \left(\frac{I_1}{I_2}\right)^2}. \quad (6)$$

Consequently,  $\eta$  represents the efficiency of the wireless charger in the simplified model of the wireless charger in Figure 4. Efficiency is commonly studied in this type of simplified model of the charger in previous research works [23]. However, the real efficiency of the whole system should include the losses of the power converters. The work in [24] demonstrates that the inclusion of the losses of these power converters does not noticeably impact the efficiency, so Equation (6) is a suitable approach to estimate the efficiency of the system. This equation is only valid under resonant conditions and, therefore, it should be considered as the upper limit of the efficiency for a real prototype. It is worth noticing that the efficiency does not depend on the primary or secondary current but on the mutual inductance and on other constant parameters.

Next, we study how the current and the efficiency vary with  $M$  for vertical, horizontal and vertical/horizontal misalignments. We will use the concept of the impedance  $Z_R$  reflected from the secondary to the primary side. By incorporating this impedance on the primary side, we only work with the mesh related to the primary side. When  $C_2$  is computed according to Equation (2), the value of  $Z_R$  is:

$$Z_R = \frac{\omega^2 M^2}{R_L + R_2}. \quad (7)$$

As can be observed, changes in the mutual impedance lead to variations on the reflected impedance. These modifications alter the primary and the secondary current.

This analysis is performed for square coils, but it could be extended for other topologies. We have opted for this topology as rectangular coils have been proven to offer a higher tolerance to coil misalignments than circular ones. An in-depth analysis of this sensitivity is presented in [25].

Other features of the considered wireless charger are summarized in Table 1.

**Table 1.** Characteristics of the analyzed wireless charger.

Frequency	85 kHz
Primary coil dimensions	0.75 m × 0.75 m
Cross-sectional area of the primary coil wire	20 mm <sup>2</sup>
Resistance of the primary coil ( $R_1$ )	195.6 mΩ
Self-inductance of the primary coil ( $L_1$ )	240.5 μH
Secondary coil dimensions	0.5 m × 0.5 m
Cross-sectional area of the secondary coil wire	20 mm <sup>2</sup>
Resistance of the secondary coil ( $R_2$ )	143.1 mΩ
Self-inductance of the secondary coil ( $L_2$ )	230.6 μH
Distance between coils assumed in the design (gd)	0.2 m
Compensation topology	Series-Series
Capacitance of the primary side ( $C_1$ )	17.05 nF
Capacitance of the secondary side ( $C_2$ )	15.88 nF
Load resistance	24 Ω
Input voltage of the primary inverter	170 V

The size and dimensions of the elements are feasible for the implementation of the wireless charger in an EV. The considered features include the 85 kHz frequency recommended by SAE J2954 [26]. When the coils are aligned, the power transferred to the load is 1.2 kW.

### 3.1. Vertical Misalignment

Vertical misalignment refers to the deviation of the distance between the coils from that assumed in the design. This displacement can occur by decreasing or increasing the distance between the two coils, which results in opposing effects that must be analyzed independently.

When a decrement in the separation of both coils happens, the value of the mutual inductance increases. As a consequence, the reflected impedance also increases according to Equation (7). When this occurs, it is not necessary to take any particular precautions because the value of the primary current decreases and the secondary current is also diminished as expressed in Equation (5).

On the other hand, increasing the vertical distance between both coils leads to the opposite effect. It decreases the mutual inductance and it reduces the reflected impedance as well. As a result, the primary and the secondary current increase. Consequently, the voltage on the secondary side increases its value and, in turn, the transferred charging power is also incremented. The augmentation of the current flowing through the components of the primary side of the charger needs to be controlled to avoid malfunctions. Figure 5 shows the evolution of the current flowing through the primary side of the charger and the coil efficiency, which has been computed as in Equation (6).

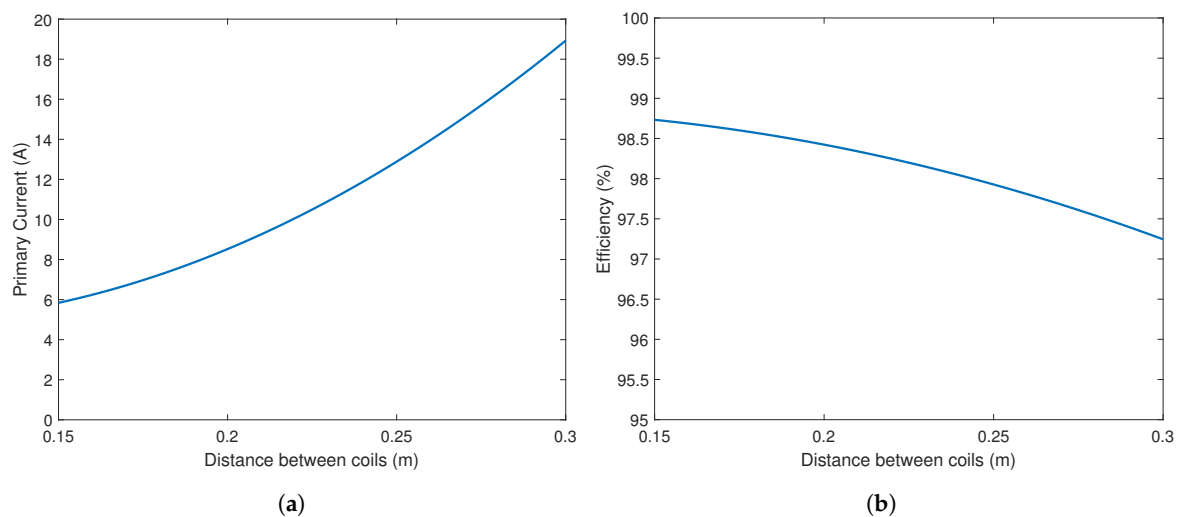


**Figure 5.** (a) primary current as a function of the distance between coils; (b) efficiency as a function of the distance between coils.

In order to avoid an excessive and even dangerous increase in the transferred power, the controller of the wireless charger has to act on the electronics. In particular, it decreases the voltage of the primary coil and, therefore, the primary and the secondary currents are also reduced. As a consequence, the secondary voltage and the load power are approximated to the design values.

### 3.2. Horizontal Misalignment

The horizontal misalignment refers to the horizontal displacement existing between the center of the primary and secondary coil, which can occur in both axes independently or simultaneously. It is the most common misalignment due to the difficulty of locating the car just above the primary coil, either in fixed or mobile situations.

This type of misalignment also affects the mutual inductance of the coils, with similar effects to the increase in the distance between coils. When a horizontal misalignment occurs, the value of the mutual inductance is reduced, increasing the transformation ratio. This results in an increment of the secondary voltage and the charging power, making it necessary for the controller to act by decreasing the transferred power. As in the previous case, the controller stabilizes the voltage and the current on the secondary side by adjusting the charging power. Figure 6 presents the evolution of the primary

current with different horizontal displacements on a single axis and the coil efficiency, which has been computed with Equation (6).

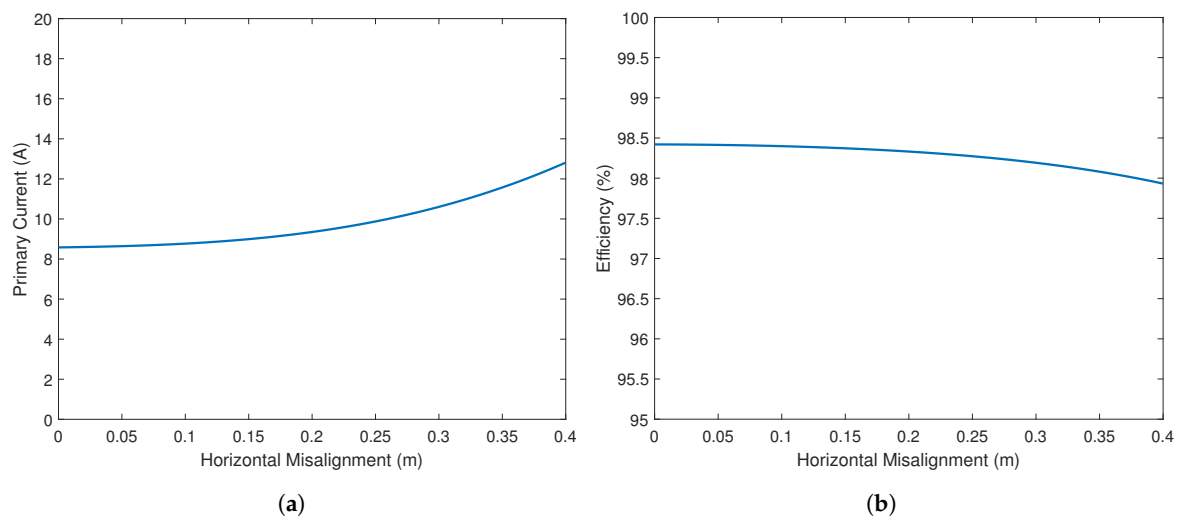


**Figure 6.** (a) primary current as a function of a horizontal misalignment; (b) efficiency as a function of horizontal misalignment.

As can be seen from Figure 6, the effects of horizontal misalignments are less than those of a vertical misalignment, having a very slight effect with small misalignments but growing exponentially with an increase in the displacement.

Although at first glance this increase in the value of the primary current may not be excessively large, it must be taken into account because its effects can be multiplied in combination with a vertical misalignment, which is discussed in the following subsection.

### 3.3. Horizontal Misalignment with 0.25 m between Coils

Finally, complementing the individualized analysis of the previous subsections, a study of the combined effects of both vertical and horizontal misalignments in both axes has been performed. In a case of actual application, it is possible to find both types of misalignment simultaneously, making the negative consequences more relevant.

In order to carry out this study, the secondary coil was located at a vertical distance of 0.25 m, which corresponds to 5 cm more than the design separation indicated in Table 1. This study is shown in Figure 7, where it is possible to observe the evolution of the primary current values with different horizontal misalignments in both axes and with a separation between coils 5 cm higher than the design.

As in the previous cases, small misalignments do not involve large increases in the values of the primary current. However, this increase in the value of the primary current occurs exponentially, exceeding 25 A with misalignments close to 40 cm.

All these analyzed cases allow the study to highlight the importance of having the primary current values under control, avoiding risks of failures and malfunctioning in the wireless charging operation. For commercial devices such as those used in our experiments, these values of current will deteriorate the semiconductors used in power converters.



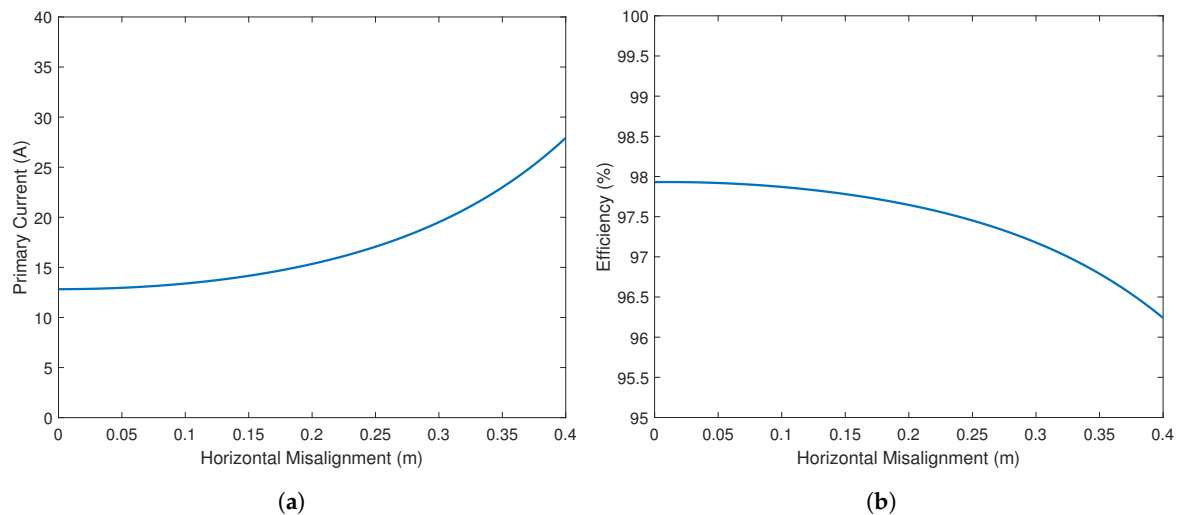


**Figure 7.** (a) primary current as a function of horizontal misalignment in both axes and a distance between the coils of 0.25 m; (b) efficiency as a function of horizontal misalignment in both axes and a distance between the coils of 0.25 m.

#### 4. Developed Control System

The generation of the high frequency current is performed by the power converter acting as a full bridge inverter in the implemented wireless charger. One of the great difficulties of the power converter of the charger is the control system, which has to be able to regulate the charge power according to the application requirements. In our design, the functionality of the control system is even more complex as we impose additional requirements relating to the maximum current value allowable on the primary side. As explained previously, this is the first electrical magnitude that experiments a relevant increment when misalignment occurs.

The function of the control system is to activate the switching of each transistor of the converter at the right time. For this, the control strategy developed in [19] has been implemented. This strategy uses the phase-shift control technique, which is used in electrical power systems, especially in converters [27–29]. The phase-shift switching control consists of applying a delay of the transistors switching of one leg in comparison with the actuation of the switches in the other leg. In this way, it is possible to adjust the output voltage of the inverter.

Using the phase-shift technique, the first harmonic of the output voltage corresponds to:

$$V_1 = \frac{4}{\pi} V_p \sin(\delta/2). \quad (8)$$

As the voltage varies with  $\delta$ , the current in the primary is also affected by this parameter (please refer to Equation (3)). Consequently, the power delivered to the load is also modified according to Equation (5). However, Equation (6) indicates that this modification does not have an impact on the efficiency of the system assuming the first harmonic approximation.

Figure 8 shows the scheme of the control algorithm developed in this work.

The implemented design controls two variables: the battery power charge and the primary current, as a result of the study performed in Section 3. In order to fulfill this goal, two PI (proportional-integral) controllers have been incorporated. In our implementation, the PI<sub>1</sub> controller constantly performs a comparison between the measured charging power and the reference charging power, storing the error between both. The PI<sub>2</sub> controller allows the primary side to be protected by limiting its current. This controller monitors the current flowing through the primary side and limits it when it exceeds the maximum value allowed. The value stored by this PI is used to modify the reference charge power of the PI<sub>1</sub> controller, indirectly reducing the current flowing through the primary side. This error is finally



used to compute the offset between the signals of both legs (the delay), which will cause a decrement of the output voltage of the primary inverter.

Tuning the parameters of these controllers is not a trivial task, since an excessively fast action by one of them can lead to an unstable behavior of the system. Therefore, the parameters of the control system have to be carefully selected, depending on the characteristics of each charger. The effects of a bad tuning of the parameters are explained in the following section.

In our implementation, the delay of the controller is 1 s. Figure 9 shows the time that the controller takes to stabilize the output power and the primary current when an abrupt change of the position of the coil occurs. This is a limit situation, as this kind of change is not expected in a real scenario.

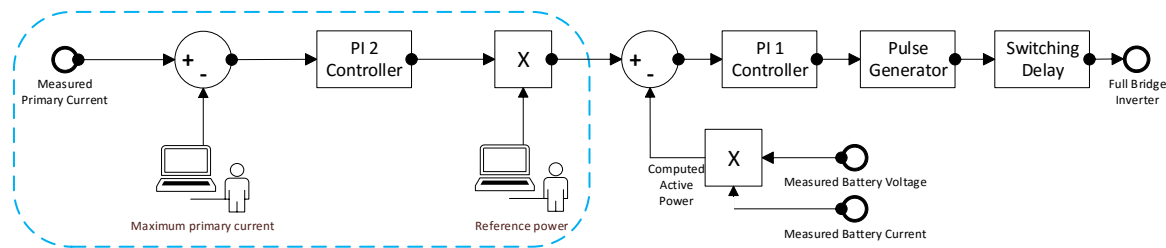


Figure 8. Scheme of the developed control system.

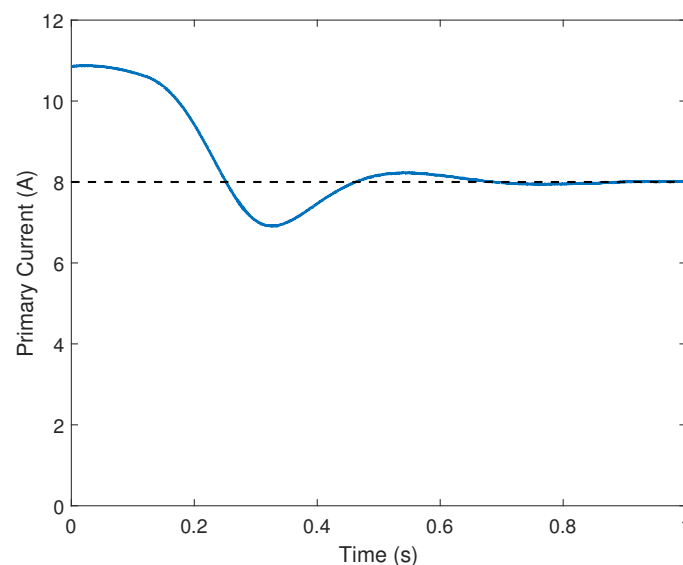


Figure 9. Actuation of the implemented controller under an abrupt change of the position of the coils.

The real delay of the system should also include the effects of the communication system, which transmit the data employed as input in the controller. Specifically, the communication delay is composed of two variables: the Analog/Digital conversion of the data and the wireless transmission of this information from the secondary side to the primary side. Based on the specification of the commercial Bluetooth Low Energy module incorporated in a typical controller such as the Intel Edison (Intel, Santa Clara, CA, USA) used in our prototype, the default conversion time is 20 ms. As a result, the format of the data is a 12-bit word that needs to be transmitted through the wireless channel. Assuming that the pairing and the connection of the Bluetooth devices have been performed previously, the communication time is computed with the rate for the transmission of the data in a Bluetooth Low Energy channel. This rate is 1 Mbps. Consequently, transmitting a 16-bit word (2 bytes) implies 15.2  $\mu$ s. Thus, the communication delays can be considered negligible.

Following the SAE J-2954 recommendations, the frequency of the magnetic field involved in the EV wireless charger should be 85 kHz. This implies that some electrical magnitudes also have this

frequency [30]. Consequently, the sampling and processing frequency should be adjusted to obtain valid estimations about the current and/or voltage in a component when this frequency is involved. Due to the limitations of the acquisition components of the controller, measurements of 85-kHz signals are not possible. Consequently, we have opted for the estimation of the primary current in the DC link. The other measurements are related to the battery so that they are DC and can be accurately obtained.

In addition, the transition from OFF to ON and vice versa of both transistors of the same leg can never occur simultaneously because the transistors require time to change their state once the switching signal has varied. In order to prevent short circuits in the inverter, the controller incorporates a dead time between the switching.

## 5. Experimental Results

The proposed system has been built in the laboratories of the Electrical Engineering Department of the University of Málaga. Figure 10 shows a picture of a part of the assembled system in which we have labeled the components. Although the results presented correspond only to the charging process, the implemented controller can work on bidirectional chargers.

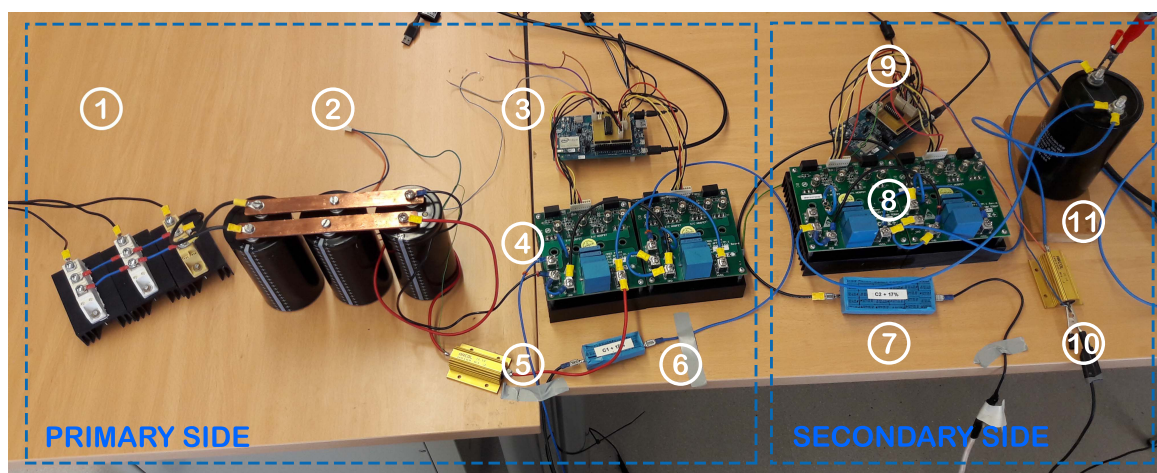


**Figure 10.** Picture of the assembled system in the Electrical Engineering Department of the Universidad de Málaga.

On the primary side, a three phase rectifier (number 1) is connected to the grid to generate a direct current. The DC is the input of DC/AC converter whose function is to generate a high frequency (85 kHz) alternating current. The DC/AC converter is labeled with number 4. Between both components, there are three capacitors connected in parallel (number 2) so that the equivalent capacity reduces the voltage ripple from the rectifier and, in turn, improves the performance of the inverter.

The DC/AC converter has been implemented with four Silicon Carbide (SiC) metal-oxide-semiconductor field-effect transistors (MOSFETs) following a full-bridge topology. These transistors are particularly suitable for this application as they support the required switching frequency and the current values. Moreover, they experiment a reduced amount of losses, which results in simple heat dissipation systems.

With the aim of reducing the assembly complexity, two protoboards KIT8020-CRD-8FF1217P-1 manufactured by CREE (Durham, NC, USA) have been used. Each protoboard incorporates two MOSFETs C2M0080120D and two diodes C4D20120D. The characteristics of these elements are summarized in Table 2. The MOSFETs, the diodes and the snubber circuits are shown in Figure 10. The protoboard also incorporates the electronics needed to avoid malfunctioning due to the simultaneous activation of two MOSFETs in the same leg as well the dissipation system appropriate for the heating exigencies.

**Table 2.** Characteristics of the C2M0080120D MOSFETs and the C4D20120D diodes.

C2M0080120D MOSFET		
$V_{DSmax}$	Drain-Source Voltage	1200 V
$I_D$	Continuous Drain Current	36 A
$R_{DS(on)}$	Drain-Source On-State Resistance	80 m $\Omega$
C4D20120D Diode		
$V_{RRM}$	Repetitive Peak Reverse Voltage	1200 V
$I_F$	Continuous Forward Current	34 A
$V_F$	Forward Voltage	1.5 V

The DC/AC converter is controlled by a PIC microcontroller model 16F18344 [31] assembled to an Intel Edison Board (number 3 in Figure 10) [32]. The PIC provides the gate signals to the converter in accordance with the designed control. With them, the inverter generates the high frequency current incorporating the phase-shift based control. The switching delay for this control is computed by the Intel Edison Board. This value is sent to the PIC through a parallel connection. The Bluetooth communication module installed in the Intel Edison boards allows the primary controller to receive the current and the voltage values from the secondary controller. Moreover, a shunt resistor is connected to an analog input of the Intel Edison Board to estimate the primary current (number 5 in Figure 10).

Between the primary and the secondary side, there are two coils made of a Litz wire winding design as shown in Figure 11. Litz wire makes it possible to reduce the Skin effect losses in the operational frequency range [18]. Theoretically, the primary coil is located on the floor, while the secondary coil is placed in the car chassis.

**Figure 11.** Picture of both coils with the parameters indicated in Table 1.

Connected in series with both coils, we find the compensation systems (numbers 6 and 7 in Figure 10), formed by polypropylene film capacitors. The main advantage of this type of capacitors is their ability to support the high voltages to which they are subjected in this type of application.

The secondary side is implemented with a topology similar to that on the primary side. After the compensation system, the energy flows to the AC/DC converter (number 8), composed of the previous CREE protoboards. When the power flows from the grid to the battery, the diodes work rectifying the alternating current and converting it to direct current, which is appropriate for a battery system.

The controller of the secondary side (number 9 in Figure 10) performs a different function than that on the primary side, since in this case it is not necessary to control the AC/DC converter. The main activity of this controller is to estimate the current flowing through the battery in the DC side,

using another shunt resistor (number 10 in Figure 10). The measurement value is sent to the primary controller employing the Bluetooth communication module installed in the Intel Edison boards.

Finally, all the energy is consumed in a resistor bank with a resistance value equivalent to the battery so that the same effects of charging a battery are simulated. A capacitor (number 11) is connected in parallel to the resistors in order to improve the battery life by reducing the ripple from the rectifier. The equivalent resistance of the battery is  $29.6 \Omega$ .

The controllers were programmed in the Intel Edison board using the high-level programming language Python. In this program, we set the following electrical restrictions:

- Maximum rms current on the primary side is 8 A.
- Maximum charging power value is 1.2 kW.

These values are easily reconfigurable for other applications. We have also set the DC voltage in the primary DC/AC converter to 170 V.

With an input voltage of 170 V in the primary AC/DC converter, the system reveals the measurements presented in Figure 12 without any coil misalignment. The voltage at the output of the primary DC/AC converter has a value of 154 V, while the current flowing through the primary coil has an RMS value of 7.6 A.

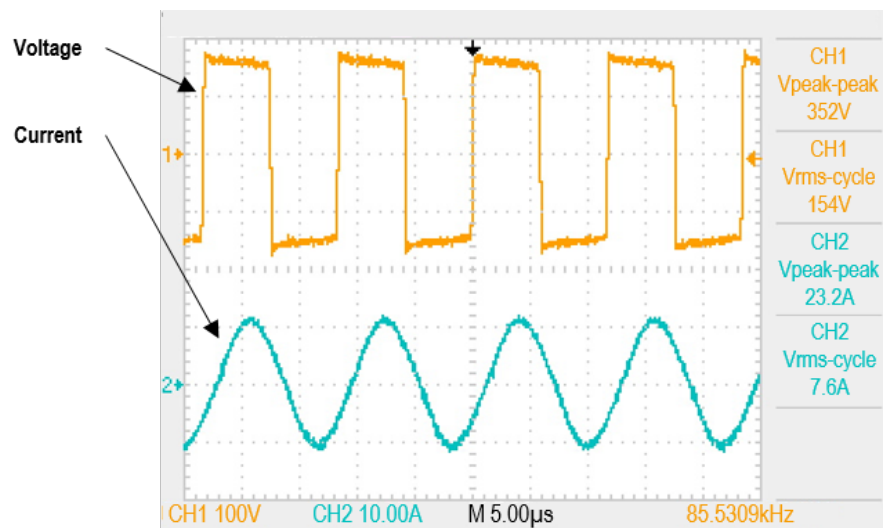


**Figure 12.** Voltage (channel 1) and current (channel 2) measurements at the output of the primary DC/AC converter without coil misalignments.

As expected from the analysis of Section 3, the value of the primary current increases when a coil misalignment occurs. Figure 13 presents the measurements of the system working with 0.2 m horizontal misalignment and 0.05 m vertical misalignment. Without the control system and keeping the primary input voltage constant (in yellow in Figure 13a), the primary current (in blue in Figure 13a) increases its value up to 11.36 A.

The developed control system detects that the current is expected to exceed the maximum value established in the program and begins to regulate the transmitted power using the phase shift technique. Figure 13b shows the electrical magnitudes with the intervention of the control system. In yellow, the primary output voltage is represented. This voltage measurement allows the observation of the action of the phase shift technique by forcing some dead times in the signal. In blue, the output primary current is presented. As can be noted, its value is 7.7 A. Due to the high frequency, the PIC cannot finely regulate the output voltage of the primary side and has a maximum number of regulation steps. For this reason, the value of the output current is not the maximum allowed, established in 8 A, but the regulation step immediately below 8 A.

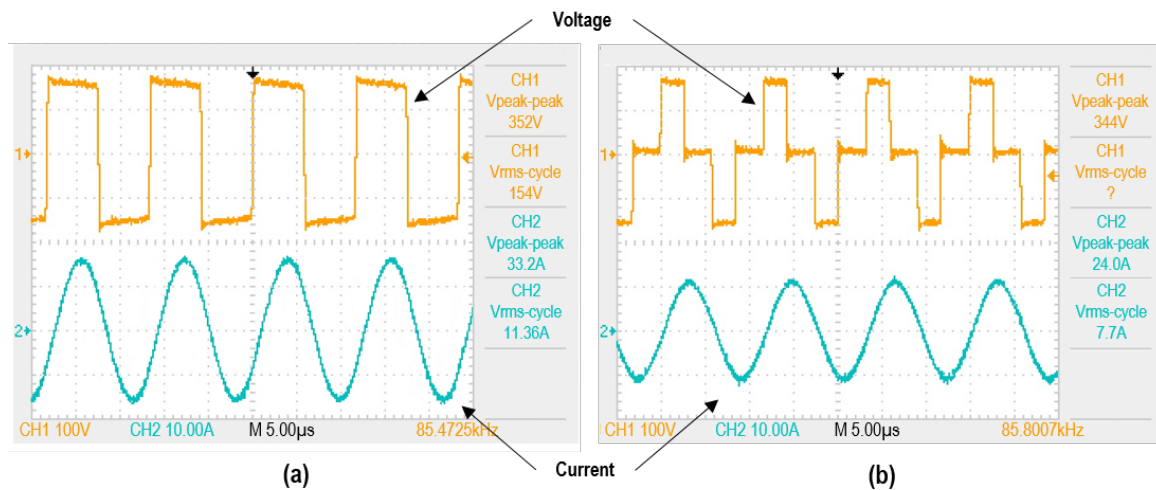


**Figure 13.** System working with 0.2 m horizontal misalignment and 0.05 m vertical misalignment. (a) primary DC voltage and current flowing through the primary coil without the proposed controller; (b) voltage output of the primary DC/AC converter and current flowing through the primary coil.

By computing the first harmonic of the voltage signals of the results presented in Figures 12 and 13, it is possible to derive the output power of the DC/AC converter in the primary side. The results are summarized in Table 3. The current on the secondary coil when no misalignment occurs is 9.83 A. This leads to a power delivered to the load equal to 1.15 kW. The application of the controller also impacts the power delivered to the load. The controller limits this metric to 775 W. This limitation is necessary to maintain the primary current in the specified range. However, the efficiency is slightly modified. In the case with misalignment and no control, its value is 99%. Alternatively, under the same circumstances but with the use of the proposed control technique, the efficiency is 97%. The small differences are due to the additional harmonics that the phase-shift control incorporates.

**Table 3.** Experimental results of the prototype.

Condition	DC/AC Output Power	Power Delivered to the Load	Efficiency
No misalignment	1.17 kW	1.15 kW	98%
Coil misalignment and no control	1.7 kW	1.69 kW	99%
Coil misalignment and control	790 W	775 W	97%

## 6. Conclusions

The design and implementation of a control algorithm for a wireless charger for an EV. The three main contributions of the paper are as follows: (i) the controller is adapted for a bidirectional system; (ii) the system works at 85 kHz as recommended by SAE J2954 and (iii) the controller alters the system operation in order to guarantee that the whole system works under safe conditions. The controllers, which are installed on the primary and secondary side to allow the two-directional power flow, restrict the input power based on a phase-shift control. Particularly, under coil misalignments, the primary current is the electrical magnitude that suffers from more noticeable increments. Consequently, this is one of the magnitudes that the controller restricts.

The proposed control is based on the advantage of a wireless data exchange between primary and secondary coils. Battery power charge and primary current are selected as the input variables of the control system.

It has been shown that the system correctly regulates the transmitted power to the established values under coil misalignments, preventing the charger from operating outside its limits.



Test results are described for the charging phase. We observed that the value of the primary current increases when a coil misalignment occurs but is maintained under its defined limits with the phase shift technique.

**Author Contributions:** The research problem addressed by the paper was identified by the three authors. The three authors proposed the methodology and José Manuel González-González conducted the simulation study and implementation of the prototype. The results were reviewed and analysed by the three authors.

**Conflicts of Interest:** The authors declare no conflict of interest.

## References

1. U.S. Energy Information Administration. *Annual Energy Outlook 2017 with Projections to 2050*; Technical Report; U.S. Energy Information Administration: Washington, DC, USA, 2017.
2. Holtmark, B.; Skonhoft, A. The Norwegian support and subsidy policy of electric cars. Should it be adopted by other countries? *Environ. Sci. Policy* **2014**, *42*, 160–168.
3. Comodi, G.; Caresana, F.; Salvi, D.; Pelagalli, L.; Lorenzetti, M. Local promotion of electric mobility in cities: Guidelines and real application case in Italy. *Energy* **2016**, *95*, 494–503.
4. Miller, J.M.; Onar, O.C.; White, C.; Campbell, S.; Coomer, C.; Seiber, L.; Sepe, R.; Steyerl, A. Demonstrating Dynamic Wireless Charging of an Electric Vehicle: The Benefit of Electrochemical Capacitor Smoothing. *IEEE Power Electron. Mag.* **2014**, *1*, 12–24.
5. Maglaras, L.A.; Jiang, J.; Maglaras, A.; Topalis, F.V.; Moschoyiannis, S. Dynamic wireless charging of electric vehicles on the move with Mobile Energy Disseminators. *Int. J. Adv. Comput. Sci. Appl.* **2015**, *6*, 239–251.
6. Chen, J.-J.; Yang, F.-C.; Lai, C.-C.; Hwang, Y.-S.; Lee, R.-G. A High-Efficiency Multimode Li-Ion Battery Charger With Variable Current Source and Controlling Previous-Stage Supply Voltage. *IEEE Trans. Ind. Electron.* **2009**, *56*, 2469–2478.
7. Jiang, W.; Xu, S.; Li, N.; Lin, Z.; Williams, B.W. Wireless Power Charger for Light Electric Vehicles. In Proceedings of the 2015 IEEE 11th International Conference on Power Electronics and Drive Systems, Sydney, Australia, 9–12 June 2015; pp. 562–566.
8. Egan, M.G.; O’Sullivan, D.L.; Hayes, J.G.; Willers, M.J.; Henze, C.P. Power-Factor-Corrected Single-Stage Inductive Charger for Electric Vehicle Batteries. *IEEE Trans. Ind. Electron.* **2007**, *54*, 1217–1226.
9. Deng, J.; Lu, F.; Li, S.; Nguyen, T.D.; Mi, C. Development of a high efficiency primary side controlled 7 kW wireless power charger. In Proceedings of the 2014 IEEE International Electric Vehicle Conference (IEVC), Florence, Italy, 17–19 December 2014; pp. 1–6.
10. Lee, J.Y.; Han, B.M. A Bidirectional Wireless Power Transfer EV Charger Using Self-Resonant PWM. *IEEE Trans. Power Electron.* **2015**, *30*, 1784–1787.
11. Deng, Q.; Liu, J.; Czarkowski, D.; Bojarski, M.; Asa, E.; de Leon, F. Design of a wireless charging system with a phase-controlled inverter under varying parameters. *IET Power Electron.* **2016**, *9*, 2461–2470.
12. Iga, Y.; Omori, H.; Morizane, T.; Kimura, N.; Nakamura, Y.; Nakaoka, M. New IPT-wireless EV charger using single-ended quasi-resonant converter with power factor correction. In Proceedings of the 2012 International Conference on Renewable Energy Research and Applications (ICRERA), Nagasaki, Japan, 11–14 November 2012; pp. 1–6.
13. Asa, E.; Colak, K.; Bojarski, M.; Czarkowski, D. A novel multi-level phase-controlled resonant inverter with common mode capacitor for wireless EV chargers. In Proceedings of the 2015 IEEE Transportation Electrification Conference and Expo (ITEC), Metro Detroit, MI, USA, 14–17 June 2015; pp. 1–6.
14. Liu, F.; Chen, K.; Zhao, Z.; Li, K.; Yuan, L. Transmitter-Side Control of Both the CC and CV Modes for the Wireless EV Charging System with the Weak Communication. *IEEE J. Emerg. Sel. Top. Power Electron.* **2017**, doi:10.1109/JESTPE.2017.2759581 .
15. Colak, K.; Bojarski, M.; Asa, E.; Czarkowski, D. A constant resistance analysis and control of cascaded buck and boost converter for wireless EV chargers. In Proceedings of the 2015 IEEE Applied Power Electronics Conference and Exposition (APEC), Charlotte, NC, USA, 15–19 March 2015; pp. 3157–3161.
16. Miller, J.M.; Onar, O.C.; Chinthavali, M. Primary-Side Power Flow Control of Wireless Power Transfer for Electric Vehicle Charging. *IEEE J. Emerg. Sel. Top. Power Electron.* **2015**, *3*, 147–162.

17. Bojarski, M.; Asa, E.; Colak, K.; Czarkowski, D. A 25 kW industrial prototype wireless electric vehicle charger. In Proceedings of the 2016 IEEE Applied Power Electronics Conference and Exposition (APEC), Long Beach, CA, USA, 20–24 March 2016; pp. 1756–1761.
18. Deng, Q.; Liu, J.; Czarkowski, D.; Kazmierczuk, M.K.; Bojarski, M.; Zhou, H.; Hu, W. Frequency-Dependent Resistance of Litz-Wire Square Solenoid Coils and Quality Factor Optimization for Wireless Power Transfer. *IEEE Trans. Ind. Electron.* **2016**, *63*, 2825–2837.
19. Gonzalez-Gonzalez, J.M.; Trivino-Cabrera, A.; Aguado, J.A. Control algorithm for wireless EV charger considering operational constraints of electrical components. In Proceedings of the 2017 11th IEEE International Conference on Compatibility, Power Electronics and Power Engineering (CPE-POWERENG), Cadiz, Spain, 4–6 April 2017; pp. 211–216.
20. Aditya, K.; Williamson, S.S. Comparative study of Series-Series and Series-Parallel compensation topologies for electric vehicle charging. In Proceedings of the 2014 IEEE 23rd International Symposium on Industrial Electronics (ISIE), Istanbul, Turkey, 1–4 June 2014; pp. 426–430.
21. González-González, J.M.; Cabrera, D.F.; Cabrera, A.T.; Aguado, J.A. Power Factor Corrector Design applied to an 85-kHz Wireless Charger. In Proceedings of the International Conference on Renewable Energies and Power Quality (ICREPQ'16), Madrid, Spain, 4–6 May 2016; pp. 521–525.
22. Otomo, Y.; Sato, Y.; Fujita, S.; Igarashi, H. Synthesis of Equivalent Circuit of Wireless Power Transfer Device Using Homogenization-Based FEM. *IEEE Trans. Magn.* **2017**, doi:10.1109/TMAG.2017.2749968 .
23. Tran, D.H.; Vu, V.B.; Choi, W. Design of a High-Efficiency Wireless Power Transfer System With Intermediate Coils for the On-Board Chargers of Electric Vehicles. *IEEE Trans. Power Electron.* **2018**, *33*, 175–187.
24. Deng, Q.; Liu, J.; Czarkowski, D.; Hu, W.; Zhou, H. An Inductive Power Transfer System Supplied by a Multiphase Parallel Inverter. *IEEE Trans. Ind. Electron.* **2017**, *64*, 7039–7048.
25. Fotopoulou, K.; Flynn, B.W. Wireless Power Transfer in Loosely Coupled Links: Coil Misalignment Model. *IEEE Trans. Magn.* **2011**, *47*, 416–430.
26. SAE International. *SAE International Approves TIR J2954 for PH/EV Wireless Charging*; SAE International: Warrendale, PA, USA, 2016.
27. Liu, X.; Wang, T.; Yang, X.; Jin, N.; Tang, H. Analysis and Design of a Wireless Power Transfer System with Dual Active Bridges. *Energies* **2017**, *10*, 1588, doi:10.3390/en10101588.
28. Berger, A.; Agostinelli, M.; Vesti, S.; Oliver, J.A.; Cobos, J.A.; Huemer, M. A Wireless Charging System Applying Phase-Shift and Amplitude Control to Maximize Efficiency and Extractable Power. *IEEE Trans. Power Electron.* **2015**, *30*, 6338–6348.
29. Chen, B.-Y.; Lai, Y.-S. Switching Control Technique of Phase-Shift-Controlled Full-Bridge Converter to Improve Efficiency Under Light-Load and Standby Conditions Without Additional Auxiliary Components. *IEEE Trans. Power Electron.* **2010**, *25*, 1001–1012.
30. Triviño-Cabrera, A.; Aguado, J.; González, J.M. Analytical characterisation of magnetic field generated by ICPT wireless charger. *Electron. Lett.* **2017**, *53*, 871–873.
31. Microchip. *PIC16(L)F18324/18344 Datasheet*; Microchip Technology: Chandler, AZ, USA, 2017.
32. Intel. *Intel Edison Compute Module Hardware Guide*; Intel: Santa Clara, CA, USA, 2016.



© 2018 by the authors. Licensee MDPI, Basel, Switzerland. This article is an open access article distributed under the terms and conditions of the Creative Commons Attribution (CC BY) license (<http://creativecommons.org/licenses/by/4.0/>).

## 3.5 Model predictive control to maximize the efficiency in EV wireless chargers

Wireless chargers are less competitive than conductive chargers in terms of efficiency. For this reason, one of the main goals is to maximize the efficiency of these chargers. Both Litz wire and SiC semiconductors help to improve the efficiency. However, higher efficiency values can be achieved by adjusting the operating parameters.

The goal of this work is to maximize the efficiency in magnetic resonant wireless chargers by reducing the losses in coils and power electronics. This is no small task as losses are strongly related to the operation mode of the power converters.

Thus, the development of this work begins with an exhaustive analysis of the losses in the system which are not related to the coupling factor between both coils. At this point, it is not only important to calculate the losses, but to identify which operating parameters of the system impact on the magnitude of the losses in each component. Moreover, losses in a wireless charger depend on the topology of the system. Our study is based on a SS topology.

By conducting a mesh-analysis (in Figure 3.8), we can infer that the operating frequency and the battery equivalent resistance are the two parameters that have the strongest impact on efficiency.

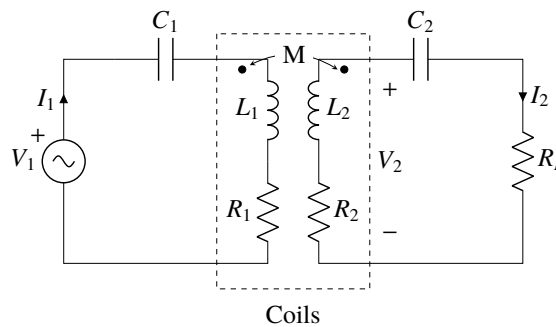


**Figure 3.8:** Generic diagram for magnetic resonance wireless chargers with SS compensation networks.

The first parameter controls whether the system is operating at resonance or not. Its importance is mainly related to the manufacturing tolerance, i.e. the coils and capacitors are not manufactured with absolute precision, causing the power factor in the circuit to be less than unity. Alternatively, the second parameter impacts on the currents that circulate through the primary and the secondary sides of the charger. Figure 3.9 shows how the efficiency varies as a function of  $R_{eq}$  for different operating frequencies in a theoretical system with the same features as the laboratory prototype.



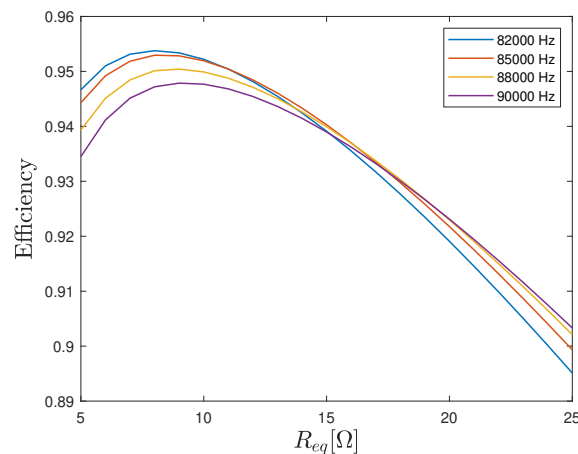


**Figure 3.9:** Efficiency as a function of  $R_{eq}$  and frequency.

From these results, we conclude that the curve corresponding to an operating frequency of 82 kHz (lower limit of the allowed range in SAE J2954) achieves the highest efficiency value with an equivalent resistance of 7  $\Omega$ . The maximum efficiency values decrease as the operating frequency of the system is increased, while these maximums are achieved with slightly higher equivalent resistance values. In the analysed range, efficiency improvements of up to 6% are achieved.

Therefore, a maximum efficiency control must determine the perfect tuning of both parameters. In addition, it should provide the capability to regulate the charging power. Controlling these parameters simultaneously requires acting on both sides of the charger, since the operating frequency is regulated on the primary inverter and the equivalent resistance on the secondary side, either by a controlled rectifier or a DC/DC converter. The charging power can be adjusted using the phase-shifting technique in the primary inverter. This makes communications essential in this type of control if misalignment is allowed.

In the related work, there are several controls that pursue the objective of maximum efficiency. The most widely used control technique for this purpose in the literature is based on Maximum Efficiency Point Tracking (MEPT), in which the controller makes small variations in the control parameters and checks for improvements in efficiency. However, MEPT controllers derive in high response times and can control two control parameters at most, such as the charging power and the equivalent resistance of the battery, or the charging power and the frequency. This restriction reduces the capability of the system to reach the optimum efficiency with the desired power delivery.

MPCs make it possible to address the configuration of all control variables (the configuration parameters of the power converters) concurrently. This is done within reduced response and calculation times. To implement a correct MPC, an accurate model is required to predict the behaviour of the system variables when the configuration parameters are changed. This model is defined by four equations for the real and imaginary part of

the primary and secondary sides. The equations are derived from a mesh-based analysis.

$$(R_1 + 2R_{m,ds})ir_1 - \left(\omega L_1 - \frac{1}{\omega C_1}\right)ii_1 - \omega Mii_2 = V_1 \quad (3.3)$$

$$(R_1 + 2R_{m,ds})ii_1 + \left(\omega L_1 - \frac{1}{\omega C_1}\right)ir_1 + \omega Mir_2 = 0 \quad (3.4)$$

$$-\omega Mii_1 + (R_{eq} + R_2 + 2R_d)ir_2 - \left(\omega L_2 - \frac{1}{\omega C_2}\right)ii_2 = 0 \quad (3.5)$$

$$\omega Mir_1 + (R_{eq} + R_2 + 2R_d)ii_2 + \left(\omega L_2 - \frac{1}{\omega C_2}\right)ir_2 = 0 \quad (3.6)$$

In these equations, the mutual inductance is a system parameter which must be measured in real time because it is affected by several factors such as coil misalignment. To achieve a feasible implementation, this parameter is estimated using the primary current and the open-circuit secondary voltage measurements.

The optimal values for control variables are computed with an optimization tool which uses the efficiency as an objective function. In addition to the losses considered in the previous theoretical analysis, the model used for the optimization also includes the losses of the power converters, i.e. losses in diodes and MOSFETs. Diode losses correspond to losses in the secondary rectifier and their calculation is based on the dynamic resistance of the diodes. Furthermore, MOSFET losses correspond to losses in the primary inverter and are related to conduction, switching, duty cycle and snubber losses.

Using the system model, its corresponding losses, the operating constraints and the objective function, the optimization algorithm provides the optimum values for the operating frequency, the inverter phase-shifting and the secondary DC/DC converter. If it is not possible to reach the established charging power with the maximum efficiency value, the algorithm opts to reduce this efficiency to guarantee the charging power.

The effectiveness of the proposed MPC has been validated in the laboratory prototype. This task has been carried out by measuring the efficiency of the charger under different operating situations and comparing the results with those provided by other controllers based on a single control variable. Table 3.1 shows the results of this analysis, with the efficiency and the operating parameters for different control algorithms and misalignments. The comparison shows a better efficiency not only in ideal situations but also when misalignments occur. The proposed control manages to increase efficiency by up to 5% compared to other controllers.

**Table 3.1:** Comparison of the efficiency under different  $M$  values.

$M$ ( $\mu H$ )	Algorithm	$\eta$ (%)	$R_L$ ( $\Omega$ )	$\alpha$	D	f (kHz)
18.9E-6	Proposed	97.2	8.5	110	0.42	82.4
	PI controller	94.2	25	80	-	85.0
	$R_{eq}$ MEPT	96.2	8.8	106	0.41	85.0
	Freq MEPT	95.6	25	116	-	89.8
17.1E-6	Proposed	95.9	7.5	104	0.45	82.1
	PI controller	92.7	25	80	-	85.0
	$R_{eq}$ MEPT	95.0	7.8	99	0.44	85.0
	Freq MEPT	94.5	25	128	-	89.8
14.9E-6	Proposed	95.1	6.3	97	0.50	81.8
	PI controller	90.7	25	84	-	85.0
	$R_{eq}$ MEPT	94.5	6.7	90	0.48	85.0
	Freq MEPT	92.4	25	180	-	90.0

Pages 119-128 are hidden due to copyright. They contain the following paper:

J. M. Gonzalez-Gonzalez, A. Trivino and J. A. Aguado, "Model Predictive Control to Maximize the Efficiency in EV Wireless Chargers," *IEEE Transactions on Industrial Electronics*, Early Access, 2020. doi: 10.1109/TIE.2021.3057006.

# Chapter 4

## Conclusions and future work

---

This chapter includes the main conclusions of the work developed throughout this Thesis. It also describes the future research lines that can provide more advanced solutions based on the contributions.



## 4.1 Conclusions

The development of this Thesis has covered the proposed research objectives in the field of wireless charging. The conclusions obtained in this work are the following:

- The review of the state of art has made it possible to establish that magnetic resonance is the most appropriate technology compared to other alternatives thanks to its power and efficiency levels. In the context of EV wireless charging, one of the main research topics is the control system, which seeks to maximize the power transfer efficiency in order to improve its competitiveness against conductive charging.
- It is essential to analyse the magnetic field when designing power transmission coils. With that in mind, we have developed an analytical characterization of the magnetic field generated by a magnetic resonance wireless charger. This model makes it possible to compute the magnetic field in any spatial position. Although this characterization has been developed for rectangular coils, which are the most tolerant to misalignment, it can easily be adapted to support other structures. The model has been validated by means of an experimental prototype.
- The transition from conductive charging to wireless charging should be a gradual process that makes it easier for the user to adopt this new technology. One of the keys to this process lies in the development of a hybrid charging system, which reduces the cost and weight of the electronics installed in the vehicle. To achieve this, this Thesis proposes a hybrid charger that improves the integration of conductive and wireless charging since it shares a large part of the on-board elements between both systems.
- One of the main limitations of the literature on this topic is the lack of experimentation in real situations, such as the use of lithium batteries and the automation and control of the entire charging process. In addition, these prototypes are usually focused on the charging of cars, when their application is also suitable for other vehicles such as e-bikes, motorbikes, drones, etc. In view of this, we have developed a charger for e-bikes. The process has included a compact design of the coils and power electronics, as well as a control that operates following a CC/CV strategy with low computational cost. The prototype has met the intended performance and efficiency targets.
- Coil misalignment is one of the most common problems affecting magnetic-resonant chargers. This fact is analysed in one of the contributions, which determines the primary intensity as the variable most affected by misalignment. In order to prevent

possible overcurrents from damaging the system components, a control strategy has been proposed. The control operates at the 85-kHz frequency; it regulates the load power and limits the current at the critical points of the system.

- Charging efficiency depends on multiple factors in the wireless charger's operation. Some of these factors, such as misalignment, cannot be controlled. However, there are variables that can be regulated by the control system and power electronics, such as the operating frequency and the equivalent resistance of the battery. In order to work with the optimal operating values of both variables, we have proposed an MPC that maximizes the efficiency. The algorithm developed includes a mesh analysis and an accurate model of the charger losses. Experimental results confirm the convenience of the MPC.

## 4.2 Future work

The following future lines of research are proposed:

- Developing an on-board hybrid charger prototype, in which the two potential power flows (conductive and wireless) share some power electronics on the secondary side. In contrast to the proposal presented in this Thesis, the hybrid charger is not based on complex coil structures but on the regulation of a common controlled rectifier on the secondary side. The bidirectional nature of the controlled rectifier will also provide V2G functionality, which will make it possible to maximize the use of self-consumption facilities or the creation of profit by providing ancillary services to the grid.
- Developing a new charger prototype for the laboratory; it should be more flexible and have a higher maximum operating power. This prototype will require redesigning the power electronics, which will provide it with bidirectional features and facilitate the implementation of new control strategies. These control strategies will be oriented to the decision of the direction of the power flow, as well as the maximization of the efficiency of this process.
- Designing, developing and testing an MPC for a V2G wireless charger. This controller aims to adjust the operation of the power electronics to control the power flow in both directions in the most efficient way. This line of development is an extension of the maximum efficiency contribution. The control will allow a four-quadrant operation, that is, any combination of the active and reactive power.



- Adapting the prototype and control strategies for operation with Li-ion batteries. In order to make this possible, the charger control has to communicate with the Battery Management System (BMS), which will provide several data regarding the status of the battery and its charging values.
- Design and evaluation of data-driven control algorithms for magnetic-resonance wireless chargers.



# Bibliography

---

- [1] United Nations, “Paris Agreement,” United Nations, Paris, Tech. Rep., 2015.
- [2] International Energy Agency (IEA), “CO2 Emissions from Fuel Combustion,” Paris, Tech. Rep., 2020.
- [3] ———, “Global EV Outlook 2020,” Paris, Tech. Rep., 2020.
- [4] S. Wee, M. Coffman, and S. La Croix, “Do electric vehicle incentives matter? Evidence from the 50 U.S. states,” *Research Policy*, vol. 47, no. 9, pp. 1601–1610, 11 2018.
- [5] “European vehicle emissions standards – Euro 7 for cars, vans, lorries and buses ,” <https://ec.europa.eu/info/law/better-regulation/have-your-say/initiatives/12313-European-vehicle-emissions-standards-Euro-7-for-cars-vans-lorries-and-buses>, accessed: 2021-03-29.
- [6] D. Pevec, J. Babic, and V. Podobnik, “Electric Vehicles: A Data Science Perspective Review,” *Electronics*, vol. 8, no. 10, p. 1190, 10 2019. [Online]. Available: <https://www.mdpi.com/2079-9292/8/10/1190>
- [7] J. Neubauer and E. Wood, “The impact of range anxiety and home, workplace, and public charging infrastructure on simulated battery electric vehicle lifetime utility,” *Journal of Power Sources*, vol. 257, pp. 12–20, 7 2014.
- [8] N. Rauh, T. Franke, and J. F. Krems, “Understanding the impact of electric vehicle driving experience on range anxiety,” *Human Factors*, vol. 57, no. 1, pp. 177–187, 2 2015. [Online]. Available: <http://journals.sagepub.com/doi/10.1177/0018720814546372>

- [9] “SAE Electric Vehicle and Plug in Hybrid Electric Vehicle Conductive Charge Coupler,” Society of Automotive Engineers, International Standard SAE J1772:201710, Nov 2017.
- [10] “Electric vehicle conductive charging system - Part 1: General requirements,” International Electrotechnical Commission, International Standard IEC 61851-1:2017, Feb 2017.
- [11] J. M. Gonzalez-Gonzalez, S. Martin, P. Lopez, and J. A. Aguado, “Hybrid battery-ultracapacitor storage system sizing for renewable energy network integration,” *IET Renewable Power Generation*, vol. 14, no. 13, pp. 2367–2375, 10 2020. [Online]. Available: <https://onlinelibrary.wiley.com/doi/10.1049/iet-rpg.2019.1310>
- [12] “Wireless Power Transfer for Light-Duty Plug-in/Electric Vehicles and Alignment Methodology,” Society of Automotive Engineers, International Standard SAE J2954:202010, Nov 2020.
- [13] A. Triviño, J. M. González-González, and J. A. Aguado, “Wireless Power Transfer Technologies Applied to Electric Vehicles: A Review,” *Energies*, vol. 14, no. 6, p. 1547, 3 2021. [Online]. Available: <https://www.mdpi.com/1996-1073/14/6/1547>
- [14] A. Triviño-Cabrera, J. M. González-González, and J. A. Aguado, *Wireless Power Transfer for Electric Vehicles: Foundations and Design Approach*, ser. Power Systems. Cham: Springer International Publishing, 2020. [Online]. Available: <http://link.springer.com/10.1007/978-3-030-26706-3>
- [15] “Information technology — Radio frequency identification for item management — Part 1: Reference architecture and definition of parameters to be standardized,” International Organization for Standardization, International Standard ISO/IEC 18000-1:2008, 7 2008.
- [16] “The Qi Wireless Power Transfer System Power Class 0 Specification,” Wireless Power Consortium, International Standard, 2 2017.
- [17] A. Kurs, A. Karalis, R. Moffatt, J. D. Joannopoulos, P. Fisher, and M. Soljačić, “Wireless power transfer via strongly coupled magnetic resonances,” *Science*, vol. 317, no. 5834, pp. 83–86, 7 2007. [Online]. Available: <https://science.sciencemag.org/content/317/5834/83>
- [18] D. S. Ricketts, M. J. Chabalko, and A. Hillenius, “Experimental demonstration of the equivalence of inductive and strongly coupled magnetic resonance wireless

- power transfer,” *Applied Physics Letters*, vol. 102, no. 5, p. 053904, 2 2013. [Online]. Available: <http://aip.scitation.org/doi/10.1063/1.4788748>
- [19] A. Triviño-Cabrera and J. Sánchez, “A Review on the Fundamentals and Practical Implementation Details of Strongly Coupled Magnetic Resonant Technology for Wireless Power Transfer,” *Energies*, vol. 11, no. 10, p. 2844, 10 2018. [Online]. Available: <http://www.mdpi.com/1996-1073/11/10/2844>
- [20] S. Sinha, A. Kumar, B. Regensburger, and K. K. Afridi, “A New Design Approach to Mitigating the Effect of Parasitics in Capacitive Wireless Power Transfer Systems for Electric Vehicle Charging,” *IEEE Transactions on Transportation Electrification*, vol. 5, no. 4, pp. 1040–1059, 12 2019.
- [21] F. Lu, H. Zhang, and C. Mi, “A Review on the Recent Development of Capacitive Wireless Power Transfer Technology,” *Energies*, vol. 10, no. 11, p. 1752, 11 2017. [Online]. Available: <http://www.mdpi.com/1996-1073/10/11/1752>
- [22] H. Zhang, F. Lu, H. Hofmann, W. Liu, and C. C. Mi, “A Four-Plate Compact Capacitive Coupler Design and LCL-Compensated Topology for Capacitive Power Transfer in Electric Vehicle Charging Application,” *IEEE Transactions on Power Electronics*, vol. 31, no. 12, pp. 8541–8551, 12 2016.
- [23] —, “Six-Plate Capacitive Coupler to Reduce Electric Field Emission in Large Air-Gap Capacitive Power Transfer,” *IEEE Transactions on Power Electronics*, vol. 33, no. 1, pp. 665–675, 1 2018.
- [24] V. B. Vu, M. Dahidah, V. Pickert, and V. T. Phan, “An Improved LCL-L Compensation Topology for Capacitive Power Transfer in Electric Vehicle Charging,” *IEEE Access*, vol. 8, pp. 27 757–27 768, 2020.
- [25] B. Luo, T. Long, L. Guo, R. Dai, R. Mai, and Z. He, “Analysis and Design of Inductive and Capacitive Hybrid Wireless Power Transfer System for Railway Application,” in *IEEE Transactions on Industry Applications*, vol. 56, no. 3. Institute of Electrical and Electronics Engineers Inc., 5 2020, pp. 3034–3042.
- [26] J. Dai and D. C. Ludois, “A Survey of Wireless Power Transfer and a Critical Comparison of Inductive and Capacitive Coupling for Small Gap Applications,” *IEEE Transactions on Power Electronics*, vol. 30, no. 11, pp. 6017–6029, 11 2015.
- [27] F. Lu, H. Zhang, H. Hofmann, and C. Mi, “A Double-Sided LCLC-Compensated Capacitive Power Transfer System for Electric Vehicle Charging,” *IEEE Transactions on Power Electronics*, vol. 30, no. 11, pp. 6011–6014, 11 2015.

- [28] D. Vincent, P. S. Huynh, N. A. Azeez, L. Patnaik, and S. S. Williamson, "Evolution of Hybrid Inductive and Capacitive AC Links for Wireless EV Charging - A Comparative Overview," *IEEE Transactions on Transportation Electrification*, vol. 5, no. 4, pp. 1060–1077, 12 2019.
- [29] Powercastco, "Wireless Power Products," <https://www.powercastco.com/>, accessed: 2021-02-01. [Online]. Available: <https://www.powercastco.com/>
- [30] "Cota: Real Wireless Power," <https://www.ossia.com/cota/>, accessed: 2021-02-01. [Online]. Available: <https://www.ossia.com/cota/>
- [31] Energous, "WattUp® Wire-Free Charging Technology," <http://energous.com/>, accessed: 2021-02-01. [Online]. Available: <http://energous.com/>
- [32] S. Nakagawa, Y. Yamanaka, K. Ohdo, J. Miyasaka, H. Shimizu, H. Nakashima, K. Hashimoto, N. Shinohara, and T. Mitani, "Development of an Electric Vehicle by Microwave Power Transmission," in *IFAC Proceedings Volumes (IFAC-PapersOnline)*, vol. 3, no. PART 1. Elsevier, 1 2010, pp. 209–214.
- [33] N. Shinohara, Y. Kubo, and H. Tonomura, "Wireless charging for electric vehicle with microwaves," in *2013 3rd International Electric Drives Production Conference, EDPC 2013 - Proceedings*. IEEE Computer Society, 2013.
- [34] W. Zhou and K. Jin, "Efficiency Evaluation of Laser Diode in Different Driving Modes for Wireless Power Transmission," *IEEE Transactions on Power Electronics*, vol. 30, no. 11, pp. 6237–6244, 11 2015.
- [35] K. J. Duncan, "Laser based power transmission: Component selection and laser hazard analysis," in *IEEE PELS Workshop on Emerging Technologies: Wireless Power, WoW 2016*. Institute of Electrical and Electronics Engineers Inc., 12 2016, pp. 100–103.
- [36] Wi-Charge, "Long-Range Wireless Charger." [Online]. Available: <https://www.wi-charge.com/products>
- [37] E. Cavallaro, "Researchers transmit energy with laser in 'historic' power-beaming demonstration," 10 2019. [Online]. Available: <https://www.nrl.navy.mil/Media/News/Article/2504007/researchers-transmit-energy-with-laser-in-historic-power-beaming-demonstration/>
- [38] A. S. Al-Ogaili, T. J. Tengku Hashim, N. A. Rahmat, A. K. Ramasamy, M. B. Marsadek, M. Faisal, and M. A. Hannan, "Review on scheduling, clustering, and

- forecasting strategies for controlling electric vehicle charging: Challenges and recommendations,” *IEEE Access*, vol. 7, pp. 128 353–128 371, 2019.
- [39] International Commission on Non-Ionizing Radiation Protection, “Guidelines for limiting exposure to time-varying electric and magnetic fields (1 Hz TO 100 kHz),” *Health Physics*, vol. 99, no. 6, pp. 818–836, 12 2010. [Online]. Available: <https://pubmed.ncbi.nlm.nih.gov/21068601/>
- [40] F. Fattori, N. Anglani, and G. Muliere, “Combining photovoltaic energy with electric vehicles, smart charging and vehicle-to-grid,” *Solar Energy*, vol. 110, pp. 438–451, 12 2014.
- [41] E. Gonzalez-Romera, F. Barrero-Gonzalez, E. Romero-Cadaval, and M. I. Milanés-Montero, “Overview of plug-in electric vehicles as providers of ancillary services,” in *Proceedings - 2015 9th International Conference on Compatibility and Power Electronics, CPE 2015*. Institute of Electrical and Electronics Engineers Inc., 8 2015, pp. 516–521.
- [42] C. Panchal, S. Stegen, and J. Lu, “Review of static and dynamic wireless electric vehicle charging system,” pp. 922–937, 10 2018.
- [43] Z. Luo and X. Wei, “Mutual Inductance Analysis of Planar Coils with Misalignment for Wireless Power Transfer Systems in Electric Vehicle,” in *2016 IEEE Vehicle Power and Propulsion Conference, VPPC 2016 - Proceedings*. Institute of Electrical and Electronics Engineers Inc., 12 2016.
- [44] D. De Marco, A. Dolara, M. Longo, and W. Yaïci, “Design and performance analysis of pads for dynamic wireless charging of EVs using the finite element method,” *Energies*, vol. 12, no. 21, p. 4139, 10 2019. [Online]. Available: [www.mdpi.com/journal/energies](http://www.mdpi.com/journal/energies)
- [45] J. T. Boys and G. A. Covic, “The inductive power transfer story at the University of Auckland,” *IEEE Circuits and Systems Magazine*, vol. 15, no. 2, pp. 6–27, 4 2015.
- [46] J. Sallán, J. L. Villa, A. Llombart, and J. F. Sanz, “Optimal design of ICPT systems applied to electric vehicle battery charge,” *IEEE Transactions on Industrial Electronics*, vol. 56, no. 6, pp. 2140–2149, 2009.
- [47] H. Feng, T. Cai, S. Duan, J. Zhao, X. Zhang, and C. Chen, “An LCC-Compensated Resonant Converter Optimized for Robust Reaction to Large Coupling Variation in Dynamic Wireless Power Transfer,” *IEEE Transactions on Industrial Electronics*, vol. 63, no. 10, pp. 6591–6601, 10 2016.

- [48] Y. Gao, C. Duan, A. A. Oliveira, A. Ginart, K. B. Farley, and Z. T. H. Tse, “3-D Coil Positioning Based on Magnetic Sensing for Wireless EV Charging,” *IEEE Transactions on Transportation Electrification*, vol. 3, no. 3, pp. 578–588, 9 2017.
- [49] W. Ni, I. B. Collings, X. Wang, R. P. Liu, A. Kajan, M. Hedley, and M. Abolhasan, “Radio alignment for inductive charging of electric vehicles,” *IEEE Transactions on Industrial Informatics*, vol. 11, no. 2, pp. 427–440, 4 2015.
- [50] A. Babu and B. George, “Sensor System to Aid the Vehicle Alignment for Inductive EV Chargers,” *IEEE Transactions on Industrial Electronics*, vol. 66, no. 9, pp. 7338–7346, 9 2019.
- [51] J. M. González-González, A. Triviño-Cabrera, and J. A. Aguado, “Design and validation of a control algorithm for a SAE J2954-compliant wireless charger to guarantee the operational electrical constraints,” *Energies*, vol. 11, no. 3, p. 604, 2 2018. [Online]. Available: [www.mdpi.com/journal/energies](http://www.mdpi.com/journal/energies)
- [52] M. Feliziani, T. Campi, S. Cruciani, F. Maradei, U. Grasselli, M. Macellari, and L. Schirone, “Robust LCC compensation in wireless power transfer with variable coupling factor due to coil misalignment,” in *2015 IEEE 15th International Conference on Environment and Electrical Engineering, IEEEIC 2015 - Conference Proceedings*. Institute of Electrical and Electronics Engineers Inc., 7 2015, pp. 1181–1186.
- [53] T. Kan, F. Lu, T. D. Nguyen, P. P. Mercier, and C. C. Mi, “Integrated Coil Design for EV Wireless Charging Systems Using LCC Compensation Topology,” *IEEE Transactions on Power Electronics*, vol. 33, no. 11, pp. 9231–9241, 11 2018.
- [54] L. Zhao, D. J. Thrimawithana, and U. K. Madawala, “Hybrid Bidirectional Wireless EV Charging System Tolerant to Pad Misalignment,” *IEEE Transactions on Industrial Electronics*, vol. 64, no. 9, pp. 7079–7086, 9 2017.
- [55] S. Cruciani, F. Maradei, and M. Feliziani, “Assessment of magnetic field levels generated by a wireless power transfer (WPT) system at 20 kHz,” in *IEEE International Symposium on Electromagnetic Compatibility*, 2013, pp. 259–264.
- [56] U. K. Madawala and D. J. Thrimawithana, “A bidirectional inductive power interface for electric vehicles in V2G systems,” *IEEE Transactions on Industrial Electronics*, vol. 58, no. 10, pp. 4789–4796, 10 2011.



- [57] X. She, A. Q. Huang, O. Lucia, and B. Ozpineci, "Review of Silicon Carbide Power Devices and Their Applications," *IEEE Transactions on Industrial Electronics*, vol. 64, no. 10, pp. 8193–8205, 10 2017.
- [58] J. McBryde, A. Kadavelugu, B. Compton, S. Bhattacharya, M. Das, and A. Agarwal, "Performance comparison of 1200V silicon and SiC devices for UPS application," in *IECON Proceedings (Industrial Electronics Conference)*, 2010, pp. 2657–2662.
- [59] Y. Li, R. Mai, M. Yang, and Z. He, "Cascaded multi-level inverter based IPT systems for high power applications," *Journal of Power Electronics*, vol. 15, no. 6, pp. 1508–1516, 2015. [Online]. Available: <http://dx.doi.org/10.6113/JPE.2015.15.6.1508>
- [60] J. Deng, S. Li, S. Hu, C. C. Mi, and R. Ma, "Design methodology of LLC resonant converters for electric vehicle battery chargers," *IEEE Transactions on Vehicular Technology*, vol. 63, no. 4, pp. 1581–1592, 2014.
- [61] T. Wang, X. Liu, N. Jin, H. Tang, X. Yang, and M. Ali, "Wireless power transfer for battery powering system," *Electronics (Switzerland)*, vol. 7, no. 9, p. 178, 9 2018. [Online]. Available: [www.mdpi.com/journal/electronics](http://www.mdpi.com/journal/electronics)
- [62] P. Guo, R. Yuan, Y. Chen, C. Cai, and L. Yang, "High-bandwidth-utilization wireless power and information transmission based on DDPSK Modulation," *IEEE Access*, vol. 7, pp. 85 560–85 572, 2019.
- [63] F. Corti, A. Reatti, A. Nepote, L. Pugi, M. Pierini, L. Paolucci, F. Grasso, E. Grasso, and M. Nienhause, "A secondary-side controlled electric vehicle wireless charger," *Energies*, vol. 13, no. 24, p. 6527, 12 2020. [Online]. Available: [www.mdpi.com/journal/energies](http://www.mdpi.com/journal/energies)
- [64] C. I. Chen, G. A. Covic, and J. T. Boys, "Regulator capacitor selection for series compensated IPT pickups," in *IECON Proceedings (Industrial Electronics Conference)*. IEEE Computer Society, 2008, pp. 932–937.
- [65] V. Jiwariyavej, T. Imura, and Y. Hori, "Coupling coefficients estimation of wireless power transfer system via magnetic resonance coupling using information from either side of the system," *IEEE Journal of Emerging and Selected Topics in Power Electronics*, vol. 3, no. 1, pp. 191–200, 3 2015.

- [66] N. A. Keeling, G. A. Covic, and J. T. Boys, "A unity-power-factor IPT pickup for high-power applications," in *IEEE Transactions on Industrial Electronics*, vol. 57, no. 2, 2 2010, pp. 744–751.
- [67] T. Li, X. Wang, S. Zheng, and C. Liu, "An Efficient Topology for Wireless Power Transfer over a Wide Range of Loading Conditions," *Energies*, vol. 11, no. 1, p. 141, 1 2018. [Online]. Available: <http://www.mdpi.com/1996-1073/11/1/141>
- [68] D. Simonetti, J. Sebastian, F. dos Reis, and J. Uceda, "Design criteria for SEPIC and Cuk converters as power factor preregulators in discontinuous conduction mode," in *Proceedings of the 1992 International Conference on Industrial Electronics, Control, Instrumentation, and Automation*. Institute of Electrical and Electronics Engineers (IEEE), 1 1992, pp. 283–288.
- [69] A. A. Mohamed and O. Mohammed, "Bilayer Predictive Power Flow Controller for Bidirectional Operation of Wirelessly Connected Electric Vehicles," *IEEE Transactions on Industry Applications*, vol. 55, no. 4, pp. 4258–4267, 7 2019.
- [70] D. Yang, S. Won, J. Tian, Z. Cheng, and J. Kim, "A Method of Estimating Mutual Inductance and Load Resistance Using Harmonic Components in Wireless Power Transfer System," *Energies*, vol. 12, no. 14, p. 2728, 7 2019. [Online]. Available: <https://www.mdpi.com/1996-1073/12/14/2728>
- [71] C. Chen, H. Zhou, Q. Deng, W. Hu, Y. Yu, X. Lu, and J. Lai, "Modeling and Decoupled Control of Inductive Power Transfer to Implement Constant Current/Voltage Charging and ZVS Operating for Electric Vehicles," *IEEE Access*, vol. 6, pp. 59 917–59 928, 2018.
- [72] W. Shi, J. Deng, Z. Wang, and X. Cheng, "The Start-up Dynamic Analysis and One Cycle Control-PD Control Combined Strategy for Primary-Side Controlled Wireless Power Transfer System," *IEEE Access*, vol. 6, pp. 14 439–14 450, 3 2018.
- [73] A. Triviño-Cabrera, M. Ochoa, D. Fernández, and J. A. Aguado, "Independent primary-side controller applied to wireless chargers for electric vehicles," in *2014 IEEE International Electric Vehicle Conference, IEVC 2014*. Institute of Electrical and Electronics Engineers Inc., 2014.
- [74] X. Dai, J. Jiang, Y. Li, and T. Yang, "A Phase-Shifted Control for Wireless Power Transfer System by Using Dual Excitation Units," *Energies*, vol. 10, no. 7, p. 1000, 7 2017. [Online]. Available: <http://www.mdpi.com/1996-1073/10/7/1000>

- 
- [75] R. Tavakoli and Z. Pantic, "Analysis, Design, and Demonstration of a 25-kW Dynamic Wireless Charging System for Roadway Electric Vehicles," *IEEE Journal of Emerging and Selected Topics in Power Electronics*, vol. 6, no. 3, pp. 1379–1393, 9 2018.
- [76] D. J. Thrimawithana and U. K. Madawala, "A primary side controller for inductive power transfer systems," in *Proceedings of the IEEE International Conference on Industrial Technology*, 2010, pp. 661–666.
- [77] K. Song, Z. Li, J. Jiang, and C. Zhu, "Constant Current/Voltage Charging Operation for Series-Series and Series-Parallel Compensated Wireless Power Transfer Systems Employing Primary-Side Controller," *IEEE Transactions on Power Electronics*, vol. 33, no. 9, pp. 8065–8080, 9 2018.
- [78] P. Tiwari and N. R. Tummuru, "Misalignment Tolerant Primary Controller for Series-Series Compensated Static Wireless Charging of Battery," in *2019 IEEE Transportation Electrification Conference, ITEC-India 2019*. Institute of Electrical and Electronics Engineers Inc., 12 2019.
- [79] E. Gati, G. Kampitsis, and S. Manias, "Variable frequency controller for inductive power transfer in dynamic conditions," *IEEE Transactions on Power Electronics*, vol. 32, no. 2, pp. 1684–1696, 2 2017.
- [80] J. M. Miller, O. C. Onar, and M. Chinthavali, "Primary-side power flow control of wireless power transfer for electric vehicle charging," *IEEE Journal of Emerging and Selected Topics in Power Electronics*, vol. 3, no. 1, pp. 147–162, 3 2015.
- [81] Y. Jiang, L. Wang, Y. Wang, J. Liu, X. Li, and G. Ning, "Analysis, design, and implementation of accurate ZVS angle control for EV battery charging in wireless high-power transfer," *IEEE Transactions on Industrial Electronics*, vol. 66, no. 5, pp. 4075–4085, 5 2019.
- [82] S. A. Sis and H. Akca, "Maximizing the efficiency of wireless power transfer systems with an optimal duty cycle operation," *AEU - International Journal of Electronics and Communications*, vol. 116, p. 153081, 3 2020.
- [83] D. Kobayashi, T. Imura, and Y. Hori, "Real-time coupling coefficient estimation and maximum efficiency control on dynamic wireless power transfer for electric vehicles," in *IEEE WoW 2015 - IEEE PELS Workshop on Emerging Technologies: Wireless Power, Proceedings*. Institute of Electrical and Electronics Engineers Inc., 6 2015.
-

- [84] X. Dai, Y. Li, P. Deng, and C. Tang, "A Maximum Power Transfer Tracking Method for WPT Systems with Coupling Coefficient Identification Considering Two-Value Problem," *Energies*, vol. 10, no. 10, p. 1665, 10 2017. [Online]. Available: <http://www.mdpi.com/1996-1073/10/10/1665>
- [85] M. Fu, H. Yin, X. Zhu, and C. Ma, "Analysis and tracking of optimal load in wireless power transfer systems," *IEEE Transactions on Power Electronics*, vol. 30, no. 7, pp. 3952–3963, 7 2015.
- [86] H. J. Lee, W.-J. Son, S. Ann, J. Byun, and B. K. Lee, "Improved Pulse Density Modulation with a Distribution Algorithm for Semi-Bridgeless Rectifier of Inductive Power Transfer System in Electric Vehicles," in *2019 10th International Conference on Power Electronics and ECCE Asia (ICPE 2019 - ECCE Asia)*, Busan, South Korea, 2019, pp. 1–6. [Online]. Available: <https://ieeexplore.ieee.org/abstract/document/8797336>
- [87] M. Fan, L. Shi, Z. Yin, and Y. Li, "A novel pulse density modulation with semi-bridgeless active rectifier in inductive power transfer system for rail vehicle," *CES Transactions on Electrical Machines and Systems*, vol. 1, no. 4, pp. 397–404, 2017.
- [88] K. Colak, E. Asa, M. Bojarski, D. Czarkowski, and O. C. Onar, "A Novel Phase-Shift Control of Semibridgeless Active Rectifier for Wireless Power Transfer," *IEEE Transactions on Power Electronics*, vol. 30, no. 11, pp. 6288–6297, 11 2015.
- [89] W. Zhong and S. Y. Ron Hui, "Charging Time Control of Wireless Power Transfer Systems Without Using Mutual Coupling Information and Wireless Communication System," *IEEE Transactions on Industrial Electronics*, vol. 64, no. 1, pp. 228–235, 1 2017.
- [90] H. Li, J. Li, K. Wang, W. Chen, and X. Yang, "A maximum efficiency point tracking control scheme for wireless power transfer systems using magnetic resonant coupling," *IEEE Transactions on Power Electronics*, vol. 30, no. 7, pp. 3998–4008, 7 2015.
- [91] X. Dai, X. Li, Y. Li, and A. P. Hu, "Maximum Efficiency Tracking for Wireless Power Transfer Systems with Dynamic Coupling Coefficient Estimation," *IEEE Transactions on Power Electronics*, vol. 33, no. 6, pp. 5005–5015, 6 2018.
- [92] W. X. Zhong and S. Y. Hui, "Maximum energy efficiency tracking for wireless power transfer systems," *IEEE Transactions on Power Electronics*, vol. 30, no. 7, pp. 4025–4034, 7 2015.

- 
- [93] D. Patil, M. Sirico, L. Gu, and B. Fahimi, "Maximum efficiency tracking in wireless power transfer for battery charger: Phase shift and frequency control," in *ECCE 2016 - IEEE Energy Conversion Congress and Exposition, Proceedings*. Institute of Electrical and Electronics Engineers Inc., 2016.
- [94] H. Li, K. Wang, J. Fang, and Y. Tang, "Pulse Density Modulated ZVS Full-Bridge Converters for Wireless Power Transfer Systems," *IEEE Transactions on Power Electronics*, vol. 34, no. 1, pp. 369–377, 2018.
- [95] S. Chen, Y. Chen, H. Li, N. A. Dung, R. Mai, Y. Tang, and J. S. Lai, "An Operation Mode Selection Method of Dual-Side Bridge Converters for Efficiency Optimization in Inductive Power Transfer," *IEEE Transactions on Power Electronics*, vol. 35, no. 10, pp. 9992–9997, 10 2020.
- [96] M. Wu, X. Yang, W. Chen, L. Wang, Y. Jiang, C. Zhao, and Z. Yan, "A Dual-Sided Control Strategy Based on Mode Switching for Efficiency Optimization in Wireless Power Transfer System," *IEEE Transactions on Power Electronics*, 2021.
- [97] "Electric vehicle wireless power transfer (WPT) systems - Part 1: General requirements," International Electrotechnical Commission, International Standard IEC 61980-1:2020, Nov 2020.
- [98] "Electric vehicle wireless power transfer (WPT) systems - Part 2: Specific requirements for communication between electric road vehicle (EV) and infrastructure," International Electrotechnical Commission, International Standard IEC 61980-2:2019, Jun 2020.
- [99] "Electric vehicle wireless power transfer (WPT) systems - Part 3: Specific requirements for the magnetic field wireless power transfer systems," International Electrotechnical Commission, International Standard IEC 61980-3:2019, Jun 2019.
- [100] "Electrically propelled road vehicles — Magnetic field wireless power transfer — Safety and interoperability requirements," International Organization for Standardization, International Standard ISO 19363:2020, Apr 2020.
- [101] MarketsandMarkets INC, "Wireless Charging for Electric Vehicle Market Size, Share, Growth and Forecast by 2027," Pune, India, Tech. Rep., 2018. [Online]. Available: <https://www.marketsandmarkets.com/Market-Reports/wireless-ev-charging-market-170963517.html>
- [102] IndustryARC, "Wireless Ev Charging Market Share, Size and Industry Growth Analysis 2020 - 2025," Hyderabad, India, Tech. Rep., 2020. [Online].
-

- Available: <https://www.industryarc.com/Research/Wireless-Ev-Charging-Market-Research-501125>
- [103] Mordor Intelligence, “Wireless Charging for Electric Vehicle Market | Growth, Statistics, Industry Forecast 2020 - 2025,” Telangana, India, Tech. Rep., 2020. [Online]. Available: <https://www.mordorintelligence.com/industry-reports/global-wireless-charging-market-industry>
- [104] Institute for Automotive Engineering (ika), “Project STILLE successfully launched - ika,” 2016. [Online]. Available: <https://www.ika.rwth-aachen.de/en/press-releases/2308-project-stille-successfully-launched.html>
- [105] Green Tech Media, “HEVO to Launch US Manufacturing for Wireless Electric Vehicle Charger | Greentech Media,” 2020. [Online]. Available: <https://www.greentechmedia.com/articles/read/hevo-to-launch-us-manufacturing-for-wireless-electric-vehicle-charger>
- [106] Momentum Dynamics, “Wireless in Action - Momentum Dynamics.” [Online]. Available: <https://momentumdynamics.com/solution/#casestudy>
- [107] A. Khaligh and M. Dantonio, “Global Trends in High-Power On-Board Chargers for Electric Vehicles,” *IEEE Transactions on Vehicular Technology*, vol. 68, no. 4, pp. 3306–3324, 4 2019.
- [108] Momentum Dynamics, “Momentum Dynamics Wireless Charging System on Jaguar I-Pace Electric Taxis: World’s First Wireless Taxi Rank,” 2020. [Online]. Available: <https://momentumdynamics.com/2020/06/24/momentum-dynamics-wireless-charging-system-on-jaguar-i-pace-electric-taxis-worlds-first-wireless-taxi-rank/>
- [109] O. C. Onar, S. L. Campbell, L. E. Seiber, C. P. White, and M. Chinthavali, “Vehicular integration of wireless power transfer systems and hardware interoperability case studies,” in *ECCE 2016 - IEEE Energy Conversion Congress and Exposition, Proceedings*. Institute of Electrical and Electronics Engineers Inc., 2016.
- [110] T. A. Nergaard and J. B. Strauble, “Integrated inductive and conductive electrical charging system,” U.S. Patent US8933661B2, Jan 2015.
- [111] S. Ichikawa, “Vehicle charging unit,” European Patent EP2431214, Mar 2012.
- [112] M. Chinthavali, O. C. Onar, S. L. Campbell, and L. M. Tolbert, “Isolated wired and wireless battery charger with integrated boost converter for PEV applications,” in

- 2015 IEEE Energy Conversion Congress and Exposition, ECCE 2015.* Institute of Electrical and Electronics Engineers Inc., 10 2015, pp. 607–614.
- [113] V. Berntsson, “Design and analysis of wireless charging combined with conductive charging,” M.S. Thesis, Chalmers University of Technology, 2017. [Online]. Available: <https://hdl.handle.net/20.500.12380/253618>
- [114] B. Vu, J. M. Gonzalez-Gonzalez, V. Pickert, M. Dahidah, and A. Trivino, “A hybrid charger of conductive and inductive modes for Electric Vehicles,” *IEEE Transactions on Industrial Electronics*, 2020.